

# **Stony Brook University**



OFFICIAL COPY

**The official electronic file of this thesis or dissertation is maintained by the University Libraries on behalf of The Graduate School at Stony Brook University.**

**© All Rights Reserved by Author.**

**Development of a Novel Immunization Platform**

A Dissertation Presented

by

**Katarzyna Magdalena Sawicka**

to

The Graduate School

in Partial Fulfillment of the

Requirements

for the Degree of

**Doctor of Philosophy**

in

**Biomedical Engineering**

Stony Brook University

**May 2014**

Copyright by  
Katarzyna M. Sawicka  
2014

**Stony Brook University**

The Graduate School

**Katarzyna Magdalena Sawicka**

We, the dissertation committee for the above candidate for the  
Doctor of Philosophy degree, hereby recommend  
acceptance of this dissertation.

**Sanford R. Simon, PhD – Dissertation Advisor**  
**Professor; Biochemistry, Cell Biology, Pathology and Biomedical Engineering**

**Richard A. Clark, MD – Chairperson of Defense**  
**Professor; Dermatology and Biomedical Engineering**

**Michael Hadjiargyrou, PhD – Committee Member**  
**Professor; Biomedical Engineering**

**Nena Golubovic-Liakopoulos, PhD – External Committee Member**  
**President and Founder, Chairman of the Board of Directors**  
**Agigma, Inc.**

This dissertation is accepted by the Graduate School

Charles Taber  
Dean of the Graduate School

Abstract of the Dissertation

**Development of a Novel Immunization Platform**

by

**Katarzyna Magdalena Sawicka**

**Doctor of Philosophy**

in

**Biomedical Engineering**

Stony Brook University

**2014**

Human skin defends against foreign pathogens with the physical barrier posed by its architecture as well as the large population of resident antigen presenting cells (APCs) that participate in launching both humoral and cellular immune responses. The equipment, storage, and personnel demands posed by intramuscular injection, the gold standard of immunization, hinder rapid distribution of vaccines to large populations under the time constraints of a spreading pandemic. Lower doses of immunogens, successfully delivered into the APC-rich layers of the skin, have been shown to elicit an immune response comparable to that achieved with intramuscular injection. The work disclosed in this dissertation addresses the drawbacks of the current vaccine paradigm through development of a novel skin patch consisting of biologically active antigen macromolecules reversibly encapsulated within a nanofibrous matrix composed of polyvinyl pyrrolidone (PVP). The large surface area to volume ratio offered by the electrospun matrix enhances the attachment of the electrospun patch to the apical skin layer, where its hygroscopic composition exploits transepidermal water transport to dissolve the solid-state patch to then temporarily swell the “brick and mortar anatomy” of the stratum corneum barrier and successfully deliver the released immunogens without resorting to abrasion and puncture of the skin. The self-administrable skin patch developed in this work has been shown to successfully encapsulate biologically active macromolecules such as immunogens for avian influenza, anthrax and whooping cough within the nanofibrous coating. The long-term storage capacity for the proteins has been significantly enhanced by encapsulation within the solid-state matrix, while their biological function and antibody recognition motifs were preserved. The patch’s efficacy in delivering antigen payloads into the immunocompetent layers of the human skin has been demonstrated *in vitro* using commercially available tissue engineered human skin models. Lastly, *in vivo* application of the patch to the skin of Sprague-Dawley rats elicited a specific immune response to the delivered antigen comparable to that elicited by the intramuscular injection.

## Dedication Page

To all those, who like molecules that move freely among themselves to form a substance with a physical state that does not resist change of shape, but change of size, and in turn contribute to a final density greater than 1.24 g/ml.

# Frontispiece

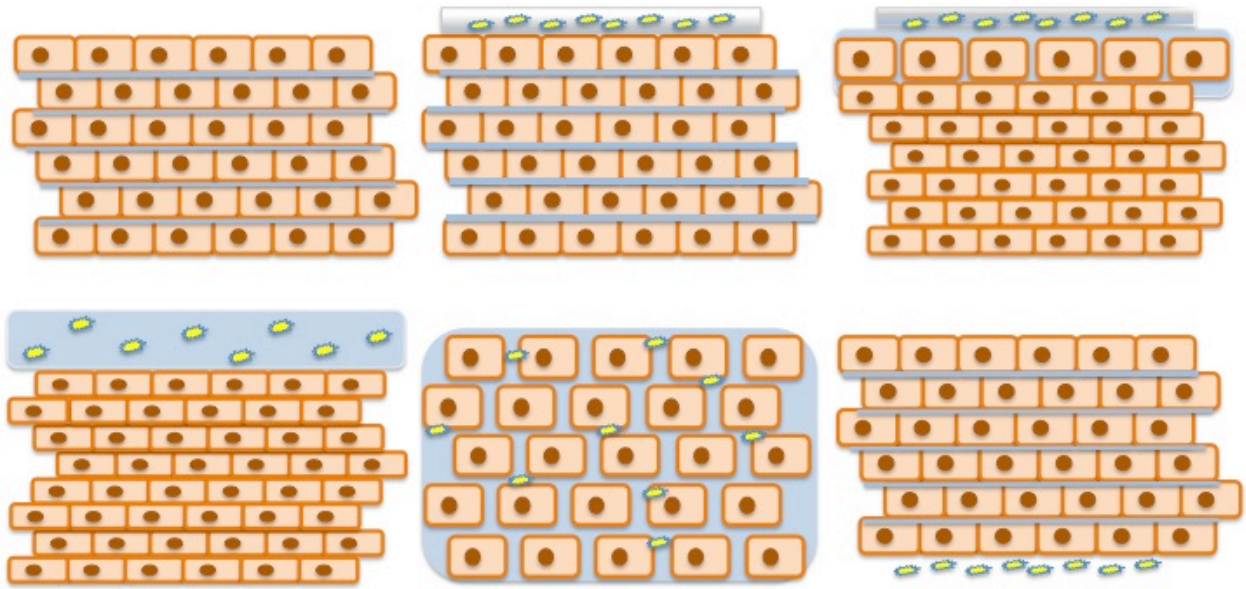


## Table of Contents

|  |             |
|--|-------------|
| <b>Abstract</b>                            | <b>iii</b>  |
| <b>Dedication</b>                          | <b>iv</b>   |
| <b>Frontispiece</b>                        | <b>v</b>    |
| <b>List of Figures</b>                     | <b>viii</b> |
| <b>List of Tables</b>                      | <b>xii</b>  |
| <b>List of Commonly Used Abbreviations</b> | <b>xiii</b> |
| <b>Preface</b>                             | <b>xv</b>   |
| <b>Acknowledgements</b>                    | <b>xvi</b>  |
| <br>                                       |             |
| <b>Chapter 1 – Introduction</b>            | <b>1</b>    |
| <i>Significance</i>                        | <b>1</b>    |
| <i>Background</i>                          | <b>1</b>    |
| <i>Currently Explored Innovations</i>      | <b>6</b>    |
| <i>Design</i>                              | <b>12</b>   |
| <i>Hypotheses and Specific Aims</i>        | <b>18</b>   |
| <br>                                       |             |
| <b>Chapter 2 – Specific Aim I</b>          | <b>20</b>   |
| <i>Introduction</i>                        | <b>21</b>   |
| <i>Materials and Methods</i>               | <b>25</b>   |
| <i>Results</i>                             | <b>30</b>   |
| <i>Discussion</i>                          | <b>37</b>   |



## Table of Contents - continued

|  |            |
|--|------------|
| <b>Chapter 3 – Specific Aim II</b>             | <b>41</b>  |
| <i>Introduction</i>                            | <b>42</b>  |
| <i>Materials and Methods</i>                   | <b>45</b>  |
| <i>Results</i>                                 | <b>52</b>  |
| <i>Discussion</i>                              | <b>65</b>  |
| <br>   |            |
| <b>Chapter 4 – Specific Aim III</b>            | <b>71</b>  |
| <i>Introduction</i>                            | <b>72</b>  |
| <i>Materials and Methods</i>                   | <b>74</b>  |
| <i>Results</i>                                 | <b>83</b>  |
| <i>Discussion</i>                              | <b>91</b>  |
| <br>   |            |
| <b>Chapter 5 – Specific Aim IV</b>             | <b>98</b>  |
| <i>Introduction</i>                            | <b>99</b>  |
| <i>Materials and Methods</i>                   | <b>102</b> |
| <i>Results</i>                                 | <b>110</b> |
| <i>Discussion</i>                              | <b>113</b> |
| <br>   |            |
| <b>Chapter 6 – Conclusions and Limitations</b> | <b>119</b> |
| <br>   |            |
| <b>References</b>                              | <b>126</b> |

## List of Figures

- Figure 1.1** The humoral antibody production upon exposure to the antigen [11]. (Pg. 3)
- Figure 1.2** The cross-section of human skin [14]. (Pg. 4)
- Figure 1.3** The microneedle design for the Macroflux patch [19]. (Pg. 7)
- Figure 2.1** The electrospinning setup. (Pg. 23)
- Figure 2.2** Dissolution study set up. (Pg. 27)
- Figure 2.3** A schematic of the PCF Millicell setup utilized for the basal media HRP release experiment. (Pg. 28)
- Figure 2.4** Release profiles observed for the HRP/PVP matrices prepared with a 0.05mM PVP; the error bars represent the standard deviation between the three matrices dissolved for each mixture. (Pg. 30)
- Figure 2.5** Release profiles observed for the HRP/PVP matrices prepared with a 0.075mM PVP; the error bars represent the standard deviation between the three matrices dissolved for each mixture. (Pg. 31)
- Figure 2.6** Release profiles observed for the HRP/PVP matrices prepared with a 0.10mM PVP; the error bars represent the standard deviation between the three matrices dissolved for each mixture. (Pg. 31)
- Figure 2.7** Comparison HRP deposition on the electrospinning collector determined from the bulk release study for nine combinations of enzyme to polymer; the error bars represent the standard error of the mean obtained for three different matrices dissolved for each mixture. Figure 2.6 Release profiles observed for the HRP/PVP matrices prepared with a 0.10mM PVP; the error bars represent the standard deviation between the three matrices dissolved for each mixture. (Pg. 32)
- Figure 2.8** Comparison of HRP release from electrospun matrices in the PCF Millicell set up for three concentrations of polymer vehicle; the error bars represent the standard deviation between the three wafers dissolved for each mixture. (Pg. 33)
- Figure 2.9** Comparison of HRP release from electrospun matrices in the PCF Millicell set up for three concentrations of polymer vehicle; the error bars represent the standard deviation between the three wafers dissolved for each mixture. (Pg. 33)

- Figure 2.10** Comparison of HRP release from electrospun matrices in the PCF Millicell set up for three concentrations of polymer vehicle; the error bars represent the standard deviation between the three wafers dissolved for each mixture. (Pg. 34)
- Figure 2.11** A representative SEM image of the 20% HRP – 80% 0.075mM PVP matrix. (Pg. 34)
- Figure 2.12** SEM images of 0.075 mM matrix electrospun at 10 $\mu$ l/min flow rate samples: no stopping, 30 second pause, 60 second pause (top to bottom). (Pg. 35)
- Figure 2.13** SEM images at a 30kX magnification of 10 $\mu$ l/min flow rate samples. The rows represent no stopping, 30 second pause, 45 second pause, 60 second pause (top to bottom). (Pg. 36)
- Figure 3.1** The electrospinning collector covered with 4x4 mm silicon wafers prior to electrospinning. (Pg. 48)
- Figure 3.2** The CHO cell assay 72 hours after dosing; top row left from right, untreated control, PT solution standard; bottom row left from right, PT/PVP electrospinning solution, and PT/PVP Matrix. (Pg. 54)
- Figure 3.3** The CHO cell assay rating scale employed 48 hours after dosing. (Pg. 55)
- Figure 3.4** The 20 week storage stability of samples stored in ambient conditions. (Pg.55)
- Figure 3.5** The 20 week storage stability of samples stored in ambient conditions in the presence of desiccant. (Pg. 56)
- Figure 3.6** The 20 week storage stability of samples stored in ambient conditions in a vacuum sealed container. (Pg. 56)
- Figure 3.7** The 20 week storage stability of samples stored in the refrigerator at 4°C. (Pg. 57)
- Figure 3.8** The 20 week storage stability of samples stored in the refrigerator at 4°C in the presence of desiccant. (Pg. 57)
- Figure 3.9** The 20 week storage stability of PT solution samples. (Pg. 58)
- Figure 3.10** The 20 week storage stability of Dry Coated PT/PVP wafers. (Pg. 58)
- Figure 3.11** The 20 week storage stability of PT/PVP Matrix. (Pg. 59)
- Figure 3.12** The SEM images obtained for freshly electrospun PT/PVP matrix (top), vacuumed stored PT/PVP matrix after two weeks of storage (bottom right), and refrigerated PT/PVP matrix after two weeks of storage (bottom left). (Pg. 60)

- Figure 3.13** The optical density of the HA standards. (Pg. 61)
- Figure 3.14** The amount of HA calculated for the samples using correlation equation. (Pg. 62)
- Figure 4.1** The electrospinning collector with 4x4 mm silicon wafer pairs used for the HRP delivery experiment in dry and tissue studies. Drawing not to scale. (Pg. 73)
- Figure 4.2** The HRP/PVP Matrix sample attached to the sterile microcentrifuge tube bottoms. (Pg. 74)
- Figure 4.3** The MatTek HRP/PVP Matrix sample attached to the sterile microcentrifuge tube bottoms. (Pg. 75)
- Figure 4.4** The standard curve for HRP. (Pg. 81)
- Figure 4.5** The average HRP delivery profile for the various platforms tested on the MatTek EFT-300 tissue engineered human skin constructs. The error bars represent the standard error of the mean between the samples within each group for a specific time point (n=6). (Pg. 82)
- Figure 4.6** The average percentage of HRP delivered by the various platforms tested on the MatTek EFT-300 tissue engineered human skin constructs. The error bars represent the standard error of the mean between the samples within each group for a specific time point (n=6). (Pg. 83)
- Figure 4.7** The alamaBlue cell viability assay absorption at 590 nm observed after the 24-hr delivery study for two tissue samples from each test group. The error bars represent the standard of deviation between the two tissue samples tested for each group (n=2). (Pg. 84)
- Figure 4.8** Comparison of HRP concentrations obtained from the electrospun HRP/PVP Matrix wafers in tissue experiment versus the control dissolution study. The error bars represent the standard error of the mean between the samples within each group for a specific time point (n=4; samples 1 and 2 of homogenized tissue were compromised with the alamar blue assay). (Pg. 85)
- Figure 4.9** Average MTS viability assay absorbance reading after the 24-hour PT delivery study (n=4 for UTC and PTSolution; n=6 PT/PVP Matrix). (Pg. 87)
- Figure 4.10** Representative images of the CHO cell clumping observed in the presence of the PT samples. (Pg. 88)
- Figure 5.1** Silicon wafers attached to aluminum foil to be wrapped over the target plate of the electrospinning apparatus. (Pg. 102)

- Figure 5.2** Electrospun PT/PVP matrix collected on the wafers. (Pg. 102)
- Figure 5.3** The PT-patch; 12 silicon wafers attached to Tegaderm. (Pg. 103)
- Figure 5.4** The PT-patch after application to the depilated dorsal surface of a rat; the sturdy backing material on the Tegaderm film was removed once the film was applied to each animal's back. (Pg. 104)
- Figure 5.5** The PT-patch bandaged over with a Vetwrap. (Pg. 105)
- Figure 5.6** Schematic representation of the PT ELISA design. (Pg. 106)
- Figure 5.7** Rat IgG standard curve. (Pg. 108)
- Figure 5.8** Mean ( $\pm$ SEM) anti-PT IgG levels in rats receiving PT either via intramuscular injection (IM) or the PT-Patch (n=5 for both groups). The blood collection occurred prior to the antigen administration at weeks 0 and 3. (Pg. 109)
- Figure 5.9** The PT-Patch being removed from the animal's back after a 24 hour occlusion. (Pg. 110)
- Figure 5.10** The PT-Patch freshly removed from the animal post experiment. (Pg. 110)
- Figure 5.11** The proposed mechanism of antigen delivery in vivo. (Pg. 115)

## List of Tables

|                  |   |
|------------------|---|
| <b>Table 1.1</b> | Outline of currently explored innovations and the their approach at the outlined drawbacks. (Pg. 10)  |
| <b>Table 2.1</b> | Outline of the initial nine solution combinations tested. (Pg. 25)  |
| <b>Table 2.2</b> | Outline of the electrospinning parameters tested. (Pg. 29)  |
| <b>Table 3.1</b> | Outline of the antibodies utilized for the HA immunorecognition experiment. (Pg. 50)  |
| <b>Table 3.2</b> | CHO cells at 24 hour observation and concentration $2.4 \times 10^4$ cells/cm <sup>2</sup> . (Pg. 52)   |
| <b>Table 3.3</b> | CHO cells at 48 hour observation and concentration $2.4 \times 10^4$ cells/cm <sup>2</sup> . (Pg. 53)   |
| <b>Table 3.4</b> | CHO cells at 72 hour observation and concentration $2.4 \times 10^4$ cells/cm <sup>2</sup> . (Pg. 53)   |
| <b>Table 3.5</b> | The 20 week storage stability of different PT formulation samples stored under different conditions. (Pg. 61)   |
| <b>Table 3.6</b> | Outline of the storage conditions tested (n=2). (Pg. 66)  |
| <b>Table 4.1</b> | The amount of HRP delivered for each sample. (Pg. 82)   |
| <b>Table 4.2</b> | The level of CHO cell clumping observed 48 hours after dosing with duplicates of the control solutions of PT standard as well as the electrospinning solution (n=2). (Pg. 86) |
| <b>Table 4.3</b> | The level of CHO cell clumping observed 48 hours after dosing with the media collected from the PT delivery EPI-200 tissue experiment. (Pg. 86)                               |
| <b>Table 5.1</b> | Methods of physical disruption of the SC used by competing technologies. (Pg. 112)  |

## List of Abbreviations

|             |                                   |
|-------------|-----------------------------------|
| <b>AFM</b>  | atomic force microscopy           |
| <b>APCs</b> | antigen presenting cells          |
| <b>cAMP</b> | cyclic adenosine monophosphate    |
| <b>CHO</b>  | Chinese hamster ovary             |
| <b>CT</b>   | cholera toxin                     |
| <b>DCs</b>  | dendritic cells                   |
| <b>DLNs</b> | draining lymph nodes              |
| <b>GI</b>   | gastrointestinal                  |
| <b>HA</b>   | hemagglutinin                     |
| <b>HRP</b>  | horseradish peroxidase            |
| <b>IM</b>   | intramuscular injection           |
| <b>LCs</b>  | Langerhans cells                  |
| <b>LF</b>   | lethal factor                     |
| <b>LPS</b>  | lipopolysaccharide                |
| <b>LT</b>   | heat-labile enterotoxin           |
| <b>MTS</b>  | tetrazolium salt                  |
| <b>PA</b>   | protective antigen                |
| <b>PT</b>   | pertussis toxin                   |
| <b>PVP</b>  | polyvinylpyrrolidone              |
| <b>rPA</b>  | recombinant protective antigen    |
| <b>SARS</b> | severe acute respiratory syndrome |

|              |   |
|--------------|---|
| <b>SC</b>    | stratum corneum                           |
| <b>SEM</b>   | scanning electron microscopy              |
| <b>SSBMS</b> | solid-state biodegradable microstructures |
| <b>TEWL</b>  | transepidermal water loss                 |
| <b>TCI</b>   | transcutaneous immunization               |
| <b>TMB</b>   | tetramethylbenzidine                      |
| <b>UTC</b>   | untreated control                         |



## **Preface**

“Without deviation from the norm, progress is not possible.”

Frank Zappa

## **Acknowledgments**

With the deepest gratitude to my very own “DEAD SEA.”

## Chapter 1

### *Introduction*

## **Significance**

The conservative base case assumption estimates that the next global pandemic could affect 25% of the world's population [1]. The predicted overall cost associated with a potential pandemic is estimated to be \$166 billion for the United States alone. This amount does not appear adequate when compared to the \$2 billion total cost endured by Canada in dealing with the contained SARS outbreak in 2002 [2]. The 44 casualties and more than 25,000 residents placed under quarantine in the greater Toronto area are far from the 25% base case assumption. To date the most successful form of pandemic eradication is a properly formulated and administered vaccine [3]. The currently employed immunization paradigm is based on an intramuscular injection, which requires the use of hypodermic needles, refrigeration, and adequate hazardous waste disposal as well as administration by trained medical staff.

## **Background**

Historically, inoculation was brought to western cultures from the Ottoman Empire in the early 18<sup>th</sup> century [4]. The man credited for the widespread use of vaccines is Edward Jenner. In the late 1790s the physician became an avid advocate for the smallpox vaccine, which called for subcutaneous delivery of pus from a fresh cowpox lesion to successfully confer smallpox immunity. Problems associated with sterility and inoculum supply have rendered the original vaccination method impractical for modern use. However the Jenner technique is to date recognized as an exceptionally effective immunization protocol, and has been credited with successfully eradicating the smallpox

pandemic. The lessons of modern immunology have led to understanding and identification of the key processes involved in conferring protection by the original smallpox vaccine [5-9]. The large population of antigen presenting cells (APCs) residing in human skin has been highlighted as the chief factor in the success of achieving immunoprotection through vaccination by the subcutaneous puncture method employed by Jenner.

The body's ability to protect itself from foreign pathogens relies on its ability to

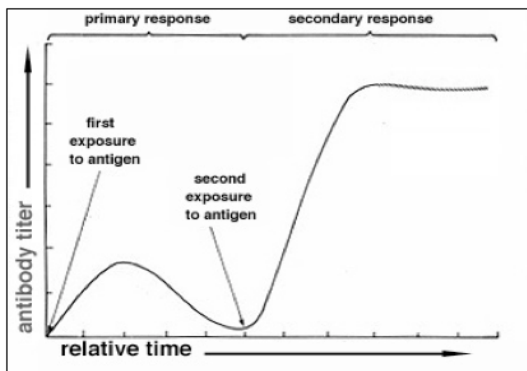


**Figure 1.1** The humoral antibody production upon exposure to the antigen [11].

recognize and react to such infectious materials once they are presented to the host immune cells, in a process known as the adaptive immune response [10]. Currently employed liquid formulations for immunization deliver antigens with a mixture of stabilizers, preservatives and components left behind by the manufacturing

process, as well as adjuvants. There are four distinct classes of vaccine formulations, reflecting the form of antigen utilized: live attenuated (e.g., smallpox), killed/inactivated (e.g., whole cell), toxoid (e.g., toxin denatured with formaldehyde) and subunit [10]. This study will focus on the optimization of protein subunit vaccines employing intradermal delivery of antigen.

The immunogen in a subunit vaccine is typically a protein component of a bacterium, virus or a DNA fragment that codes for the protein sequence and is transcribed and translated in the host. Subunit vaccines have been reported to induce both humoral and cellular responses to the administered antigen. The effectiveness of

such vaccination largely depends on the antigen's immunogenicity, which is in turn a function of the antigen's size, molecular complexity, degree of "foreignness" and capacity to be cleaved into peptides by APCs [12]. The antigen-stimulated and activated APCs migrate to draining lymph nodes (DLNs), where the antigen is then presented to naïve T helper cells. Subsequently the antigen is presented to B cells resulting in systemic antibody production as well as priming of memory B cells [7]. It has been long recognized that the amount of antigen delivered is often less significant than the frequency of antigen administration [12]. The initial production of antibodies begins to decline approximately three weeks post-primary exposure, but can be further enhanced via a second contact with the same antigen, as illustrated in Figure 1.1 [11]. Therefore, booster shots are strongly advocated and generally induce high concentrations of antigen-specific antibodies.

The integumentary system of the human body is its largest organ, and represents the first line of defense against foreign materials. In the field of intradermal delivery the human skin is composed of

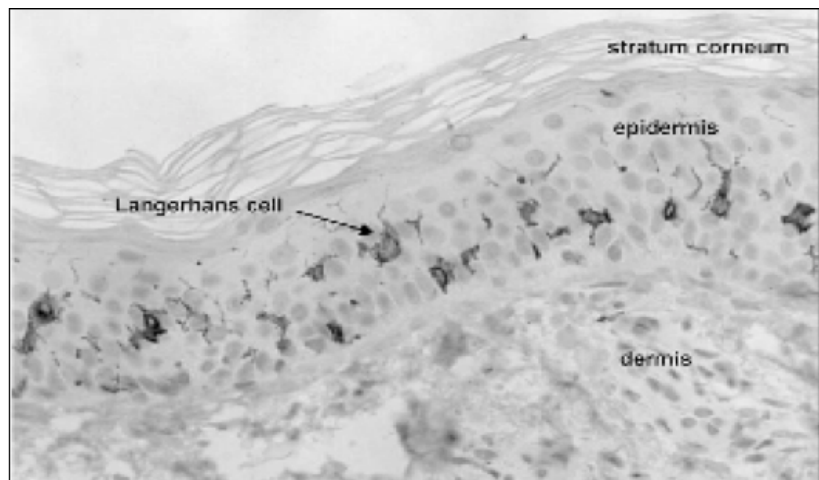


**Figure 1.2** The cross-section of human skin [14].

three main layers: the stratum corneum (SC), epidermis and dermis as shown in Figure 1.2 [13,14]. The 10-20 $\mu$ m thick SC is predominantly made up of cornified keratinocytes, which release lipids into the intercellular spaces. The resulting brick-and-

mortar structure serves as a competent, but breachable barrier [14]. The 50-100µm thick epidermis is mainly made up of keratinocytes and bone marrow-derived APCs known as Langerhans cells (LCs) [5].

The surveillance network of LCs occupies 25% of the skin's total surface. The cells continuously migrate out of the skin to the draining lymph nodes (DLN), but the rate of migration drastically increases upon exposure to activating stimuli such as antigens and adjuvants [8, 9]. The innermost of the three layers, the dermis, provides structural support to the skin. It is mostly composed of connective tissue, and is populated with its own resident APCs, the dendritic cells (DCs), as well as hair and sweat glands. Due to the presence of blood vessels the dermis has been considered the major target of transdermal drug delivery [15]. Successful delivery of antigens to the epidermis as well as the dermis has been shown to generate cellular as well as humoral immune responses via mechanisms involving participation of major histocompatibility antigens on both classes of APCs found in the human skin [10, 16]. The skin's constant surveillance function and active participation in immunoprotection renders it an optimal destination for antigen delivery [13].

Recent attempts to utilize the intradermal route of antigen delivery have been motivated by stockpile shortages of vaccines for avian and swine influenza. Two large-scale studies of vaccination against avian influenza compared the efficacy of a lowered (3µg) dose intradermal immunization to that of a full 15µg dose of the intramuscularly injected vaccine formulation [17, 18]. Although inconsistent, the findings showed that a lower dose of the intradermal vaccine induces antibody titers that offer protection comparable to that achieved after a full dose of intramuscular vaccine in young

individuals; however intradermal vaccination may not have the same effect in the elderly. Nevertheless, the reported efficacy of dose sparing intradermal injection supports the conclusion that the skin can serve as a primary target for antigen delivery under pandemic conditions. The Mantoux method of intradermal administration requires that approximately 2 mm of the needle penetrate the skin at a 15 degree angle followed by a slow release of the liquid into the superficial layers [17]. Efficacy of the method requires employment of highly trained medical personnel, and the protocol is therefore unsuitable for efficient and rapid vaccination of large populations to contain a spreading pandemic.

### **Currently Explored Innovations**

To eliminate the cumbersome delivery method, yet capitalize on the efficacy of the dose sparing intradermal delivery regimen, numerous novel methods of inoculation have been developed within the last decade. Each of the below highlighted technologies attempts to overcome the permeability barrier of the SC.

#### IS™ Patch

The efforts of Gregory M. Glenn, originally from Carl R. Alving's group, to develop an effective transcutaneous vaccine have culminated in the development of a so-called "universal immunostimulating" IS™ patch (Iomai, MD, USA). This transcutaneous immunization (TCI) delivery platform has been employed with adjuvants such as cholera toxin (CT) or heat-labile enterotoxin (LT) and has been shown to induce systemic and mucosal immune responses in animal and human subjects [13, 14, 18-



24]. The initial patch design consisted of a moist gauze dressing placed over murine skin in which the SC had been compromised by disruption methods such as hydration alone, hydration with tape stripping or abrasion with a pumice pad or emery paper [13, 20]. The decade-long process of evaluating the efficacy of the IS patch has centered on its capacity to serve as an independent vaccine against bacterial toxins, as well as its use as an adjuvant delivery system to augment the response to traditionally delivered anthrax and avian flu immunizations. The patch has been marketed as a band aid-like product to be placed over an injection site to enhance the immunogenicity of liquid vaccine formulations with weak intrinsic capacity to achieve seroconversion or to be used in immunosuppressed populations such as the elderly [13]. TCI has been reported to induce both IgG and IgA antibodies in mucosal secretions of mice [19]. The later version of the patch, which has successfully passed Phase I clinical trials, and has since been acquired by Intercell AG (Austria), consists of a dry patch paired with a disposable skin penetration device for mild disruption of the SC [22].

MACROFLUX®

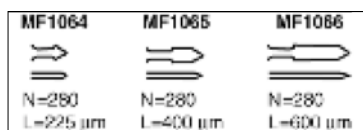


**Figure 1.3** The microneedle design for the Macroflux patch [19].

The Macroflux patch technology employs a titanium microneedle array patented by ALZA Corporation [25, 26] to disrupt the barrier function of the SC. As a proof of principle to demonstrate how immunization can be accomplished with

this platform, the microneedles were dip coated with a 45kDa antigen, ovalbumin (OVA), to induce a specific immune response in hairless guinea pigs, which was then compared to traditionally administered intramuscular (IM) injection. The OVA dry coated arrays delivered only 12.16%, 13.74%, 4.16% of the deposited coating, believed

to have originated from the tips as represented in Figure 1.3. System improvements aimed at optimizing the microneedle design and confining deposition of the immunogen to tips only resulted in delivery efficiency of 48-58% [26]. The anti-OVA titers induced by Macroflux® immunization favorably compared to those achieved after intramuscular injection. The greatest drawbacks of the Macroflux system are the cost associated with titanium microarray fabrication, the need to optimize the stability of the antigen coatings and the relative inflexibility of the delivery system, which incorporates a spring-loaded applicator to drive the microneedle array into the epidermis.

#### Solid State Biodegradable MicroStructures (SSBMS)

The solid-state biodegradable microstructure (SSBMS) arrays utilize a spring-loaded high velocity impactor to penetrate the stratum corneum with easily dissolved microneedles that will, upon dissolution, deliver incorporated macromolecules into the skin [27]. The technology was recently employed to deliver a booster dose of recombinant protective antigen (rPA) anthrax vaccine 28 days following the initial dose delivered as a traditional intramuscular injection in Sprague-Dawley Rats. Upon delivery of an array of 200µm tall microneedles into the skin, approximately 75% of the array patch dissolved within two minutes. The superior anti-PA IgG levels obtained after administration of immunogen via a microneedle patch containing an antigen content equal to that of a traditionally administered liquid vaccine further supports the rationale behind efforts to improve the intradermal immunization method. The main drawbacks of the dissolvable microneedle system are the multistep fabrication of the microstructures, and the cost associated with production and disposal of the spring loaded impactor.

## PVP MICRONEEDLES

A similar dissolvable microneedle array patch was developed and reported by Prausnitz et al [28]. A preparation of inactivated avian influenza virus was mixed with a solution of vinyl pyrrolidone followed by photopolymerization at room temperature within a microneedle mold. The resulting polymeric cast had the form of a patch containing an array of 650µm antigen containing polyvinyl pyrrolidone (PVP) microneedles. These photopolymerized PVP patches were applied to the surface of the skin without any additional apparatus for penetration, and therefore offer a simpler delivery strategy than the microneedle devices that are paired with impactors. A simple thumb press of the patch into the skin of pigs or BALB/c mice provided sufficient delivery to achieve an immune response. Approximately 89% of the soluble polymer vehicle dissolved away within five minutes, thus releasing the antigen into skin. The profile of antibody titers 14 days after a single immunization showed that the antigen/polymer microneedles induced a slightly diminished humoral response compared with that achieved with an intramuscular injection, or after application of a metal microneedle array coated with the same formulation. A placebo patch containing no payload induced titers that were comparable to those detected in untreated controls. At day 28 the titers achieved in the samples from animals immunized via dissolvable microneedle patches were higher than those for the other groups. The dissolving PVP microneedle patch successfully eliminated the employment of accessory devices such as the high velocity impactor; however its fabrication did involve a multistep manufacturing requirement, and the in situ polymerization process may or may not be compatible with other antigens.

| Technology      | Storage | Trained Personnel | Antigen Dose | Equipment | Biohazardous Waste |
|-----------------|---------|-------------------|--------------|-----------|--------------------|
| IS Patch™       | ?       | +                 | +            | -         | +                  |
| Macroflux       | ?       | +                 | +            | -         | -                  |
| SSBMS           | ?       | +                 | -            | -         | +                  |
| PVPMicroneedles | ?       | +                 | +            | -         | +                  |

**Table 1.1** Outline of currently explored innovations and the their approach at the outlined drawbacks.

The appeal of intradermal methods for delivery of antigens that might obviate the need for the Mantoux technique of injection has become a priority in novel vaccine development. A self-administered system that could utilize the skin's immunocompetence offers promise that immunity could be achieved with lowered antigen doses when compared to the commonly employed intramuscular route of delivery. Successful delivery of antigens through the 10-20 layers of cornified keratinocytes, known as the stratum corneum, will be facilitated by employment of an electrospun payload laden nanofibrous matrix.

The 10-20  $\mu\text{m}$  thick stratum corneum has been identified as an effective, but fragile barrier of the body's integumentary system [31-35]. Its composition and structure pose a physical barrier to penetration of liquids, large molecules and microbial agents. The transdermal route of drug delivery has been claimed to be limited to molecules smaller than 500Da due, in part, to the impermeability of the stratum corneum, but,

more important, to the skin's metabolism of macromolecular payloads [13]. Inter-subject and inter-site differences in permeability have been attributed to variation of SC thickness and lipid content, as well as differences in skin type and age [15]. Regional site-specific permeation rates have been directly linked to local transepidermal water loss (TEWL) [36, 37]. Regardless of the physicochemical properties of the compound tested, regions with the highest TEWL and, in turn, permeation values were reported to be the forehead and area behind the ear [36]. The “brick and mortar” lamellae that are actively involved in the management of water transport in skin have been said to resemble an accordion that flexes during lipid swelling and drying events [37]. The external hydration of the skin induces swelling, causing reversible changes in the SC microstructure, consequently allowing passage of normally inadmissible molecules [15]. The most obvious enhancement of skin permeation is achieved by maximizing the surface area of contact between the patch and skin. A lack of stable adhesion of the delivery system to the skin can result in detachment, thus breaking the payload permeation process [38]. The work proposed here will concentrate on exploiting the benefits of enhancing the surface area of contact, controlling transepidermal water loss (TEWL), and inducing a temporary swelling of the “brick and mortar anatomy” of the stratum corneum as the most significant factors for penetration of the barrier, without resorting to abrasion and puncture.

Recent advances in intradermal immunization have concentrated on various forms of mechanical disruption of the stratum corneum to effectively deliver the antigen to the immunocompetent regions of the skin. Ranging from physical abrasion to puncture penetration, each of the described solutions complicates the design, and cost

for production and distribution of the vaccination product, and still requires education of patients and health care providers. The proper disposal of biohazardous materials to avoid blood borne pathogen spread may become more crucial during a pandemic threat. Furthermore it has been reported that some of the longer needle arrays can draw blood, and thus fail to eliminate the risk of transmitting blood borne pathogens associated with the use and disposal of hypodermic needles. The waste generated by the use of metal microneedle arrays in some of the currently proposed devices would simply substitute, replace, or add to the amount of waste produced by the current disposal of conventional hypodermic needles. Other explored methods of administration, Table 1.1, such as high velocity spring loaded impactors or a multistep skin treatment prior to administration, add more complexity to the system and therefore present the potential for lower patient compliance and suboptimal utilization by health care providers.

## **Design**

### *Polyvinylpyrrolidone*

This project aims to address the hurdle of intradermal delivery of antigens through the use of reversible antigen encapsulation within a hygroscopic nanofibrous matrix composed of polyvinylpyrrolidone (PVP). PVP, commonly known as povidone, is a synthetic polymer of a wide range of molecular weights varying from 30,000 to 1,300,000 g/mol. Vinylpyrrolidone, PVP's monomer, has been found to be carcinogenic and toxic to aquatic life [39]. However the virtually nondegradable polymer is generally

regarded as safe and has been employed in many biomedical applications [40]. In its pure form, unlike most of the commonly used polymers, PVP is amorphous, and presents no crystal structure [41]. When dry it is a light flaky powder, which readily absorbs up to 18% of its weight in atmospheric water [42]. Hydrophilic PVP is readily soluble in water as well as other polar solvents, due to its own polarity. In solution, it has excellent wetting properties and readily forms films, often earning it the role of a disintegrant for caplets and tablets used by nutraceutical and pharmaceutical companies [43]. Oral, topical, or intraperitoneal administration of PVP has not been reported to result in any immunogenicity or toxicity [44]. It is said to be completely inert to humans and simply passes through the GI tract [44-48].

One of the earliest biomedical applications of PVP was in Betadine® [46], an antiseptic solution of iodine and PVP applied to topical wounds to prevent infection. The polymer was successfully used as a blood plasma expander during the Second World and Korean Wars [49]. Due to the shortage of both blood and plasma in the battlefield, the supplies were diluted with PVP to increase the available volume and increase the number of injured treated. Polyvinylpyrrolidone has been identified as an enhancer for dermal delivery due to its superior adhesive properties between the substrate and skin [44-48].

Polyvinylpyrrolidone was the main ingredient of the first successful hairspray, responsible for the beehive hairdos of the early 1950s [39]. The polymer's adhesive properties as well as solubility in water made it an ideal hairspray, but its affinity for water became a drawback, as it tended to adsorb moisture giving hair an unnatural appearance. Manufacturers overcame the hindrance by adding silicone to the mixture,

which formed an exterior film and prevented humidity from binding to the PVP. Currently the polymer can be found in many personal care products, such as shampoos, toothpaste and contact lens solutions [39]. Other commonplace uses of PVP are as a food additive, glue, old-style postage stamps and envelopes [49], as well as in coatings for photo-quality ink-jet papers, transparencies and inkjet printer inks.

### *Electrospinning*

Fiber synthesis techniques of wet, dry, melt and gel spinning are capable of producing polymer fibers with diameters down to the micrometer range. Electrospinning, also known as electrostatic spinning, is a process capable of producing polymer fibers with nanoscaled diameters [50]. The ultra fine solid fibers are notable for small diameters, large surface area to volume ratio, and small pore size [51]. The choice of polymer can effect fiber properties such as strength, weight, porosity and surface functionality [52]. A series of patents describing an experimental setup for the production of polymer threads using an electrostatic force were awarded to Anton Formhals between 1934 and 1944 [53]. To date more than a hundred synthetic and natural polymers have been electrospun into nanofibers [51]. The very large surface area to volume ratio, flexibility in surface functionalities, superior mechanical performance, and versatility of design are some of the characteristics that make the polymer nanofibers optimal candidates for biomedical applications, such as tissue engineering, wound dressing, drug delivery as well as a variety of others [54].



The cost efficient electrospinning technique provides the capacity to lace together a variety of polymers and particles to produce nonwoven nanocomposite membranes. The method so widely explored with polymer solutions has been translated into forming composites of soluble drugs, bacterial agents and inorganic compounds [55]. During the process a polymer solution or composite mixture is ejected out of the fine needle and into an electric field as high as 3 kV/cm. The build up of electrostatic charges on the surface of a liquid droplet overcomes its surface tension and induces the formation of a jet [56]. The likely charged jet expands via repulsion, and travels towards the oppositely charged or ground collector, where it deposits as a solid nonwoven nanofibrous matrix. Polyvinylpyrrolidone has become one of the most utilized polymers due to its compatibility with various composites [57].

### *Whooping Cough*

*Bordetella pertussis* is a gram negative bacterium named for Jules Bordet, who together with Octave Gengou was the first to isolate and identify the gram-negative microbe as the causative agent for whooping cough in 1906 [58]. First mention of the disease appeared in 15<sup>th</sup> century France, while the first epidemic was reported in 1578 [59]. The name pertussis comes from Latin for intensive cough, and accurately describes the presentation of this respiratory disease that can be particularly severe and potentially lethal in infants and non-immunized children [59-62]. The clinical features of the disease can be divided into three specific stages. The first, catarrhal, stage is similar to the common cold with a cough. Within two weeks the illness advances to the

paroxysmal stage, characterized by bursts of frequent coughs followed by a distinctive high-pitched whoop when the patient attempts to take a deep breath. Such episodes may occur repeatedly throughout this phase of the disease, with an average of 15 attacks per day. Infant patients may not possess the strength to have a whoop. Vomiting and exhaustion often follow the episodes. The paroxysmal stage may persist up to 10 weeks, and gradually decreases in frequency and intensity. The final stage of convalescence lasts approximately three weeks; however cough attacks may persist for months from the initial onset.

The virulence of the infection is instigated by the sophisticated medley of bacterial factors released in host, once the bacterium attaches to the ciliated epithelium [63-65]. Each of the proteins fulfills a specific function to damage the respiratory tract and evade the immune response of the host. The toxin identified to be essential for the pathogenicity of whooping cough is pertussis toxin (PT). PT has been employed as an effective antigen in acellular vaccines for whooping cough. Structured as an AB toxin PT is composed of five different subunits. The A promoter contains one subunit which deactivates heterotrimeric G-proteins with its ADP-ribosyltransferase activity, resulting in accumulation of cAMP disrupting signaling pathways [66]. One of the G-protein dependent effects of PT observed is inhibition of lymphocyte and neutrophil migration. The B oligomer is a pentamer structured as two dimers (S2-S3, S2-S4) held together via noncovalent bonds with the S5 subunit. Its chief role is to bind to sugar residues of target cells' plasma membranes to effectively release the A-promoter into the cytosol. The PT B-oligomer has been identified to have its own G-protein independent activities,

such as inducing dendritic cell maturation, contributing to the various pathological effects in host cells [67-69].

The currently employed acellular vaccine combines inactivated PT with diphtheria and tetanus toxoids [70-71]. The pediatric immunization used in infants, known as DTaP was first approved by the FDA in 1996 for administration at 2, 4 and 6 months of age with booster shots given at 18 months and at 4 to 6 years. Although the acellular vaccine confers lower protection than the previously employed whole cell vaccine it eliminates many of the unwanted side effects. Recently there has been a six-fold increase in the global incidence of pertussis, mostly in adolescents and adults [72-92]. The steady resurgence of reported cases of pertussis in adolescents and adults has been connected to the waning immunity from acellular childhood immunization as well as improved diagnostics and reporting. The newly licensed adolescent and adult formulation known as Tdap has been advised for administration in place of the traditional tetanus immunization to confer whooping cough immunity in older populations, who have been shown to be the carriers and infecting the unprotected infant population. The Advisory Committee on Immunization Practices has recommended that pregnant women receive the Tdap immunization, preferably in the third trimester to result in the highest antibody concentration in infants.

Both formulations are said to result in protection from pertussis by eliciting antibodies specific to PT, particularly to the A-promoter of the toxin. Recent reports of pertussis outbreaks in regions with high incidence of vaccination, such as Oregon, have pointed to apparent changes in pertussis epidemiology in the United States that justify development of a novel approach to whooping cough immunization that is capable of

conferring long-lived protection against the bacterium, without the logistical hindrances of the currently employed repeated booster immunization.

## **Hypotheses and Specific Aims**

Within the last decade various innovative immunization methods have been investigated. The integumentary system is not only highly accessible, but the skin's immunocompetence appears to allow for significantly lowered antigen doses to achieve an immune response comparable to that achieved by intramuscular injection, thus allowing protection of larger population sectors with lower amounts of precious vaccines. The cumbersome injection method required for subcutaneous or intramuscular administration of vaccine formulations has hampered the use of traditional vaccination protocols in pandemic situations, and has called for development of novel delivery systems.

The long-term goal of this project is to generate a novel antigen delivery platform that will aim to eradicate some of the stringent requirements posed by the use of traditional liquid formulations for immunizations. The typical inability of macromolecular antigens to penetrate into the skin will be overcome through the use of nanotechnology to reversibly encapsulate such antigens within a hygroscopic nanofibrous matrix with a large surface area to mass ratio. Beyond the application for developing a pertussis vaccine, this study has the potential to expand the field of intradermal immunization in a novel direction by promoting delivery of biologically relevant antigens, such as intact,

unmodified proteins, to achieve broader protection from antibodies geared to recognize pathogens in their native state.

***The global hypothesis guiding this project is that the nanofibrous antigen composite matrix offers a highly adaptable and versatile strategy for logistically feasible deployment of an intradermal immunization patch.***

#### **Specific Aim I**

*To optimize the electrospinning process parameters for synthesis of nanofibrous matrices with maximized reversible inclusion of macromolecule payloads.*

#### **Specific Aim II**

*To establish retention of antigen functionality and immunoreactivity, as well as long-term storage stability for a variety of antigens encapsulated within a nanofibrous matrix.*

#### **Specific Aim III**

*To establish the proposed delivery system's capacity to facilitate passage of an antigen into commercially available engineered human skin models.*

#### **Specific Aim IV**

*To evaluate the efficacy of the proposed whooping cough vaccine in vivo in the Sprague Dawley rat model of dermal delivery.*

## Chapter 2

### *Specific Aim 1*

## **Specific Aim I**

*To optimize the electrospinning process parameters for synthesis of nanofibrous matrices for maximized reversible inclusion of macromolecule payloads.*

## **INTRODUCTION**

Preservation of enzymes, produced from plants, animals or microorganisms has been a longtime focus of research due to their widespread use in molecular biology as well as industrial applications i.e. food, biofuels, paper and rubber industries [93]. The extensive employment of enzymes is motivated by their selective catalytic properties. The food enzyme market has been predicted to increase to \$2.3 billion dollars by 2018 [93]. Traditionally one of five immobilization methods would be applied to enhance storage and utilization of a given enzyme.

The simplest of the methods is adsorption, where the enzyme is allowed to physically attach to the substrate without the use of harsh chemical reagents, therefore not causing significant loss of catalytic function [94]. The lack of strong interactions between the enzyme and the carrier can result in enzyme leakage from the substrate. To aid in retention of the bound enzyme multiple modifications have been proposed. For example the immobilization method of covalent attachment, which limits leakage via the formation of covalent linkage between the enzyme and carrier. However, this method requires expensive substrates, such as agarose, and some loss of enzyme functionality has been reported due to misalignment of the enzymes on the carrier [93-95]. By contrast, the method of entrapment restricts leakage of enzyme molecules by

imposing a spatially tight lattice structure. This technique allows for a high rate of enzyme loading, however requires a highly controlled microenvironment. The lattice structure should not be too large to retain the enzyme nor too tight for free diffusion of enzymatic substrate and product. The fourth method for enzyme immobilization is that of encapsulation. The technique locks biological components within semipermeable membranes forming lysosomes. The physical enveloping restricts passage of large biomolecules, but allows for exchange of small enzymatic reaction components. This method allows for co-immobilization of any combination of components that benefit the given application. Some of the disadvantages seen with encapsulation are associated with the restricted diffusion of reactants as well as the stability of the encapsulating structure [95]. The final method of enzyme immobilization, cross-linking, relies on the use of physical or chemical methods to form links between the enzyme molecules. Cross-linking of the enzyme to itself results in a stable, complex 3D structure, which immobilizes the enzyme without the use of a supporting matrix. The harsh reagents required represent a significant limiting factor in employing the method, as they may partially denature or inactivate the enzyme through unintentional active site crosslinking. Although each of the traditional methods has been found useful for specific enzymes, each of the methods presents a set of drawbacks thus posing a need for a novel, cost effective and straightforward technique of enzyme immobilization that restricts the payloads denaturation and leaching.

The original idea of electrospinning dates back almost eighty years ago, the recognition of its potential to advance material properties has resulted in a rapid expansion of information within the last decade [50-53]. The principle behind this



technology involves the use of an electric field as high as 3000 V/cm to overcome the surface tension of a droplet formed at the tip of a needle, as illustrated in Fig2.1. The charged jet is accelerated toward a grounded or oppositely charged collector.

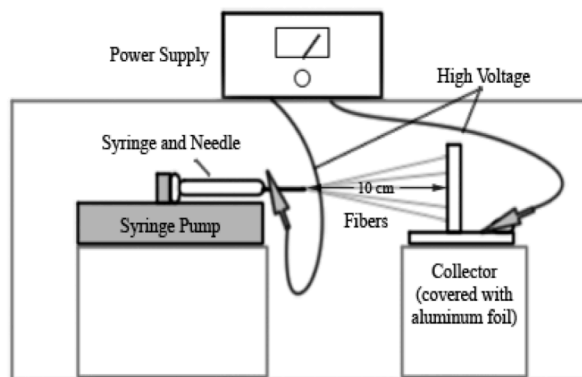


**Figure 2.1.** The electrospinning setup.

The process can be divided into three specific zones of initiation, thinning and solidification [96]. Once the jet reaches the collecting plate, it deposits as a non-woven matrix of polymeric fibers with fine diameters ranging from a few nanometers to micron scale, depending on the characteristics of the solution and process parameters employed [97, 98]. Fiber properties such as strength, weight, porosity, and surface functionality can be tailored, as they depend on the specific polymer incorporated into the vehicle. The greatest benefit of the electrospinning method has been its capacity to produce nanofibrous mats of high surface area to volume and mass ratios, characterized by continuous three-dimensional planes of surface reactivity and porosity, in a straightforward and inexpensive manner.

Horseradish Peroxidase (HRP; EC1.11.1.7), a 44,000 Dalton enzyme, comes from the *Cochlearia armoracia* root [99-100]. Its function is to catalyze the oxidation of substrates, such as the chromogenic 3,3',5,5' tetramethylbenzidine (TMB), with hydrogen peroxide to produce a colorimetric signal. The direct, sensitive reaction is widely utilized in commercially available enzyme linked immunosorbent assays (ELISA) and was one of the reasons we chose the enzyme as a representative macromolecule

to be encapsulated with the electrospinning process. Understanding the stability of HRP throughout the electrospinning process would allow for further expansion of the encapsulation method to other macromolecules, such as immunogens, that would lead to the development of a novel intracutaneous vaccine patch.

Maximum compatibility between the biologically relevant payload and the polymer vehicle solution may be obtained by using water-miscible solvents and salts. Employment of aqueous solvents and addition of salts to the electrospinning mix increases the solution's surface tension as well as its boiling point. The modifications result in lowered efficiency of the electric field to elongate the jet and present a hurdle toward formation of a uniform nanofibrous matrix. The high charge density of the jet results in acceleration towards the collector, resulting in insufficient flight time to allow for complete solvent evaporation [96]. This combination of factors has been known to cause the jet to collapse partially into droplets before the solvent completely evaporates, resulting in a "beads-on-a-string" morphology of the nanofibrous mat deposited on the target. The presence of beading is presumed to decrease the surface area reactivity of the matrix.

In this study we explored the process of electrospinning as a novel enzyme immobilization method. We optimized the solution and process parameters to obtain enzyme laden composite matrices characterized by high surface area to volume ratio as well as continuous 3D porosity of the nanofibrous mats. We also tested a novel modification of the electrospinning process, an ordinary pause to help and decrease the presence of beading in the obtained electrospun matrices.

## MATERIALS AND METHODS

### *Solutions*

Immuno Pure Horseradish Peroxidase (HRP) obtained as a salt-free lyophilized powder from [Pierce; Rockford, IL] was reconstituted in phosphate buffered saline (PBS) at a concentration of 0.598 units/ $\mu$ l.

The HRP standard curves were obtain through dilutions of the stock solution with PBS.

Polyvinylpyrrolidone (PVP) of M.W. 1,300,000 from Sigma-Aldrich [St. Louis, MO] was dissolved at 0.1mM, 0.075mM or 0.05mM concentrations in absolute ethanol, allowing for a variety of viscosities to maximize the inclusion of payload within the matrix.

The electrospinning solutions tested varied in percent volume of the polymer solution as presented in Table 2.1.

| <b>Payload Volume %</b> | POLYVINYL PYRROLIDONE (PVP) 1,300,000 MW |                |              |
|-------------------------|--|----------------|--------------|
| <b>20%</b>              | 80%<br>0.05mM                            | 80%<br>0.075mM | 80%<br>0.1mM |
| <b>25%</b>              | 75%<br>0.05mM                            | 75%<br>0.075mM | 75%<br>0.1mM |
| <b>30%</b>              | 70%<br>0.05mM                            | 70%<br>0.075mM | 70%<br>0.1mM |

**Table2.1.** Outline of the initial nine solution combinations tested.

All of the outlined solutions were constructed with various dilutions of HRP with PBS to obtain the final HRP concentration of 0.00208 units of enzyme per microliter of the mixture.

### *HRP/PVP Matrix*

The electrospinning solutions outlined above were magnetically stirred for five minutes before being placed into a 2cc glass syringe, Popper&Sons [New Hyde Park, NY], and placed into the programmable syringe pump [KD Scientific; Holliston, MA]. The HRP/PVP coating was generated by ejecting 300  $\mu$ l of the given electrospinning solution at a flow rate of 10  $\mu$ l/min into an electric field of 1.5 kV/cm with a 10 cm distance between the needle and the target.

The matrix was collected onto an 8x10 cm block covered with aluminum foil. Three mats were obtained for each of the nine solutions.

### *Bulk Solubilization and Release of Payloads*

The highly hygroscopic nanocomposite matrix containing HRP as the payload was employed to assess the dissolution of the polyvinylpyrrolidone matrix and release of the incorporated macromolecular payload. The aluminum foil containing the electrospun matrix was dissolved by a triple wash with 5 ml of PBS, collecting liquid into a reagent reservoir that was placed onto a gentle rocker to allow for mixing of the solutions, as seen in Figure 2.2. The time dependency of dissolution is evaluated by



**Figure 2.2.** Dissolution study set up.

collection of sequential 100  $\mu$ l wash at 0.5, 1, 1.5, 2, 2.5, 3, 4, 5, 6, 8 and 10 minutes, and analyzed for the HRP concentration present.

#### *Payload inclusion analysis*

The colorimetric HRP assay was carried out in 96-well microplates, where 10  $\mu$ l duplicates were mixed with 100  $\mu$ L stabilized TMB (3,3',5,5'-Tetramethylbenzidine) from Pierce [Rockford, IL] and recorded the kinetic reaction at 650 nm. The reaction was stopped after 30 minutes by addition of 100  $\mu$ l of 2.0 M sulfuric acid and endpoint values were obtained at 450 nm. A standard curve of known HRP concentrations was generated simultaneously to allow for accurate quantification of the HRP content in

unknown samples. The optical density measurements were obtained using the Versa Max Microplate Reader [Molecular Devices, Sunnyvale, CA].

### *Basal Media Solubilization of HRP/PVP Matrix*

The electrospun matrix for each of the nine HRP/PVP solutions outlined above was collected onto three 4x4mm silicon wafer [Silex, Boston, MA]. Each wafer was faced down onto the 0.4  $\mu\text{m}$  PCF Millicell® tissue sample holder [Millipore, Billerica, MA]. The device's polycarbonate filter bottom made basal contact with 500  $\mu\text{l}$  of the subjacent aqueous medium (PBS), and allowed for slower payload release.

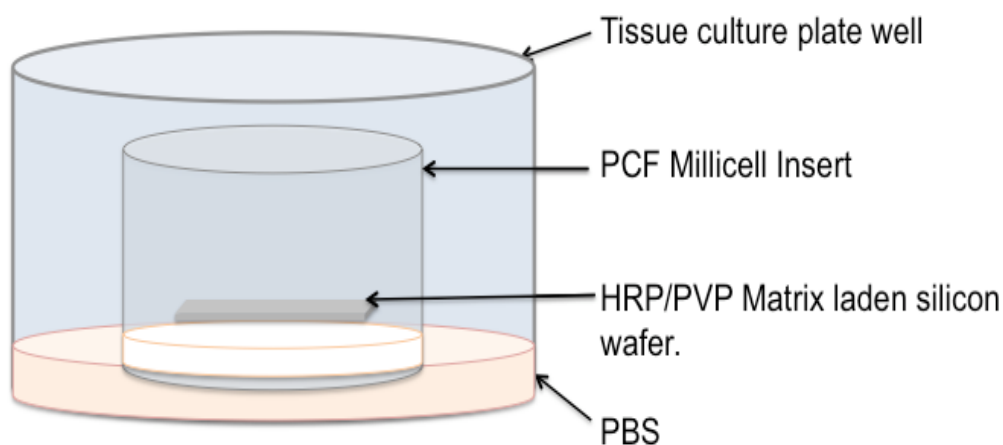


**Figure 2.3.** A schematic of the PCF Millicell setup utilized for the basal media HRP release experiment.

The tissue holder units were relocated to a fresh volume of 500  $\mu\text{l}$  of PBS at 5, 30, 60 and 120 minutes followed by a final wash of the wafer in the absence of the Millicell unit. The collected buffer was analyzed for functional HRP with the colorimetric assay explained above. Control wafers were dissolved in equal volumes to obtain the average deposition of HRP on the wafers.

### *SEM Analysis*

Polyvinylpyrrolidone (PVP) (Mw~1,300,000; Sigma Aldrich, St. Louis, MO) solutions were prepared in a mixture of 80% by volume ethanol and 20% of 0.1% bovine serum albumin (BSA) in phosphate buffered saline (PBS). The composition of the solutions aimed to imitate the surface tension, viscosity and ionic charge of the HRP/PVP mixtures examined. The three polymer concentrations used were 0.05, 0.075, and 0.10 mM.

| <b>Flow rates</b>                                 | <b>Voltage</b> | <b>Distance</b> | <b>Volume</b> | <b>Pause Intervals</b>                 |
|---|----------------|-----------------|---------------|--|
| 5 $\mu$ l/min<br>10 $\mu$ l/min<br>20 $\mu$ l/min | 15 kV          | 10 cm           | 250 $\mu$ l   | No pause<br>30 sec<br>45 sec<br>60 sec |

**Table2.2.** Outline of the electrospinning parameters tested.

The process was paused by stopping the fluid ejection and turning off the voltage supply. Each condition was run in multiples, and a representative area from each sample was examined with the scanning electron microscope (SEM).

### *Statistical Analysis*

All of the data used for statistical evaluations were checked for normality and equality of variance, using the Shapiro-Wilk and Levene's tests, followed by appropriate tests for the given experiment. All statistical tests were performed using SPSS software [IBM, Somers, NY] assuming a significance level of  $p < 0.05$ .

## RESULTS

### *Bulk Dissolution*

The release profiles for the nine enzyme-polymer mixtures were represented in concentrations of HRP as well as the percentage of the expected enzyme concentration.

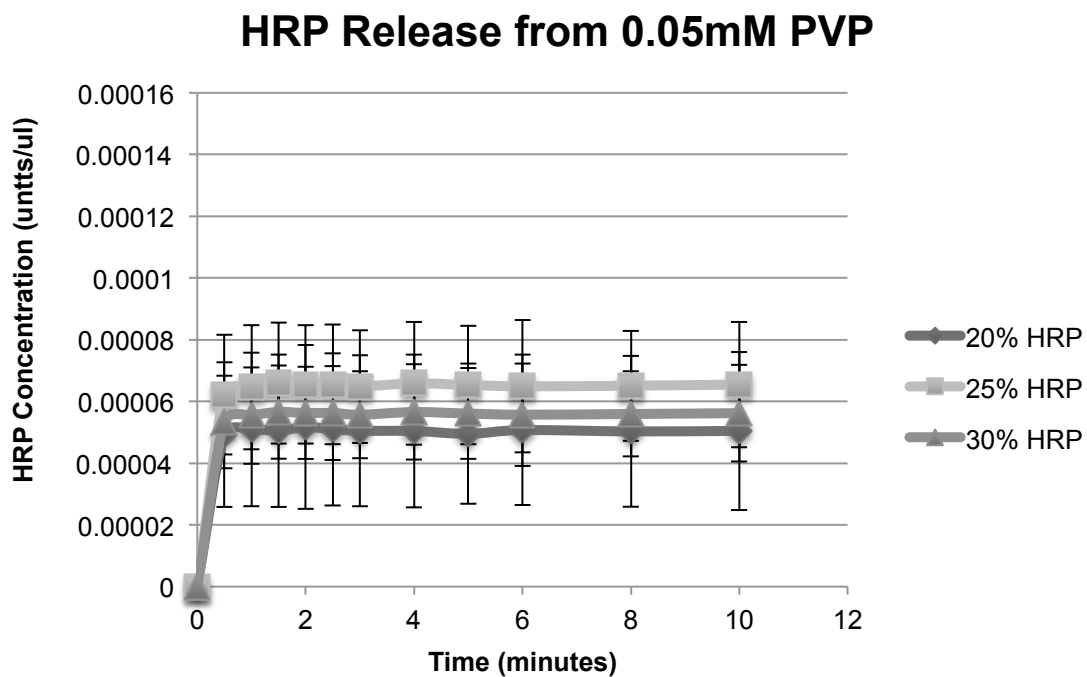


**Figure 2.4.** Release profiles observed for the HRP/PVP matrices prepared with a 0.05mM PVP; the error bars represent the standard deviation between the three matrices dissolved for each mixture.



### HRP Release from 0.075mM PVP

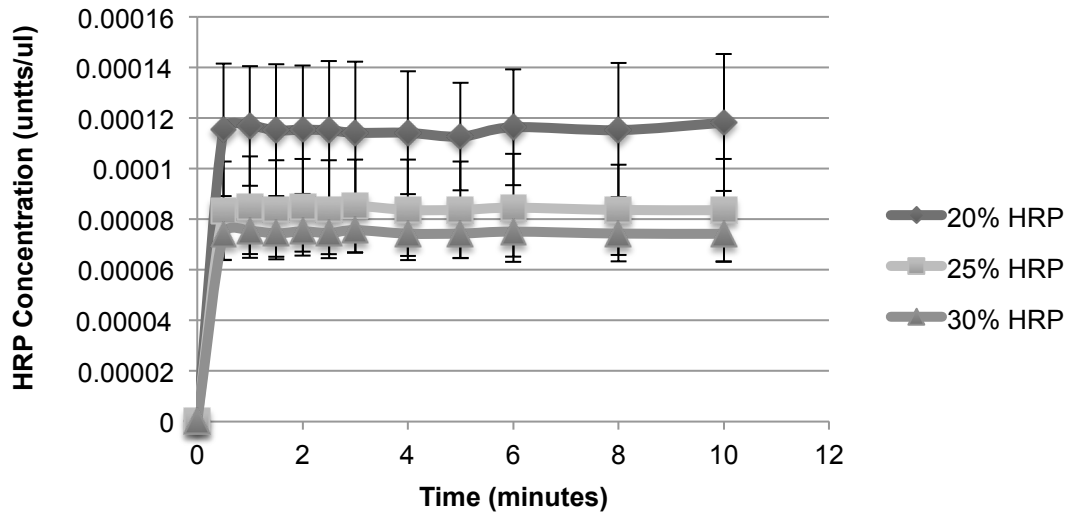


**Figure 2.5.** Release profiles observed for the HRP/PVP matrices prepared with a 0.075mM PVP; the error bars represent the standard deviation between the three matrices dissolved for each mixture.

### HRP Release from 0.10mM PVP

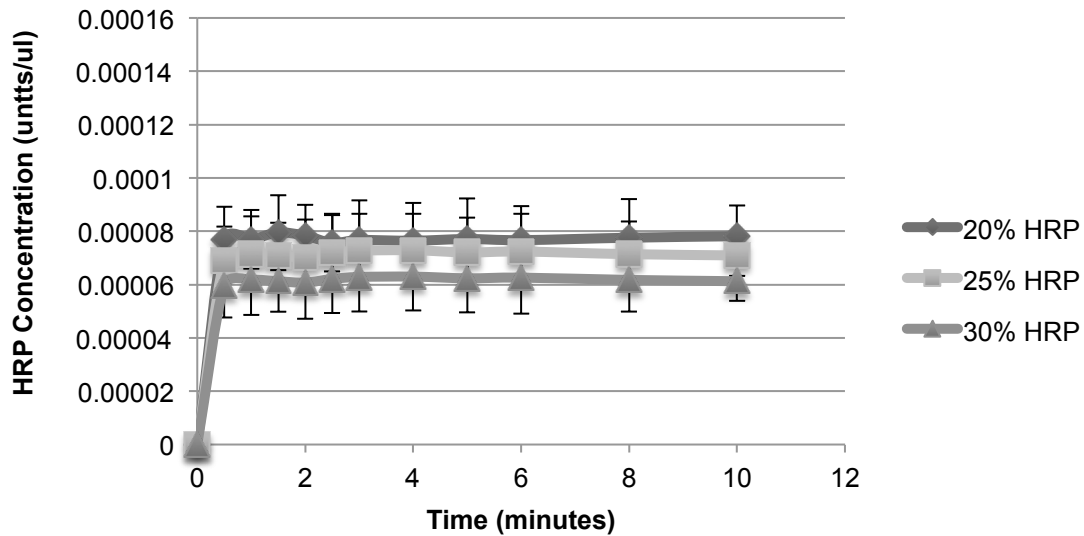


**Figure 2.6.** Release profiles observed for the HRP/PVP matrices prepared with a 0.075mM PVP; the error bars represent the standard deviation between the three matrices dissolved for each mixture.

The percentage of HRP deposition was calculated by relating the observed enzyme concentrations to that expected for all of the samples, 0.000125 units/ $\mu$ l.

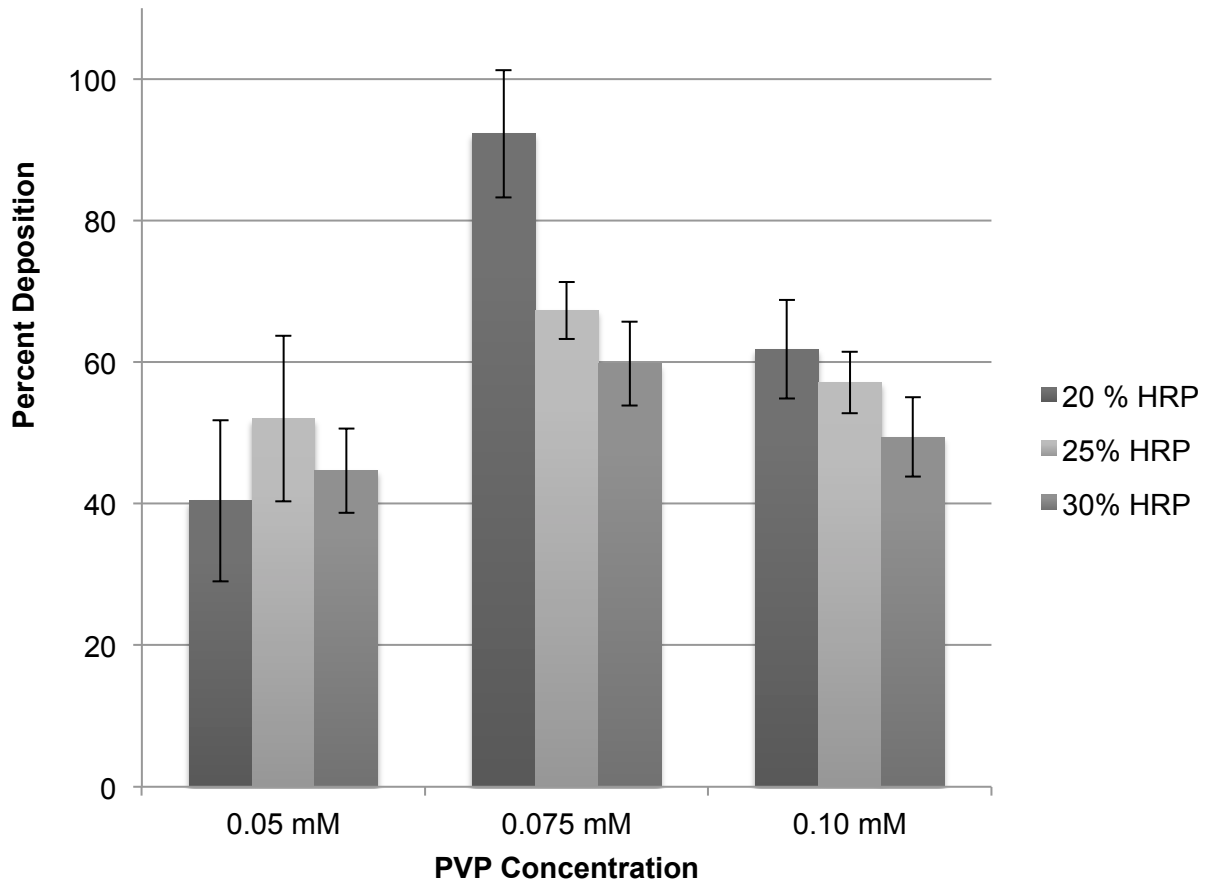


**Figure 2.7.** Comparison HRP deposition on the electrospinning collector determined from the bulk release study for nine combinations of enzyme to polymer; the error bars represent the standard error of the mean obtained for three different matrices dissolved for each mixture.

An overall comparison of the different PVP/HRP compositions showed that the deposition of HRP differed significantly between conditions ( $p=0.05$ ; Kruskal-Wallis test). The deposition (%) observed for the 20% HRP 0.075mM PVP mixture was significantly higher than that of the other compositions ( $p=0.05$ ; Mann-Whitney test) with the exception of the 25% HRP 0.075mM PVP mixture ( $p=0.13$ ).

Basal Media Solubilization of HRP/PVP Matrix

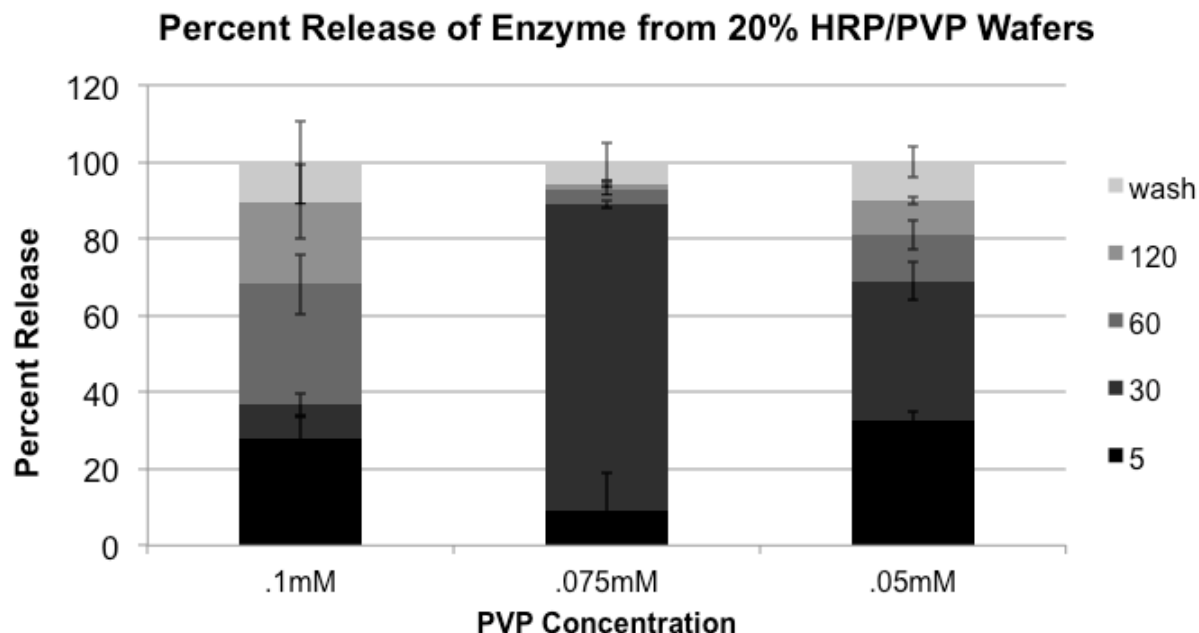


**Figure 2.8.** Comparison of HRP release from electrospun matrices in the PCF Millicell set up for three concentrations of polymer vehicle at 5, 30, 60, 120 minutes; the error bars represent the standard deviation between the three wafers dissolved for each mixture.

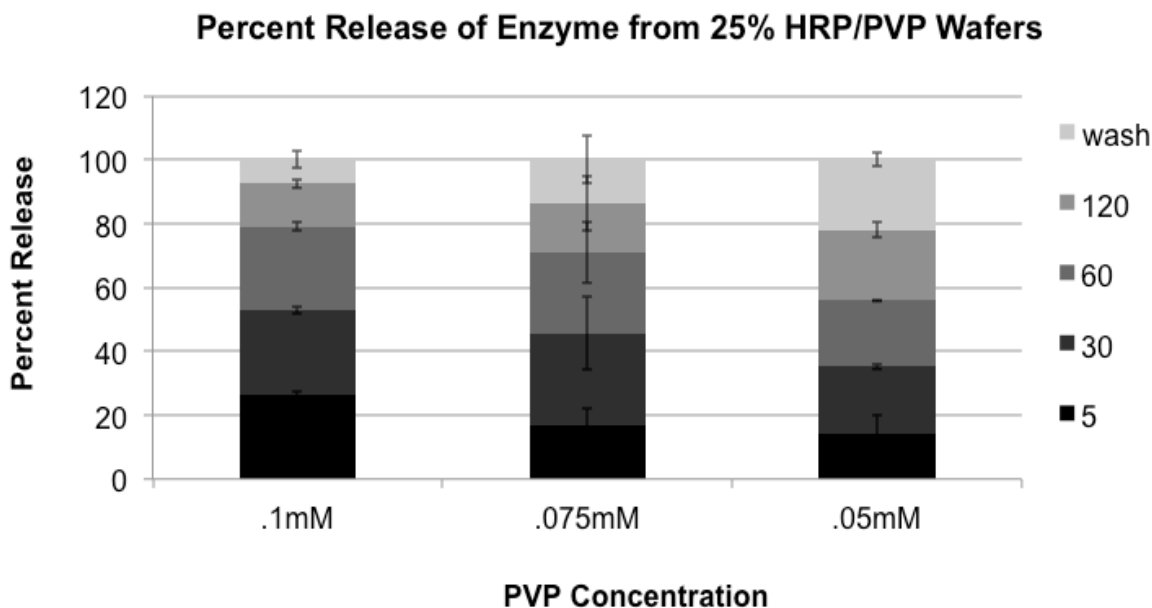


**Figure 2.9.** Comparison of HRP release from electrospun matrices in the PCF Millicell set up for three concentrations of polymer vehicle at 5, 30, 60, 120 minutes; the error

bars represent the standard deviation between the three wafers dissolved for each mixture.

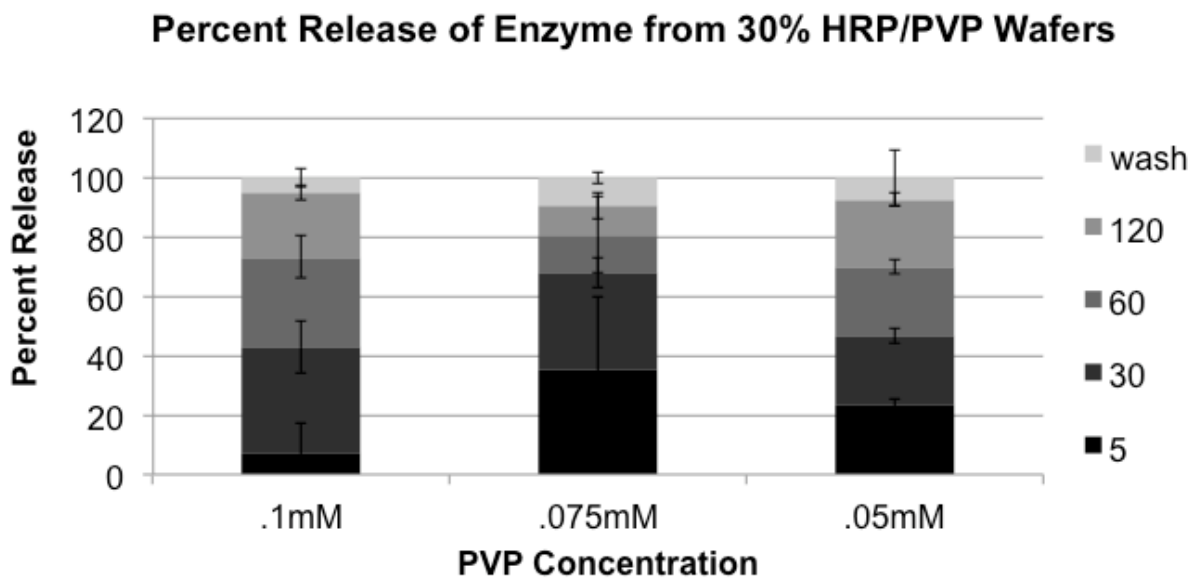


**Figure 2.10.** Comparison of HRP release from electrospun matrices in the PCF Millicell set up for three concentrations of polymer vehicle at 5, 30, 60, 120 minutes; the error bars represent the standard deviation between the three wafers dissolved for each mixture.

#### *SEM Analysis*

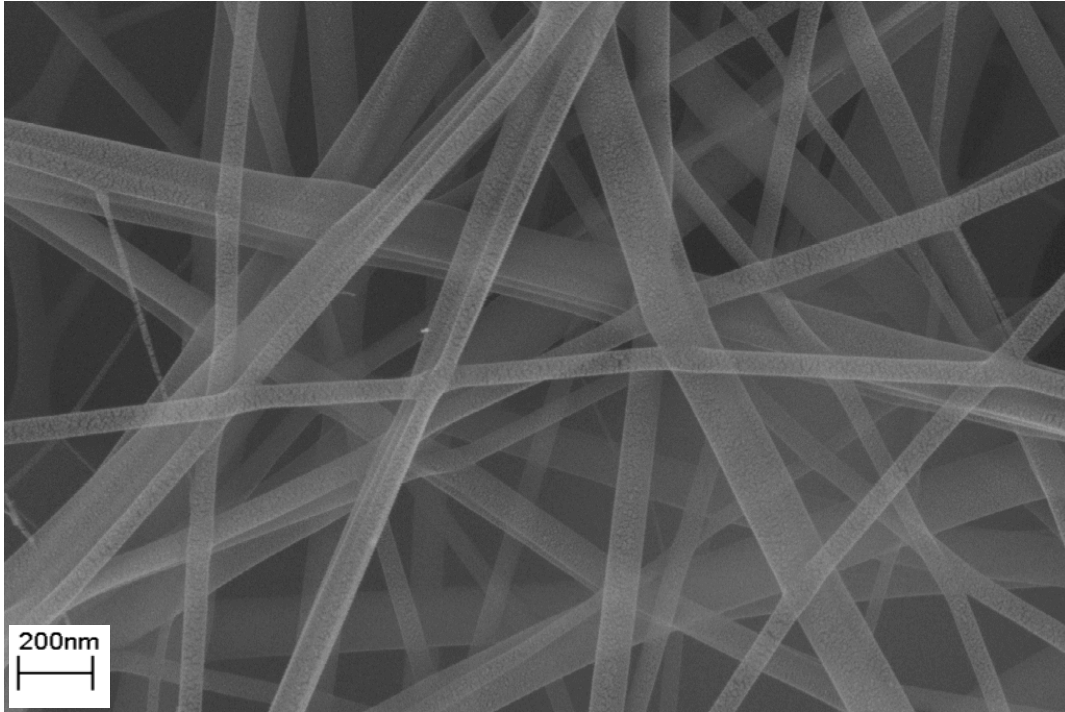


**Figure 2.11.** A representative SEM image of the 20% HRP – 80% 0.075mM PVP matrix.

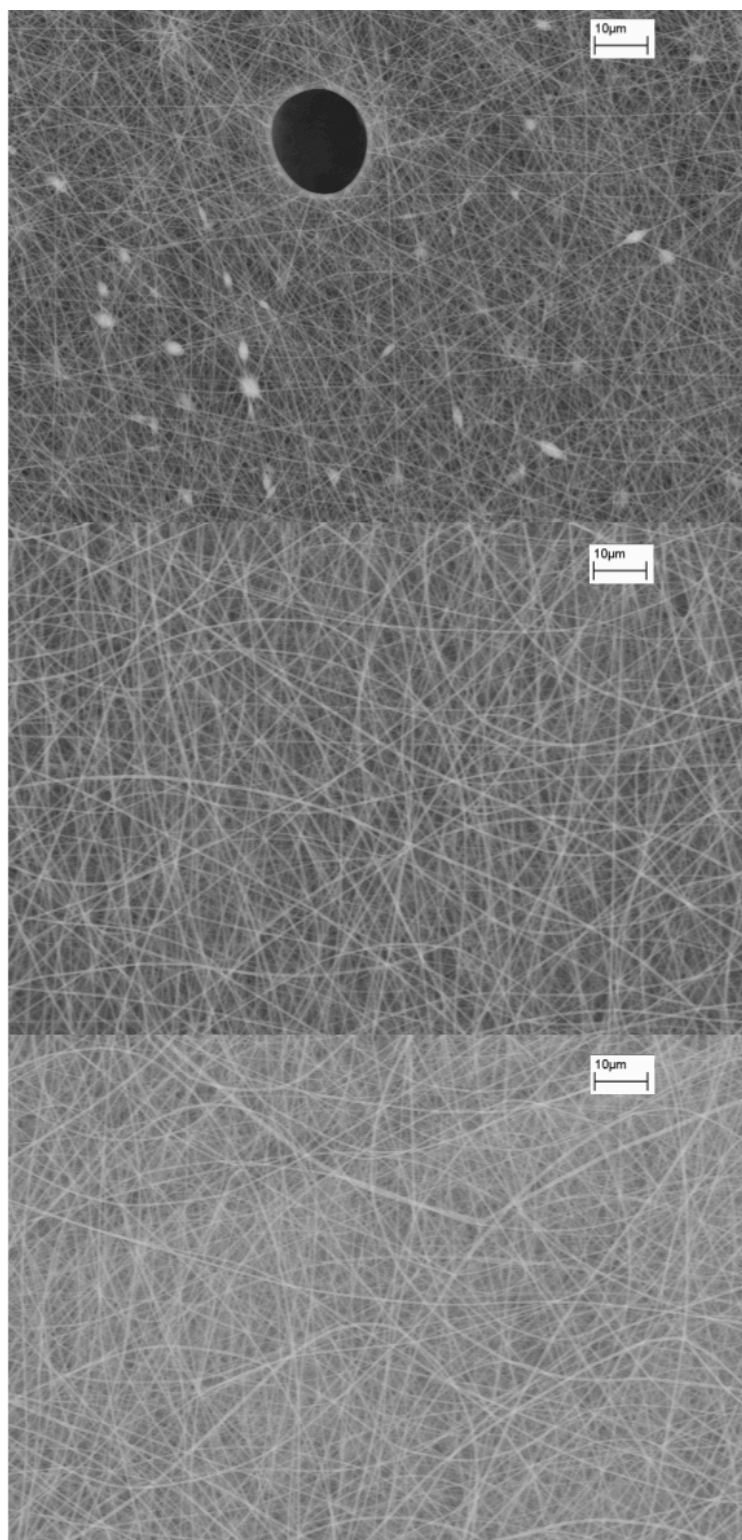


**Figure 2.12.** SEM images of 0.075 mM matrix electrospun at 10 $\mu$ l/min flow rate samples: no stopping, 30 second pause, 60 second pause (top to bottom).

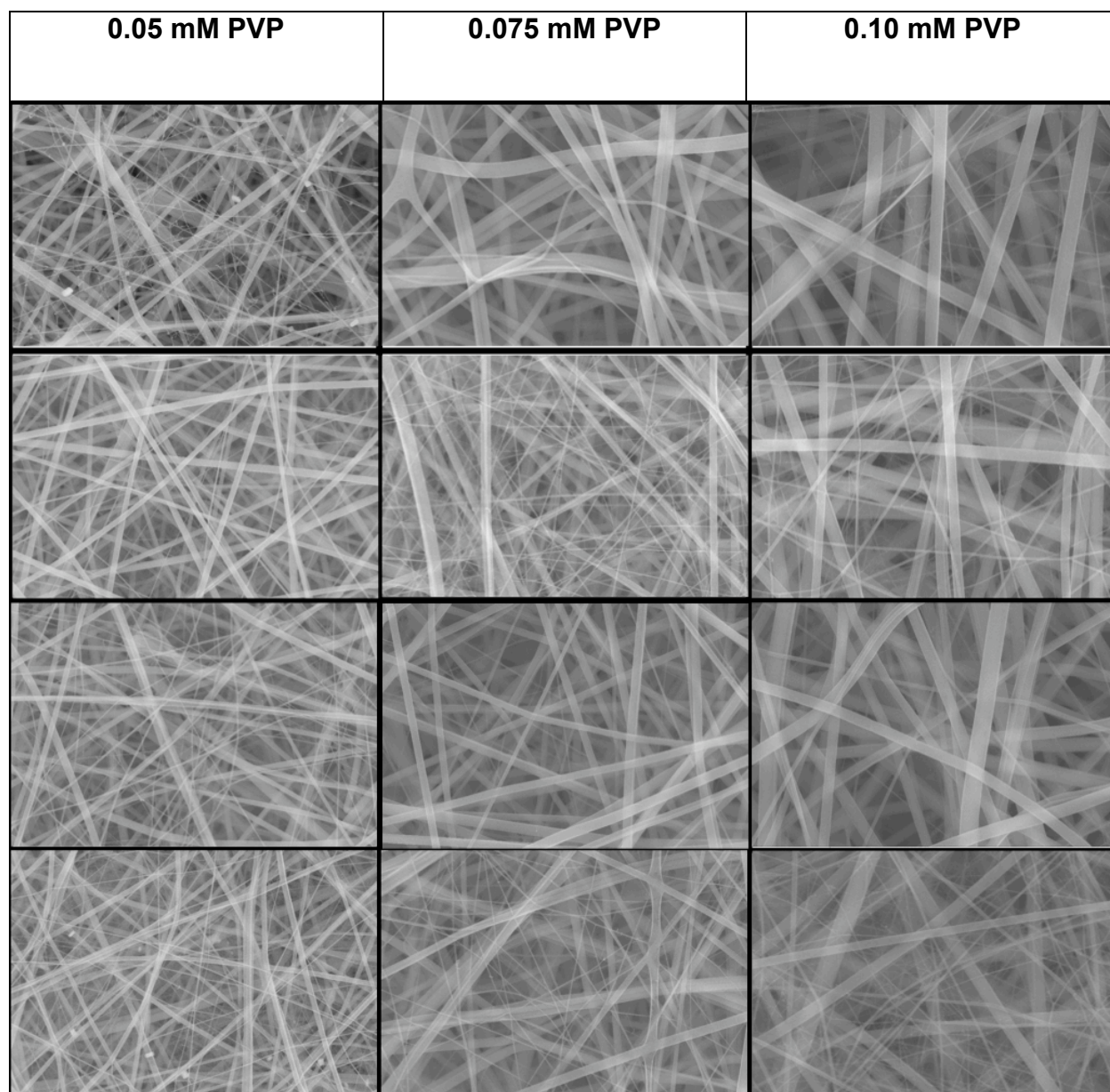


**Figure 2.13.** SEM images at a 30kX magnification of 10 $\mu$ l/min flow rate samples. The rows represent no stopping, 30 second pause, 45 second pause, 60 second pause (top to bottom).

## DISCUSSION

The goal of this study was to optimize the electrospinning process parameters for synthesis of nanofibrous matrices of a model macromolecule, horseradish peroxidase. By performing a bulk dissolution study we were able to illustrate the preservation of enzymatic activity of the enzyme throughout the process of electrospinning. The highly hydrophilic nature of PVP aided in the instantaneous release of HRP from the electrospun biocomposite matrix regardless of its composition within the first 30 seconds. The concentration of the extracted enzyme was evaluated as a percentage of the total amount of protein electrospun. We established the most favorable mixture for HRP stability to be 20% HRP – 80% 0.075 mM, with the highest percentage of functional HRP released from the matrix. The bolus release of HRP in the presence of a large volume, led to the development of a novel release study, that utilized a 0.4  $\mu\text{m}$  PCF Millicell® tissue sample holder to create a barrier between the electrospun coating and available moisture. The developed setup resulted in a steady release of the enzyme from the electrospun wafers during a 2 hour time period. The final aim of this study was to evaluate the matrix morphology through the use of SEM. We were able to successfully encapsulate HRP within matrices of PVP that presented an average diameter of 40nm, presenting with continuous 3D porosity and an advantageous surface area to volume ratio. Lastly we were able to validate the effect of brief pausing on the matrix morphology i.e. bead formation.

The successful incorporation of biological molecules into electrospun fibers without apparent loss of activity has been widely reported within the last decade [101-109]. It was therefore hypothesized that despite the harsh process of electrospinning,



HRP would maintain its catalytic function. Through the use of a colorimetric assay where HRP oxidizes a chromogenic substrate we were able to confirm preservation of as much as 92% of enzyme activity with the most advantageous combination of polymer to enzyme 20% HRP – 80% 0.075 mM, as seen in Figure 2.7. It appeared that the lowest polymer concentration, and therefore the least viscous of the mixtures resulted in the smallest percentage of deposition or function retention. The two terms are used interchangeably throughout the study, as it is not clear if the loss of enzyme is due to its denaturation or limited deposition on the electrospinning collector. The sizeable error bars depicted represent the variation between three mats of the same composition. The main source of deviation came from the third, consecutively electrospun mat for each of the nine conditions (data not presented). Analysis of enzymatic activity of the solution after the completion of three mats showed a dramatic drop in HRP activity. The loss of enzymatic activity is said to be a result of the prolonged exposure to the polymer solvent, absolute ethanol. The other possibility for this drop may be due to the exposure to room temperature for the duration of the experiment.

The bolus release of enzyme from the electrospun mats in the presence of 5 ml of PBS may not adequately showcase the surface solubility of the electrospun nanofibrous matrices when applied directly to the skin, as is expected to occur upon close contact with the SC. Therefore a novel approach to matrix dissolution, utilizing the 0.4  $\mu\text{m}$  PCF Millicell® tissue sample holders, presented an improved model for electrospun matrix dissolution. The polycarbonate filter of the unit posed a permeable barrier between the buffer and the nanofibrous matrix, which allowed for a controlled release of the enzyme, as depicted in Figures 2.8-10. The optimal combination of

HRP/PVP determined above to be 20% HRP – 80% 0.075mM PVP, exhibited the most robust excretion of the enzyme in the first 30 minutes, where the other compositions required double that time to achieve a similar amount of resolubilized enzyme. The control wafers dissolved in buffer determined that on average the electrospun matrix deposited approximately 0.18% of the total deposition on the 4x4 mm wafers, which occupy 0.2% of its total surface area.

One of the chief aims of this study was optimize the electrospinning technique to obtain maximized payload inclusion into random, nonwoven nanofibrous mats of the highly biocompatible polymer, polyvinylpyrrolidone (PVP). We found that the hygroscopic polymer's capacity to readily absorb moisture is further enhanced by the high surface area to volume and mass ratios observed for electrospun mats. Although the obtained biocomposite matrices confirmed the nanofibrous morphology, the large proportion of aqueous solvent for enzyme stability resulted in a large density of beading, thus limiting the surface area available for a given electrospun coating [56]. To address the morphological drawback, we proposed to introduce an interval pause to the process. The effect of process stoppage was examined through the employment of the optimal proportionality of the enzyme to polymer, where HRP was substituted for BSA. The introduction of the process pause was shown to result in a decrease of the average fiber diameter for a given polymer concentration, Figure 2.12. Another significant consequence of introducing a pause was the elimination of the beads-on-the-string morphology, Figure 2.13. At this point it is not fully understood why a brief break in the matrix production has an effect on the final morphology. It was hypothesized that the solvent vaporization during the jet flight from the tip of the needle towards the collector

may influence the local humidity that limits further liquid evaporation. By introducing the pause, we allowed the present humidity to fully evaporate or condense and deposit at the bottom of apparatus, away from the jet path. This simple alteration of the procedure was employed in all further experiments.

In summary the study successfully identified optimal solution and process parameters that effectively immobilize functional horseradish peroxidase within nanofibrous matrices of a generally regarded as safe synthetic polymer, PVP. Through the use of a bulk dissolution study we were able identify the 20% HRP – 80% 0.075 mM solution to result in as much as 92% of immobilized HRP to be after being dissolved from the matrix. The study offered a novel approach to release studies that better illustrate the TEWL transport dissolution of the matrix through the use of a 0.4  $\mu\text{m}$  PCF Millicell® tissue holder. SEM analysis of the collected matrices showed an average diameter of 40 nm for the HRP/PVP matrix. The high surface area to volume ratio as well as continuous 3D porosity of nanofibrous mats was shown to be preserved even in the presence of aqueous solvents via a simple process alteration, a 60 second pause every 10 minutes.

## Chapter 3

### *Specific Aim 2*

## **Specific Aim II**

*To establish retention of antigen functionality and immunoreactivity, as well as long-term storage stability for a variety of antigens encapsulated within a nanofibrous matrix.*

## **INTRODUCTION**

The manufacturing, storage and distribution of currently employed vaccines often pose stringent temperature requirements due to the inherent instability of biologically relevant payloads in aqueous solutions [110]. The added costs, as well as the previously stated roadblocks associated with existing technologies encourage the development of a novel immunization paradigm that would prove to be more cost effective as well as more suitable for use in pandemic situations. The versatility of the electrospinning process has been extensively utilized to lace together a variety of polymers and particles to produce nonwoven nanocomposite thin mats. Our group has previously reported the use of the technique to reversibly encapsulate enzymatically active urease [57]. The incorporation of biologically relevant antigens within such nanomatrices could result in superior surface attachment between the patch and skin, and therefore increase efficacy of antigen delivery [27].

Global resurgence of pertussis, whooping cough, raised questions of the current preventative and treatment technologies [70-92]. As a highly contagious disease caused by the fastidious gram-negative aerobic *coccobacillus Bordetella pertussis*, whooping cough is primarily considered a pediatric illness. Recent trends show a shift

in the pertussis epidemiology towards adolescents and adults, who can infect the most vulnerable population of neonates and infants. The most frequent misconception about the disease is that protection provided by childhood immunization is life long, whereas in fact adolescents become susceptible to whooping cough approximately 6 to 10 years after childhood vaccination. The aim of this study was to develop a novel non-invasive whooping cough vaccine by the immobilization of Pertussis Toxin in electrospun polymer (Polyvinylpyrrolidone, PVP) nanofibers. Pertussis toxin (PT) is a 117kDa multi-component protein comprised of six non-covalently bound subunits arranged in a pyramid-like structure. The largest of the subunits, known as the enzymatic A promoter, relies on the B oligomer, composed of the remaining 5 subunits, to enter most cells [63-69]. The active promoter has been shown to then inactivate target G proteins via its ADP-ribosyltransferase activity.

To verify the functionality of the protein immobilized within electrospun matrices we adapted the sensitive *in vitro* assay initially published in 1980s [111]. The qualitative analysis relied on the morphological change that Chinese hamster ovary (CHO) cells undergo in the presence of ng/ml concentrations of bioactive pertussis toxin [111-115]. The cellular assay was also utilized to establish the long-term storage profile for the antigen immobilized within electrospun matrices and compared it to that of dry-coated and liquid formulations of PT.

Aside from preservation of antigen functionality, a robust immunogenic payload must be able to generate, and be recognized by, antibodies produced to the intact protein, namely neutralizing antibodies. To examine the capacity of the electrospun nanocomposite membrane to successfully preserve antigenic immunoreactivity

throughout the harsh process we encapsulated the 15 amino acid H5-hemagglutinin (HA) peptide, recognized as a candidate immunogen against bird flu [116]. Within the last decade avian influenza was responsible for 206 deaths around the world with a mortality rate of 61% [117]. Although the viruses transmit readily within bird flocks, animal to human expansion requires virus mutations resulting in a moderately low number of reported cases to date, however an imminent threat of a possible pandemic exists. H5N1 has been identified as the most pathogenic strain of avian flu, and therefore has been the most studied in development of prospective vaccine strategies [116-121].

The long-term goal of this study aims to employ the electrospun matrix as a novel intradermal vaccine. In this chapter we evaluate the technology's ability to preserve antigen functionality and immunorecognition as well as the long-term storage observed for the immobilized immunogen. The versatility of the electrospinning method was established by forming composites containing three different antigens. We selected molecules that represent a variety of biological functions, sizes, solubility, and stability to showcase the adaptability of the proposed system. The model molecules chosen for this study were pertussis toxin (PT), hemagglutinin (HA), and protective antigen (PA), although only PT and HA data are presented in this chapter.

## **MATERIALS AND METHODS**

### *PT Functionality*

#### *Solutions*

50 µg of lyophilized, salt-free, 117 kDa Pertussis Toxin (PT) [List Biological Labs, Campbell, CA] was reconstituted in 0.80ml of sterile Hank's buffered saline (HBSS) resulting in a concentration of 62.5 ng/µl PT in HBSS.

The PT standards employed as positive controls for the cell culture assay were made with HBSS dilutions of stock PT to obtain a range of concentrations from 2-5 ng/ml PT in HBSS.

Polyvinylpyrrolidone (PVP) of M.W. 1,300,000 from Sigma-Aldrich was dissolved at 0.10 mM concentration in absolute ethanol.

The electrospinning solution consisted of 70% of the polymer solution by volume and 30% of the PT stock solution, to result in a final concentration of 18.75 ng/µl.

#### *PT/PVP Matrix*

The electrospinning solution consisting of 30% PT by volume was magnetically stirred for five minutes before being placed into a glass syringe, and placed into the programmable syringe pump. The PT/PVP coating was generated by ejecting 320 µl of the electrospinning solution at a flow rate of 10 µl/min into an electric field of 1.6 kV/cm with a 10 cm distance between the needle and the target. Based on the results



obtained with HRP, it was assumed that 50% of the total matrix, or 3 µg of PT, would deposit on the collector. The mat was cut into 4 pieces, each presumed to represent 750ng of PT, placed into a glass vial and dissolved in 5ml of HBSS then further diluted for the cellular assay.

### *Chinese Hamster Ovary (CHO) Cells*

Confluent CHO-K1 ATCC CCL-61 cells were trypsinized and plated in sterile 96-well flat bottomed cell culture plates at a concentration of  $2.7 \times 10^4$  cells/cm<sup>2</sup>, equivalent to 0.20 ml of  $3.78 \times 10^4$  cells/ml, except for the peripheral rows and columns with HBSS to avoid the edge effect previously observed for CHO cells cultured in 96-well plates. The cells were allowed to adhere over a 24-hour incubation period, at the end of which the original medium was replaced with triplicate 200 µl aliquots of the samples listed below:

- PT standards: 0.0, 2.0, 2.5, 3.0, 3.5, 4, 4.5, 5 ng/ml in HBSS.
- PT/PVP Solution diluted to concentrations of 0.0, 2.0, 2.5, 3.0, 3.5, 4, 4.5, 5 ng/ml in HBSS.
- Dissolved PT/PVP Matrix diluted to concentrations of 0.0, 2.0, 2.5, 3.0, 3.5, 4, 4.5, 5 ng/ml in HBSS.
- Dissolved PVP Matrix diluted to represent equivocal amounts of polymer as the dissolved PT/PVP Matrix samples.

The plates were examined for the characteristic CHO cell clumping in the presence of functional PT at 24-hour intervals for a 72-hour time period. The

microscopic observations were recorded using a qualitative grading range from 0 to 2, where a grade of zero indicated no observable clumping.

### *Storage Stability*

The above outlined solutions were utilized to generate three formulations of PT that were evaluated in the storage stability study:

- PT Solution samples consisted of 20  $\mu\text{l}$  of the 0.75 ng/ $\mu\text{l}$  stock PT solution diluted with HBSS, stored in small glass vials.
- Dry Coated PT/PVP wafers were constructed by depositing 10  $\mu\text{l}$  of the electrospinning solution that was previously diluted down to a concentration of 0.75 ng/ $\mu\text{l}$  PT with HBSS onto a silicon wafer and let to air dry, thus consisting of 7.5 ng of PT per wafer.
- PT/PVP Matrix was deposited onto 4x4mm silicon wafers such that each wafer contained 7.5 ng PT.

All of the samples were diluted in 500  $\mu\text{l}$  of CHO media, to represent equivocal concentrations two dry coated and matrix wafers were dissolved. 200  $\mu\text{l}$  duplicates of each mixture were dosed onto CHO cells. At each time point two samples were tested for each condition. The CHO media consisted of RPMI 1640 with 2.05 mM L-Glutamine, 5% Fetal Bovine Serum and 1% Penicillin/Streptomycin.

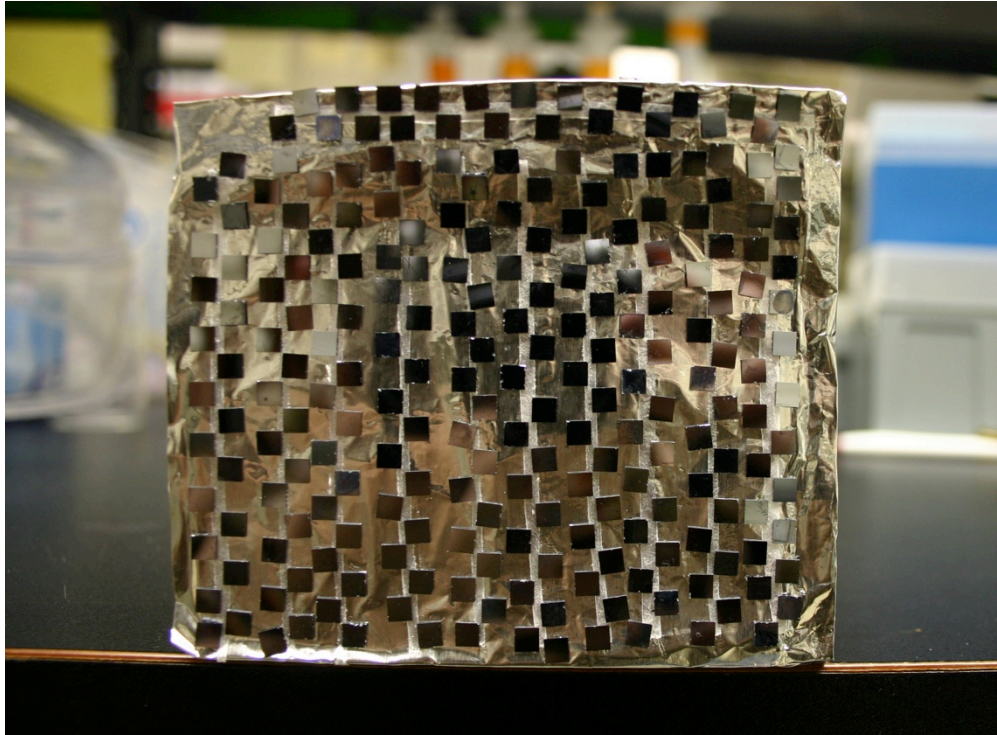


**Figure 3.1.** The electrospinning collector covered with 4x4 mm silicon wafers prior to electrospinning.

Equal numbers of wafers and solutions for each method were divided among and stored at the following conditions:

1. Ambient- The wafers and solutions were stored in contact with air at room temperature and ambient humidity.
2. Ambient Desiccant- The wafers and solutions were stored in room temperature and in an environment where the humidity was controlled using water absorbent materials.
3. Ambient Vacuum- The wafers were stored inside a vacuum at room temperature.
4. Ambient Refrigerated- The wafers and solutions were stored at 4 °C and in contact with air at ambient humidity.

5. Desiccant Refrigerated- The wafers and solutions were stored at 4 °C and in an environment where the humidity was controlled using water absorbent materials.

Samples were solubilized and evaluated for antigen activity at day 0, weeks 1, 2, 4, 8, 12, 15 and 20 weeks through the previously outlined CHO cell assay. Each microplate consisted of freshly prepared PT standards ranging in concentration from 2 to 30 ng/ml.

The positive control for loss of activity was a PT solution denatured through a boiling of the native protein.

### *Immunorecognition*

The 15 amino acid peptide derived from the N-terminal domain of the H5-heammaglutinin (HA) [Meridian Life Science, Inc., Saco, ME], represents a small (~2kDa) antigenic domain on the avian influenza virus. It was reconstituted in 0.1% BSA PBS at a concentrations of 200 ng/μl.

The electrospinning solution consisted of 30% by volume of the stock HA solution and 70% by volume of 0.05mM PVP dissolved in a mixture of 2.5 mL of 0.1% BSA PBS and 7.5 mL of ethanol.

Previous studies exposed that approximately 80% of the electrospun volume deposits on the collecting surface consisting of a 10 cm x 12 cm aluminum foil to which 4 mm x 4 mm silicon wafers were adhered. To quantify deposition of the samples, they

were dissolved in 0.1% BSA PBS to match the standards. The silicon wafers were placed into a 24-well plate and covered by 500 µl of 0.1% BSA PBS per well followed by 1 hour incubation to ensure complete dissolution of the coating. The foil sample was dissolved in a reagent reservoir containing 32.0 ml of 0.1% BSA PBS.

### *Immunoreactivity Assay*

The assay employed the Bio-Dot SF Microfiltration [Bio-Rad Laboratories, Los Angeles, CA] apparatus by modifying the standard protocol. The modifications included the use of a 0.2µm nitrocellulose membrane as the capture membrane, and 5.0 mg of non fat dry milk in 100.0 ml of TTBS was utilized for one hour as the blocking wash.

| <b>PRIMARY ANTIBODY<br/>[Overnight Incubation]</b>           |                                 | <b>SECONDARY ANTIBODY (HRP-conjugated)<br/>[4 hour Incubation]</b> |                                  |
|--|---------------------------------|--|----------------------------------|
| Rabbit anti-HA<br>(Meridian Life Science, Inc.,<br>Saco, ME) | 1.0 mg/ml<br>1:2,500<br>25.0 ml | Goat anti-Rabbit<br>(Jackson Immunoresearch,<br>West Grove, PA)    | 0.8 mg/ml<br>1:80,000<br>80.0 ml |

Table 3.1. Outline of the antibodies utilized for the HA immunorecognition experiment.

The stock HA solution was diluted down to standard concentrations using 0.1% BSA PBS. The primary rabbit polyclonal antibody to HA (Meridian Life Science, Inc., Saco, ME) was diluted down to a concentration of 0.4 µg/ml utilized was and used for an overnight. The secondary horseradish peroxidase (HRP) conjugated goat anti-rabbit IgG was diluted down to a 0.01 µg/ml concentration and the membrane incubated with the membrane for 4 hours. The SuperSignal West Pico Chemiluminescent (Pierce

Biotechnology) was utilized to obtain signal that was transferred to the Clear Blue X-Ray Film (Pierce Biotechnology) that was in turn analyzed using the ImageJ software.

### *Statistical Analysis*

The qualitative nature of the data collected in this chapter did not allow for statistical analysis.

## RESULTS

### *PT Functionality*

The assessment of CHO cell morphological changes was recorded for each of the samples, and tabulated below. The following designation was utilized to represent the samples: ES = Electrospun, SOL = Solution, STD = Standard, UTC = Untreated Control. The previously explained rating system was employed to assess for the presence of functional PT.

#### *24 Hour Observation*

| <b>2.4 x 10<sup>4</sup><br/>cells/cm<sup>2</sup></b> | <b>PVP (ES) /<br/>HBSS</b> |          |          | <b>PT (STD) /<br/>HBSS</b> |          |          | <b>PT-PVP (SOL) /<br/>HBSS</b> |          |          | <b>PT-PVP (ES) /<br/>HBSS</b> |           |           |
|--|----------------------------|----------|----------|----------------------------|----------|----------|--------------------------------|----------|----------|-------------------------------|-----------|-----------|
|  | <b>1</b>                   | <b>2</b> | <b>3</b> | <b>4</b>                   | <b>5</b> | <b>6</b> | <b>7</b>                       | <b>8</b> | <b>9</b> | <b>10</b>                     | <b>11</b> | <b>12</b> |
| <b>5.0 ng/mL</b>                                     | 0                          | 0        | 0        | 0                          | 0        | 0        | 0                              | 0        | 0        | 0                             | 0         | 0         |
| <b>4.5 ng/mL</b>                                     | 0                          | 0        | 0        | 0                          | 0        | 0        | 0                              | 0        | 0        | 0                             | 0         | 0         |
| <b>4.0 ng/mL</b>                                     | 0                          | 0        | 0        | 0                          | 0        | 0        | 0                              | 0        | 0        | 0                             | 0         | 0         |
| <b>3.5 ng/mL</b>                                     | 0                          | 0        | 0        | 0                          | 0        | 0        | 0                              | 0        | 0        | 0                             | 0         | 0         |
| <b>3.0 ng/mL</b>                                     | 0                          | 0        | 0        | 0                          | 0        | 0        | 0                              | 0        | 0        | 0                             | 0         | 0         |
| <b>2.5 ng/mL</b>                                     | 0                          | 0        | 0        | 0                          | 0        | 0        | 0                              | 0        | 0        | 0                             | 0         | 0         |
| <b>2.0 ng/mL</b>                                     | 0                          | 0        | 0        | 0                          | 0        | 0        | 0                              | 0        | 0        | 0                             | 0         | 0         |
| <b>UTC</b>   | 0                          | 0        | 0        | 0                          | 0        | 0        | 0                              | 0        | 0        | 0                             | 0         | 0         |

**Table 3.2.** CHO cells at 24 hour observation and concentration 2.4 x 10<sup>4</sup> cells/cm<sup>2</sup>.

*48 Hour Observation*

| <b>2.4 x 10<sup>4</sup><br/>cells/cm<sup>2</sup></b> | <b>PVP (ES) /<br/>HBSS</b> |          |          | <b>PT (STD) /<br/>HBSS</b> |          |          | <b>PT-PVP (SOL) /<br/>HBSS</b> |          |          | <b>PT-PVP (ES) /<br/>HBSS</b> |           |           |
|--|----------------------------|----------|----------|----------------------------|----------|----------|--------------------------------|----------|----------|-------------------------------|-----------|-----------|
|  | <b>1</b>                   | <b>2</b> | <b>3</b> | <b>4</b>                   | <b>5</b> | <b>6</b> | <b>7</b>                       | <b>8</b> | <b>9</b> | <b>10</b>                     | <b>11</b> | <b>12</b> |
| <b>5.0 ng/mL</b>                                     | 0                          | 0        | 0        | 1                          | 1        | 1        | 1                              | 1        | 1        | 2                             | 2         | 2         |
| <b>4.5 ng/mL</b>                                     | 0                          | 0        | 0        | 1                          | 1        | 1        | 1                              | 1        | 1        | 2                             | 2         | 2         |
| <b>4.0 ng/mL</b>                                     | 0                          | 0        | 0        | 1                          | 1        | 1        | 1                              | 1        | 1        | 2                             | 2         | 2         |
| <b>3.5 ng/mL</b>                                     | 0                          | 0        | 0        | 1                          | 1        | 1        | 1                              | 1        | 1        | 2                             | 2         | 2         |
| <b>3.0 ng/mL</b>                                     | 0                          | 0        | 0        | 1                          | 1        | 1        | 1                              | 1        | 1        | 2                             | 2         | 2         |
| <b>2.5 ng/mL</b>                                     | 0                          | 0        | 0        | 1                          | 1        | 1        | 1                              | 1        | 1        | 2                             | 2         | 2         |
| <b>2.0 ng/mL</b>                                     | 0                          | 0        | 0        | 0                          | 0        | 0        | 0                              | 0        | 0        | 0                             | 0         | 0         |
| <b>UTC</b>   | 0                          | 0        | 0        | 0                          | 0        | 0        | 0                              | 0        | 0        | 0                             | 0         | 0         |

**Table 3.3.** CHO cells at 48 hour observation and concentration 2.4 x 10<sup>4</sup> cells/cm<sup>2</sup>.

*72 Hour Observation*

| <b>2.4 x 10<sup>4</sup><br/>cells/cm<sup>2</sup></b> | <b>PVP (ES) /<br/>HBSS</b> |          |          | <b>PT (STD) /<br/>HBSS</b> |          |          | <b>PT-PVP (SOL) /<br/>HBSS</b> |          |          | <b>PT-PVP (ES) /<br/>HBSS</b> |           |           |
|--|----------------------------|----------|----------|----------------------------|----------|----------|--------------------------------|----------|----------|-------------------------------|-----------|-----------|
|  | <b>1</b>                   | <b>2</b> | <b>3</b> | <b>4</b>                   | <b>5</b> | <b>6</b> | <b>7</b>                       | <b>8</b> | <b>9</b> | <b>10</b>                     | <b>11</b> | <b>12</b> |
| <b>5.0 ng/mL</b>                                     | 0                          | 0        | 0        | 1                          | 1        | 1        | 1                              | 1        | 1        | 1                             | 1         | 1         |
| <b>4.5 ng/mL</b>                                     | 0                          | 0        | 0        | 1                          | 1        | 1        | 1                              | 1        | 1        | 1                             | 1         | 1         |
| <b>4.0 ng/mL</b>                                     | 0                          | 0        | 0        | 1                          | 1        | 1        | 1                              | 1        | 1        | 1                             | 1         | 1         |
| <b>3.5 ng/mL</b>                                     | 0                          | 0        | 0        | 1                          | 1        | 1        | 1                              | 1        | 1        | 1                             | 1         | 1         |
| <b>3.0 ng/mL</b>                                     | 0                          | 0        | 0        | 1                          | 1        | 1        | 1                              | 1        | 1        | 1                             | 1         | 1         |
| <b>2.5 ng/mL</b>                                     | 0                          | 0        | 0        | 1                          | 1        | 1        | 1                              | 1        | 1        | 1                             | 1         | 1         |
| <b>2.0 ng/mL</b>                                     | 0                          | 0        | 0        | 0                          | 0        | 0        | 0                              | 0        | 0        | 0                             | 0         | 0         |
| <b>UTC</b>   | 0                          | 0        | 0        | 0                          | 0        | 0        | 0                              | 0        | 0        | 0                             | 0         | 0         |

**Table 3.4.** CHO cells at 72 hour observation and concentration 2.4 x 10<sup>4</sup> cells/cm<sup>2</sup>.



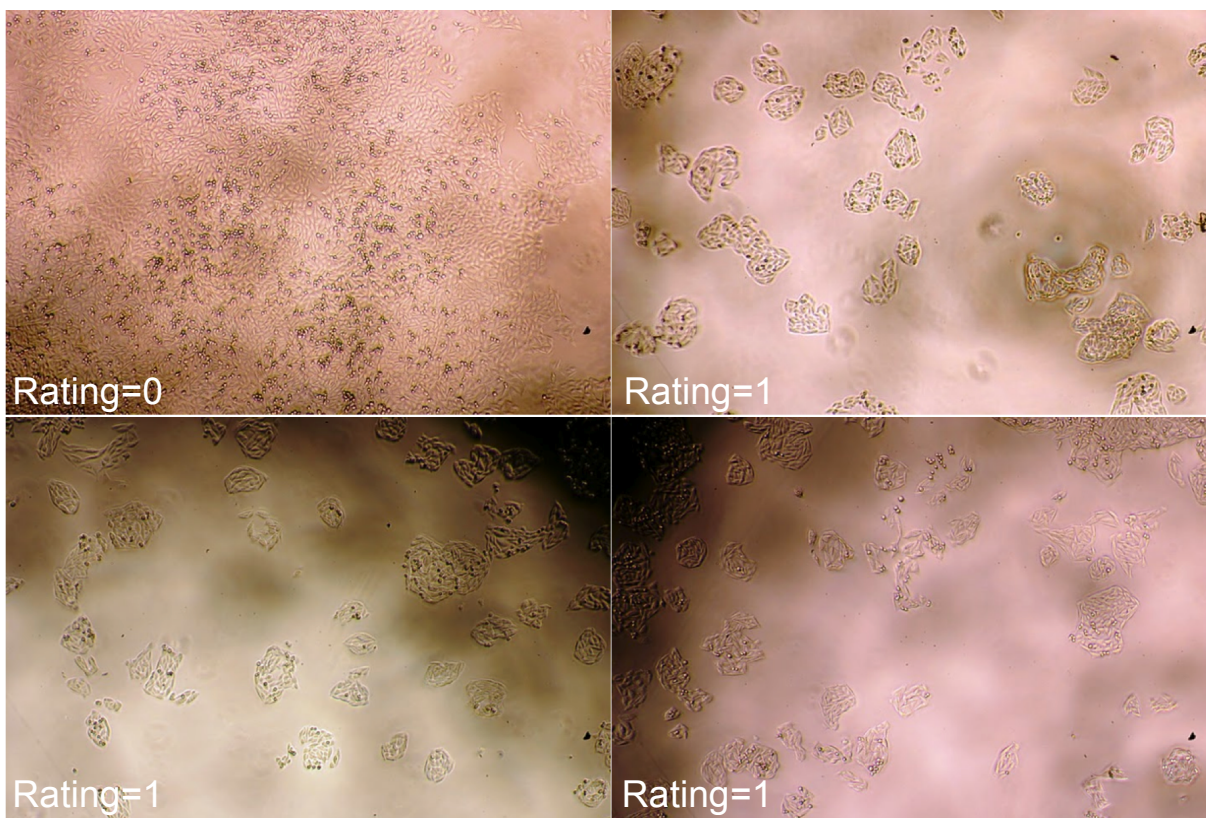


**Figure 3.5.** The CHO cell assay 72 hours after dosing; top row left from right, untreated control, PT solution standard; bottom row left from right, PT/PVP electrospinning solution, and PT/PVP Matrix.

### *Storage Stability*

The long-term stability of PT was assessed for PT solution, dry coated PT wafers, and electrospun PT/PVP matrix. To simplify the presentation of the data, we employed a rating of zero for samples that presented no clustering of CHO cells and a rating of 1, for those samples that exhibited the presence of the specific morphological changes expected in the presence of functional PT.

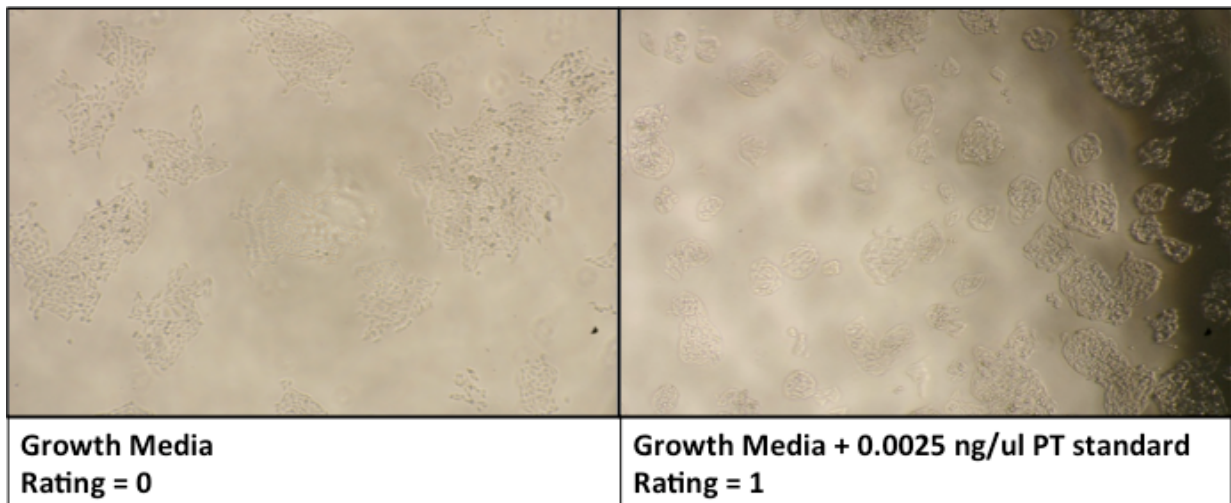


**Figure 3.6.** The CHO cell assay rating scale employed 48 hours after dosing.

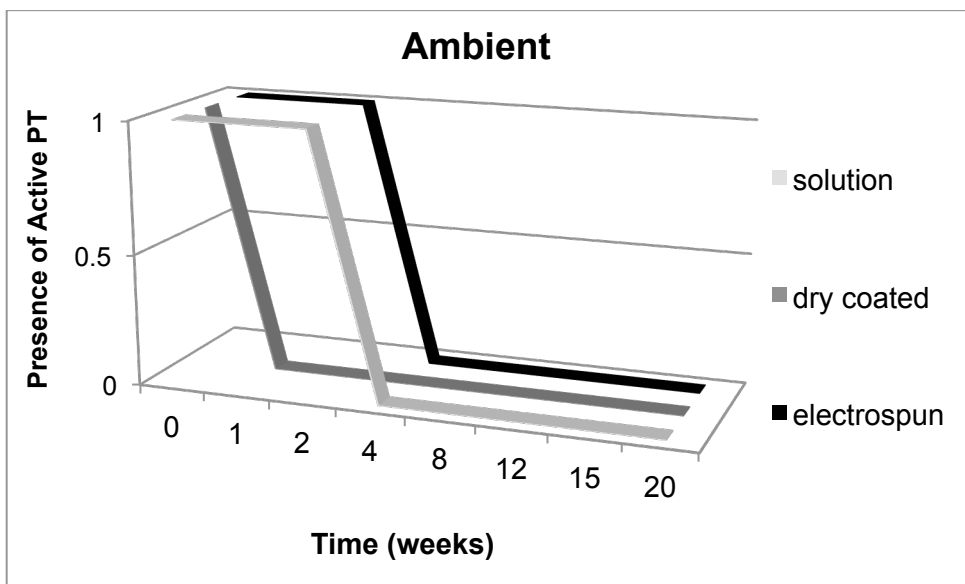


**Figure 3.7.** The 20 week storage stability of samples stored in ambient conditions.

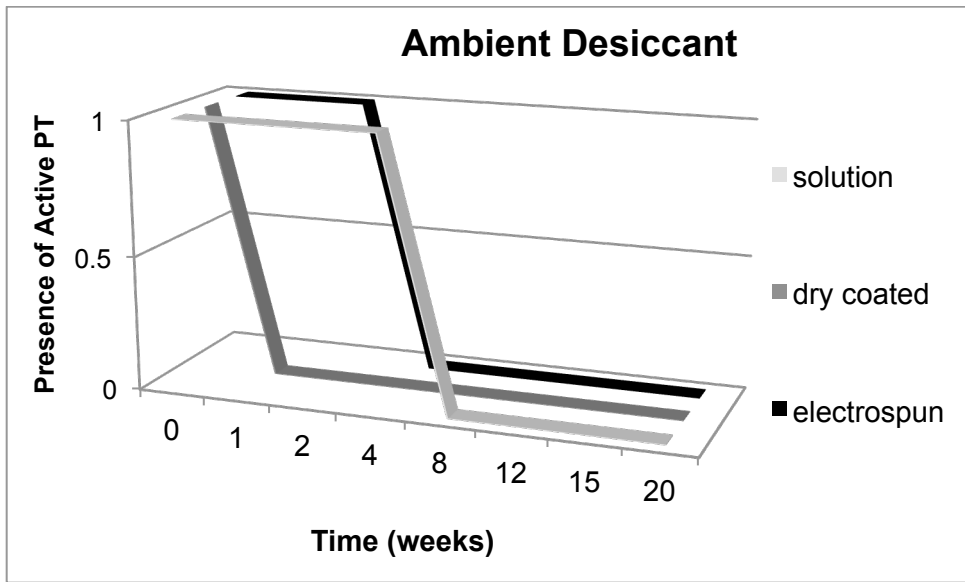


**Figure 3.8.** The 20 week storage stability of samples stored in ambient conditions in the presence of desiccant.

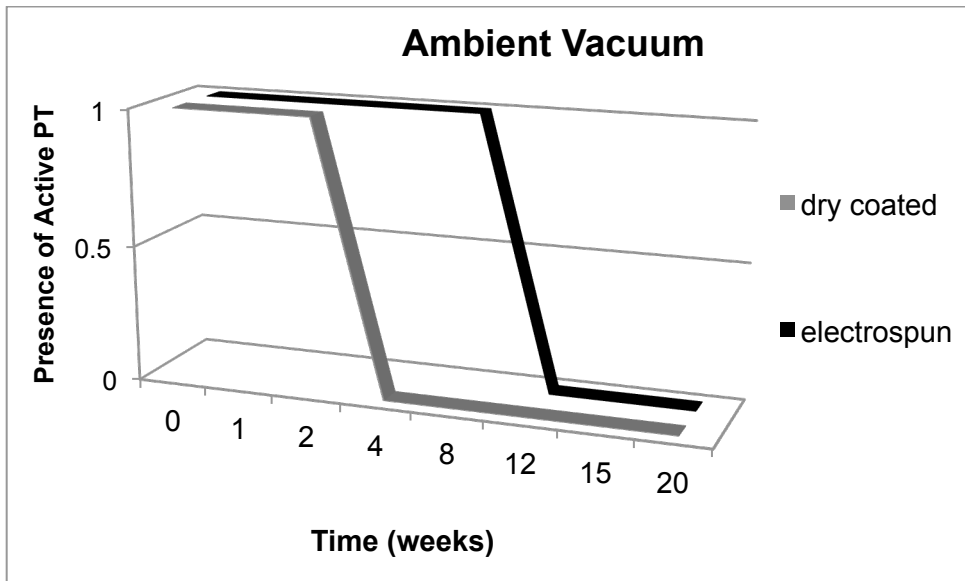


**Figure 3.9.** The 20 week storage stability of samples stored in ambient conditions in a vacuum sealed container.

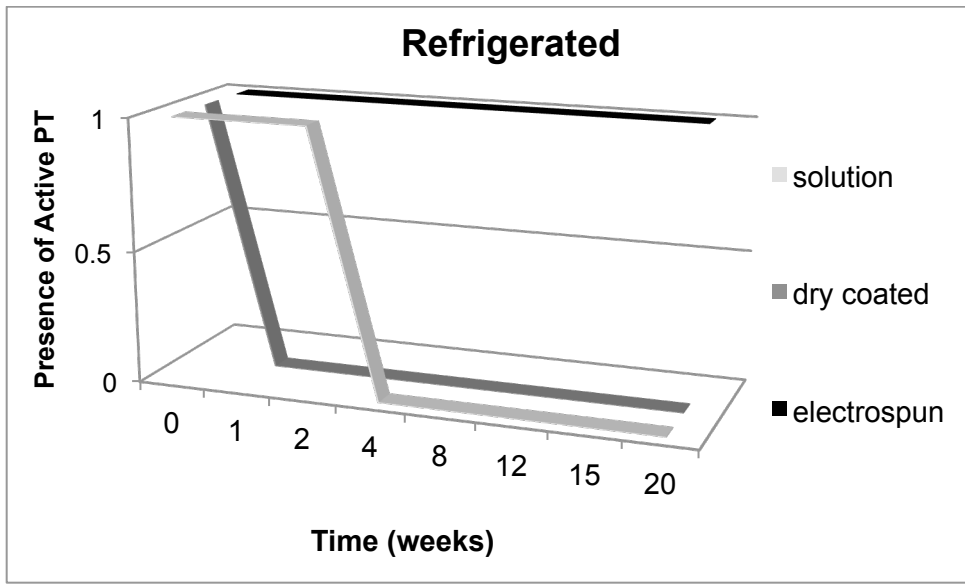


**Figure 3.10.** The 20 week storage stability of samples stored in the refrigerator at 4°C.

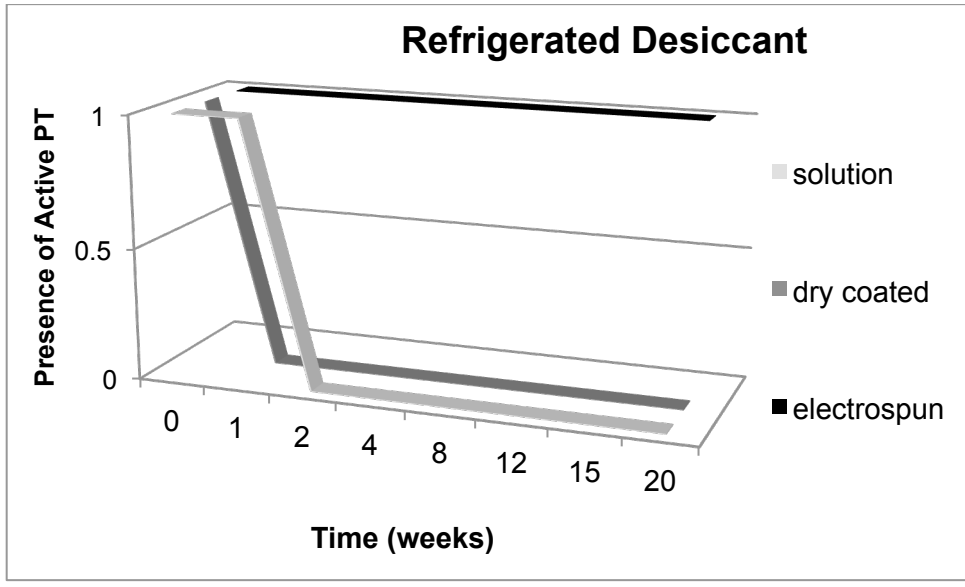


**Figure 3.11.** The 20 week storage stability of samples stored in the refrigerator at 4°C in the presence of desiccant.

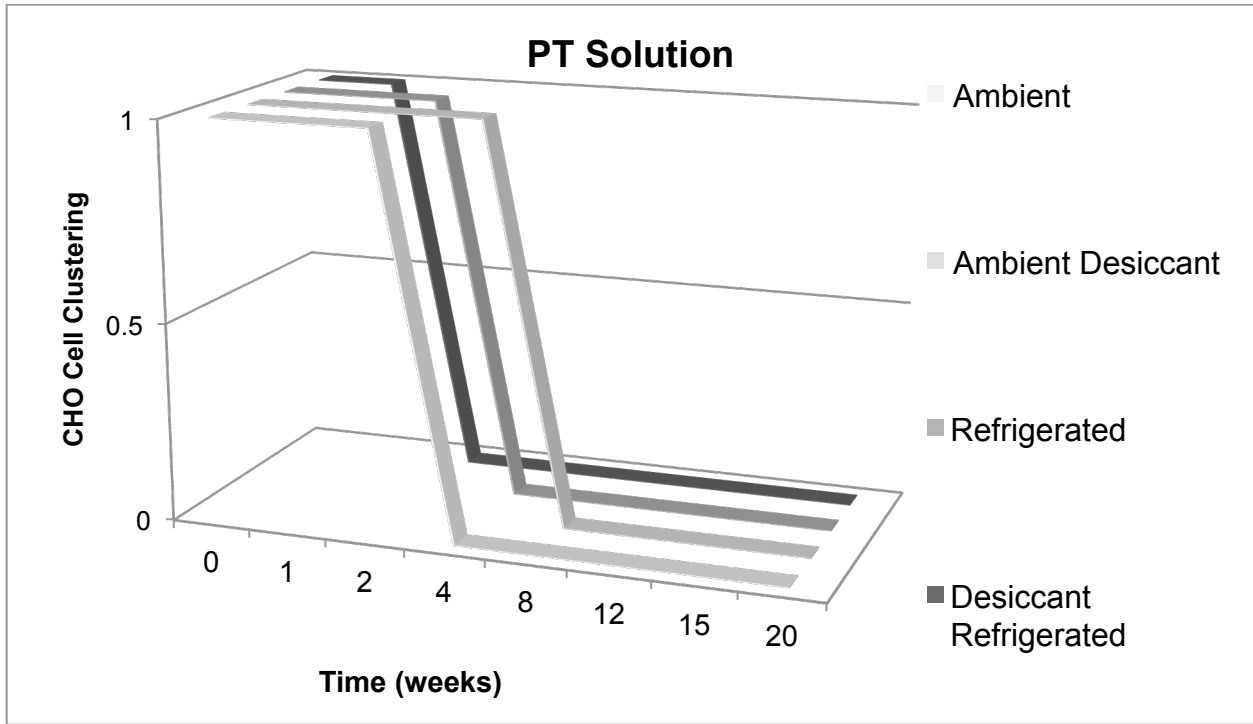


**Figure 3.12.** The 20 week storage stability of PT solution samples.

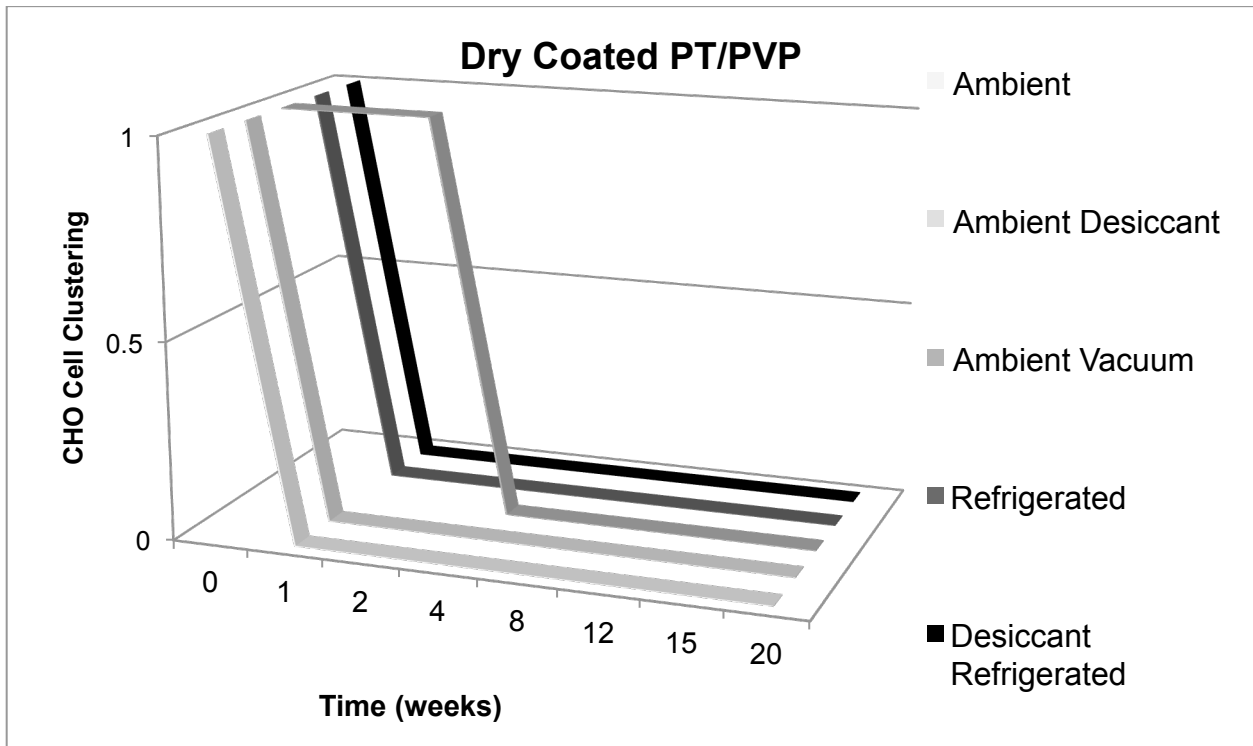


**Figure 3.13.** The 20 week storage stability of Dry Coated PT/PVP wafers.

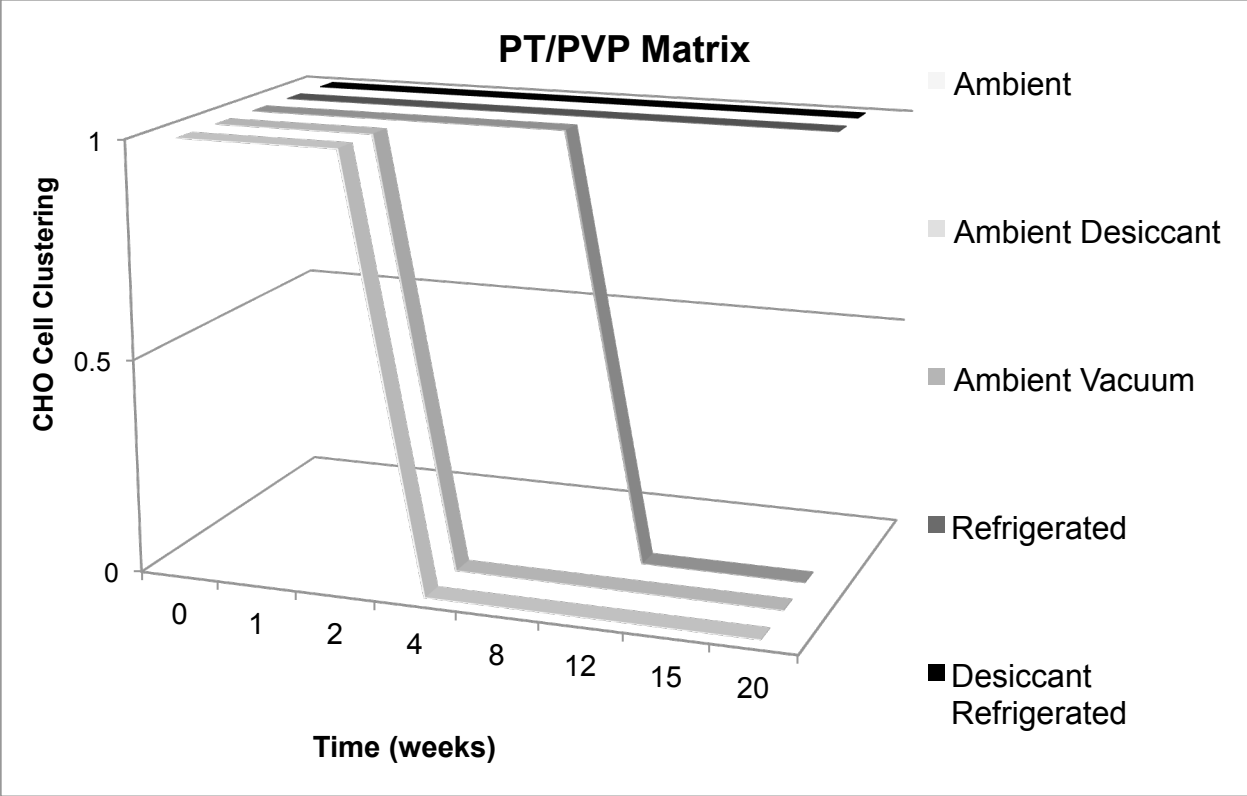


**Figure 3.14.** The 20 week storage stability of PT/PVP Matrix.

| <b>WEEKS</b>                  |             | <b>0</b> | <b>1</b> | <b>2</b> | <b>4</b> | <b>8</b> | <b>12</b> | <b>15</b> | <b>20</b> |
|-------------------------------|-------------|----------|----------|----------|----------|----------|-----------|-----------|-----------|
| <b>ambient</b>                | solution    | 1        | 1        | 1        | 0        | 0        | 0         | 0         | 0         |
|                               | dry coated  | 1        | 0        | 0        | 0        | 0        | 0         | 0         | 0         |
|                               | electrospun | 1        | 1        | 1        | 0        | 0        | 0         | 0         | 0         |
| <b>ambient desiccant</b>      | solution    | 1        | 1        | 1        | 1        | 0        | 0         | 0         | 0         |
|                               | dry coated  | 1        | 0        | 0        | 0        | 0        | 0         | 0         | 0         |
|                               | electrospun | 1        | 1        | 1        | 0        | 0        | 0         | 0         | 0         |
| <b>ambient vacuum</b>         | dry coated  | 1        | 1        | 1        | 0        | 0        | 0         | 0         | 0         |
|                               | electrospun | 1        | 1        | 1        | 1        | 1        | 0         | 0         | 0         |
| <b>ambient refrigerated</b>   | solution    | 1        | 1        | 1        | 0        | 0        | 0         | 0         | 0         |
|                               | dry coated  | 1        | 0        | 0        | 0        | 0        | 0         | 0         | 0         |
|                               | electrospun | 1        | 1        | 1        | 1        | 1        | 1         | 1         | 1         |
| <b>desiccant refrigerated</b> | solution    | 1        | 1        | 0        | 0        | 0        | 0         | 0         | 0         |
|                               | dry coated  | 1        | 0        | 0        | 0        | 0        | 0         | 0         | 0         |
|                               | electrospun | 1        | 1        | 1        | 1        | 1        | 1         | 1         | 1         |

**Table 3.5.** The 20 week storage stability of different PT formulation samples stored under different conditions.

The SEM analysis of the electrospun PT/PVP Matrix exhibited limited bead on a string morphology, and presented a matrix of high surface area to volume ration of continuous 3D porosity, with an average diameter of 72 nm.

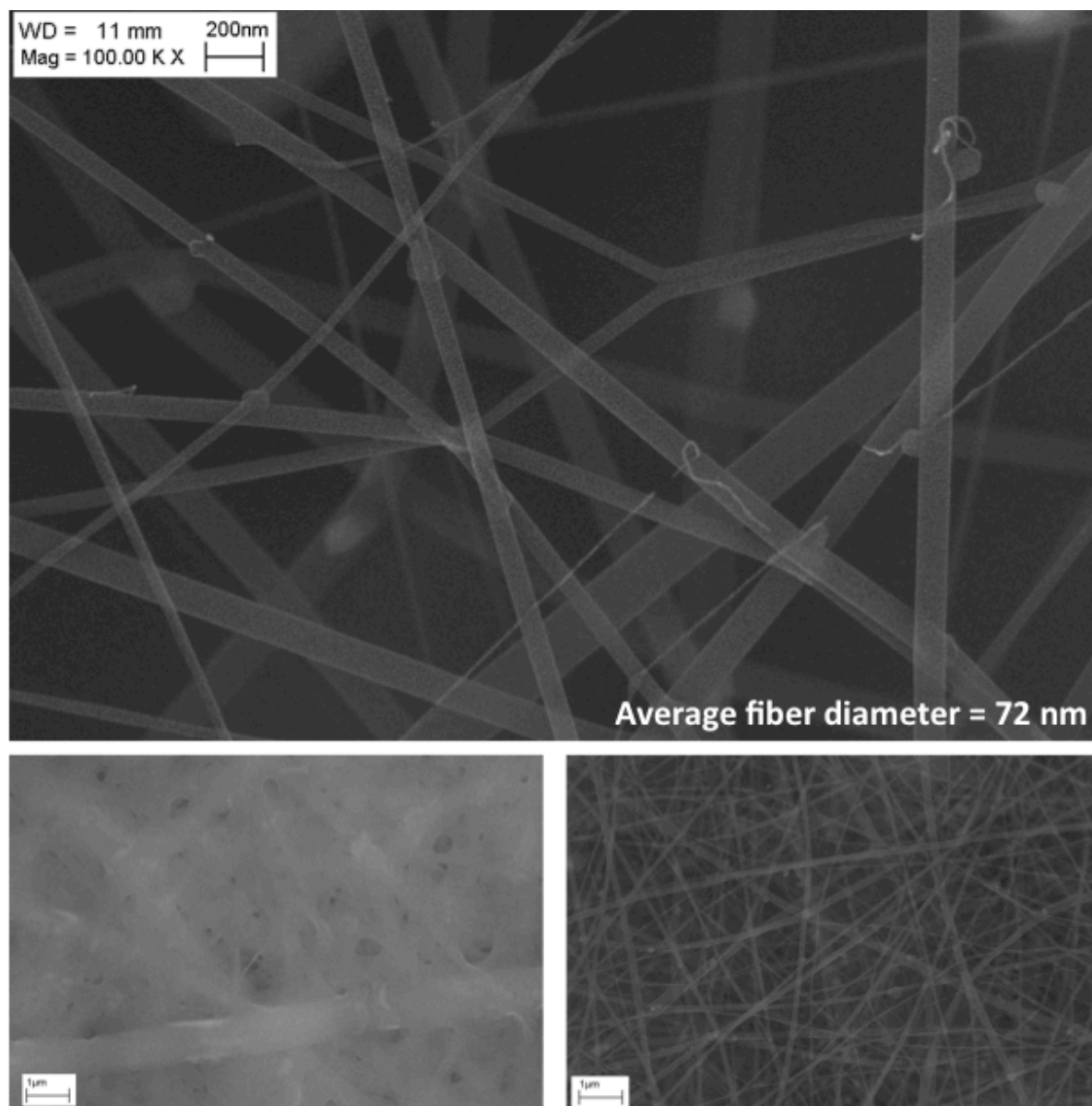


**Figure 3.15.** The SEM images obtained for freshly electrospun PT/PVP matrix (top), vacuumed stored PT/PVP matrix after two weeks of storage (bottom right), and refrigerated PT/PVP matrix after two weeks of storage (bottom left).



## Immunorecognition

The HA standards presented in Figure 3.16 were analyzed using ImageJ software and the values were correlated to the known HA concentrations. The equation was then utilized to identify concentrations of the wafer samples, as well as the dissolved foil and electrospinning solution.

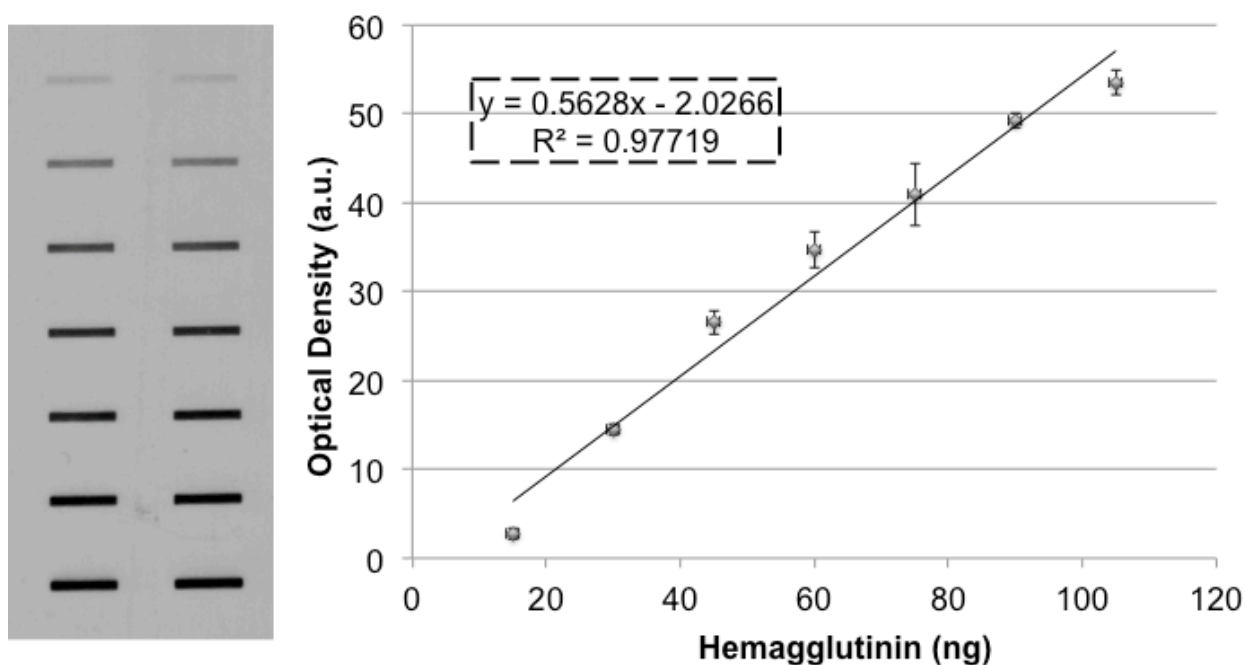


**Figure 3.16.** The optical density of the HA standards.

The electrospun membrane was expected to deposit 80.0% of the total electrospun antigen based on previous findings. It was further expected that silicon wafers would contain 0.20% of the deposition found on the foil, as that is the surface area each wafer takes up on the foil. The presence of immunoreactive HA extracted from the electrospinning solution, HA/PVP Matrix wafer and collector was graphed against that expected to be found in each sample.

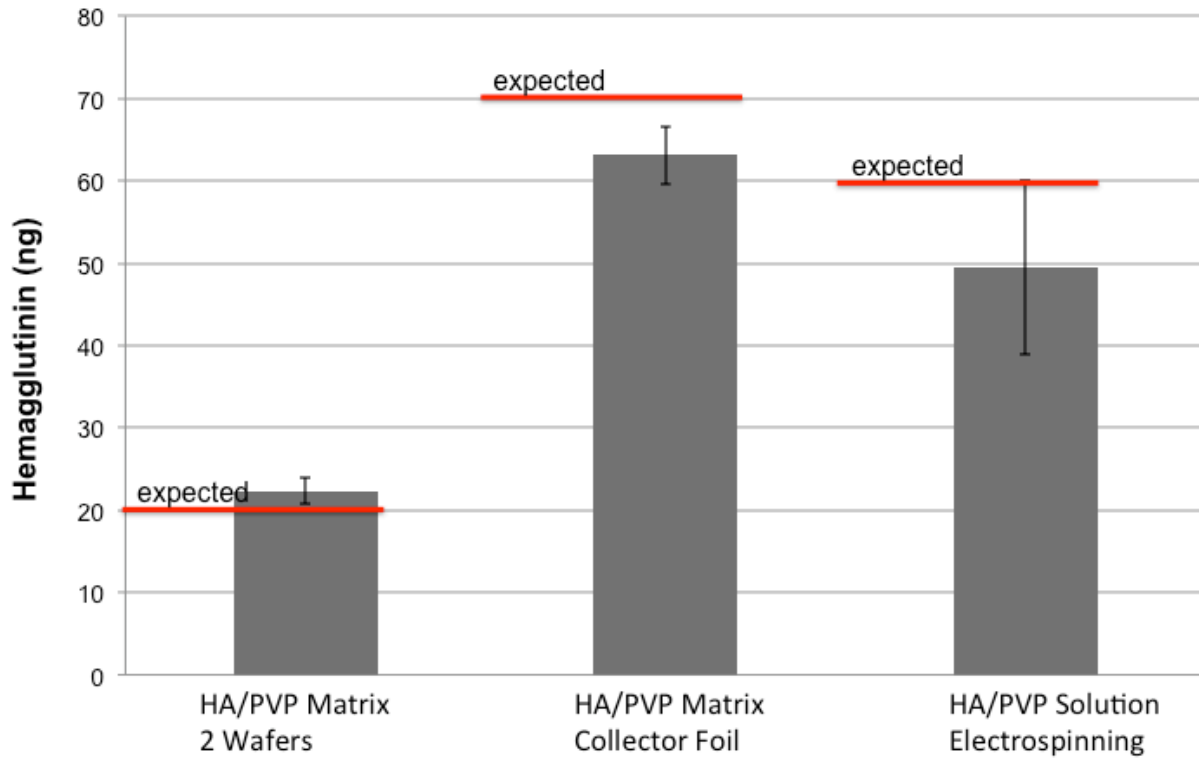


**Figure 3.17.** The amount of HA calculated for the samples using correlation equation.

## DISCUSSION

The purpose of this study was to establish retention of functionality and immunoreactivity for an antigen immobilized within a nanofibrous matrix, as well as to evaluate the long-term storage stability of the antigen-containing matrix. Functionality of Pertussis toxin (PT) evaluated through the highly sensitive CHO cell *in vitro* assay showed preservation of antigen activity in the presence of the polymer vehicle as well as after being resolubilized from the electrospun nonwoven nanofibrous matrix. The same assay was employed to evaluate the long-term stability of PT formulated in solution, as a dried PT/PVP coating and finally the novel PT/PVP Matrix. The 20-week observation period successfully showcased the denaturation of the dry coated and solution samples, and established the superior storage capacity of the novel matrix. Scanning electron microscopy evaluation of the matrix morphology confirmed the presence of a highly porous nonwoven mat of fibers with an average diameter of 72 nm. The preservation of antigen's immunorecognition was established using the 15 amino acid hemagglutinin peptide, widely utilized as an antigen in the developed avian influenza vaccines. The utilization of the Slot-Blot apparatus allowed for quantification of HA exuded from the dissolved matrix to be within the acceptable range of the expected concentration.

Biomolecules can be successfully immobilized, traditionally by methods of entrapment, microencapsulation, covalent attachment, adsorption, and more recently via electrospinning in PVP [122]. The strict limitations on use of aqueous solvents for electrospinning have been explained in the previous section on fabrication of electrospun nanofibrous payload composites. However the delicate nature of the

antigen payloads employed required specific accommodations based on the protein's stability in liquid formulations. Precise and sensitive quantification of each of the chosen antigen or antigen-like molecules necessitated employment of highly selective, specific and sensitive assays. The most straightforward assay utilized for the purpose of payload quantification was the HRP assay discussed previously. The other macromolecules employed in this study required adaptation of *in vitro* functionality assays that utilized cellular responses to the active forms of the payload.

The CHO cell assay employed to confirm the presence of functional PT, has been widely reported since its initial publication almost 30 years ago [111]. Morphological changes in cultures of CHO cells have been previously reported in the presence of other toxins, i.e. cholera toxin. However the specific clustering of the cell line dosed with PT was not reproduced in the presence of *H. influenza*, *B. paraptussis* or other microorganisms common to the upper respiratory tract [113], thus establishing the CHO cell clustering assay as a valuable tool for detection of active PT [114]. The morphological change observed in CHO cells dosed with functional PT was explained to be a result of blocked transmembrane signaling caused by ADP ribosylation of the relevant G proteins by the toxin's A-promoter [70]. Comparable intoxication of the cells reported here in the presence of stock PT to that of antigen released from the novel electrospun PT/PVP Matrix further advocates for the use of electrospinning for reversible immobilization of bioactive molecules.

Recent reports of improved efficacy of the LT-IS patch developed by Glenn et al. have highlighted the utility of an advanced so-called "dry patch" formulation [23]. In comparison to a wet formulation, the dry patch, prepared by dip coating, presented a

logistically more appealing solution for intradermal immunization due to the ease of use as well as improved stability conferred by the absence of water. The enhanced efficacy of the dry patch has been attributed to its capacity to undergo rapid solubilization via transepidermal water loss, creating a favorable local concentration gradient, in turn resulting in a more robust delivery of antigens into the skin [21]. However, the dip coating method of payload deposition presents its own drawbacks: the drying step requires deposition of a limited volume to effectively form a solid coating, the liquid formulation must be extensively evaluated for each mixture to prevent payload denaturation. Even under optimal conditions the method presents a major drawback for intradermal delivery, namely that of suboptimal surface reactivity. The single plane of reactivity offered by the thin film morphology limits surface interaction between the film and the subjacent skin. The long-term storage study employed here compared the stability of PT formulated as dry coated film to that of the PT/PVP Matrix, and regardless of the storage condition employed showed that the thin film was unable to stabilize the antigen beyond two weeks. Furthermore it presented no improvement for long-term storage stability to that of antigen in solution.

Due to the hygroscopic nature of the polymer employed we evaluated the effects of humidity conditions outlined in Table 3.5. We were able to demonstrate that the electrospun matrix preserved the immobilized antigen's activity for the entire duration of the 20 week long study, when refrigerated with as well as without desiccant, approximately 16 weeks longer than the other PT formulations evaluated here. The prolonged stability of antigen observed for the novel PT/PVP Matrix when stored under vacuum at room temperature indicates that humidity affects the stability of the antigen

|             |           |           |           |
|-------------|-----------|-----------|-----------|
| Temperature | -20°C     | 4°C       | 20°C      |
| Humidity    | Ambient   | Ambient   | Ambient   |
| Control     | N/A       | N/A       | Vacuum    |
|             | Desiccant | Desiccant | Desiccant |

**Table3.5.** Outline of the storage conditions tested (n=2).

laden matrix. The use of the electrospinning method for immobilization of various biomolecules has been widely reported; however, the specific location of the encapsulated payload (e.g. on or within the individual fibers of the nanofibrous matrix) is to date uncertain. By comparing the loss of antigen functionality in equivocally constructed pertussis formulations of dry coated films to that of electrospun mats, the study indicated that the presence of the polymer vehicle has no effect on stability as much as its morphology. This implies that the electrospun immunogen was encased within the nanofibrous mats rather than the surface deposition observed for dry coated samples. Temperature, pH, and concentration are three major factors for preserving protein stability [122]. The variation in temperature as well as pH may alter the protein's tertiary structure and therefore enhance or inhibit its activity [148]. In aqueous solutions proteins arrange themselves so that the hydrophobic amino acids form a core surrounded by the hydrophilic amino acids exposed to the solvent [93-95]. It has been suggested that PVP's hygroscopic nature simulates the proteins' behavior in aqueous solution, thus preserving the immunogens' function. The storage stability of an antigen encapsulated within a nanofibrous PVP matrix was also established for protective

antigen (PA), key immunogen of the anthrax vaccine [123-129], and further validates the novel immobilization method.

To date numerous attempts have been undertaken to create a functional pandemic avian influenza immunization [130]. The subunit antigen vaccines have been identified as the most likely to induce strain specific immunity, and to offer the most efficient coverage if multiple epitopes of a given antigen subunit were contained. We have utilized the novel nanofibrous matrix to immobilize a 15 amino acid hemagglutinin peptide. The preservation of the antigen's immunoreactivity throughout the harsh process of electrospinning was verified with the developed immunoreactivity assay. The analysis utilized the slot blot apparatus to confirm the antigen's immunorecognition and allowed for quantification of the HA-composite accumulation on proposed delivery platforms. The maintenance of antigen's reactivity to a specific antibody renders the electrospinning process an adequate method for antigen encapsulation. As presented in Figure 3.16, the deposition on both the silicon wafer and foil samples were within the margin of error of the expected values presenting a low variability between the group samples. The ease of use and cost effectiveness of the approach can be postulated to effectively translate to other epitopes of the influenza virus thus offering an improved coverage against the varying strains of the flu.

In summary, the results obtained in this study established the retention of functionality and immunoreactivity for PT and HA respectively. The whooping cough and avian flu immunogens were successfully immobilized within a nanofibrous matrix of PVP, a generally regarded as safe polymer. The improved storage stability exhibited by the PT/PVP matrix further validated the employment of the electrospinning method to

encase antigens within its hygroscopic nonwoven matrix. The high surface area to volume and mass ratio of the nanofibrous composite reported here, offers the potential for improved surface interaction between the novel immunization patch and the outermost layers of the skin thus allowing for successful antigen delivery.



## Chapter 4

### *Specific Aim 3*

### **Specific Aim III**

*To establish the proposed delivery system's capacity to facilitate passage of an antigen into commercially available engineered human skin models.*

## **INTRODUCTION**

The outermost layer of mammalian skin is known as the stratum corneum (SC). The 10-20  $\mu\text{m}$  thick SC is composed of 10-20 layers of cornified keratinocytes encased in lipids secreted by the epithelial layers of the epidermis [131-132]. This “brick and mortar structure” poses an effective, but fragile barrier to the penetration of fluids, large molecules, and particles as well as microbes.

Disruption of the SC enhances permeation, and can be successfully achieved through physical and chemical treatments to the topical surface of the skin. Traditionally employed dermal delivery techniques such as electroporation or iontophoresis are limited to specific molecule types and require the use of bulky and costly equipment. The simplest mode of skin permeation relies on hydration of the skin through occlusion, wetting or other methods [132]. Moistening of the brick and mortar layer leads to lipid swelling, which results in temporary microstructural changes that allow for efficient passage of payloads through the otherwise “impermeable” SC.

Fick's first law of diffusion states that the rate of infusion, known as flux ( $J$ ) is proportional to the concentration gradient across a given distance ( $dC/dx$ ) and a diffusivity constant ( $D$ ) for a given permeant.

$$J = -D \left( \frac{dC}{dx} \right)$$

[Equation1]

The directionality of particle movement from high to low concentration holds true in the skin; however, the skin's complexity limits the law's applicability, as the skin is a live, dynamic organ, and not simply a porous membrane [33]. Delivery of drugs to the skin has been reported to vary from site to site, species to species, and individual to individual. This variation is attributable to a number of factors, such as skin type, ethnic group, site, thickness, temperature, hydration status, sweat gland function, temperature, endogenous enzymatic activity as well as any area pre-treatments (e.g., cleansing, dermabrasion) [133, 134].

The main objective of this aim was to evaluate the efficacy of the nanofibrous matrix to transport biologically functional antigen-like macromolecules into and across human skin *in vitro*. The commercially available EpiDerm FT™ and EpiDerm™ human skin models manufactured by MatTek Corp (Ashland, MA) were utilized to observe the delivery of 44 kDa horseradish peroxidase (HRP) and 117 kDa pertussis toxin (PT) respectively. Both of the tissue models possess the stratified keratinocyte layers of the epidermis as well as a morphologically and functionally relevant cornified stratum corneum [135]. In addition, the EpiDerm FT™ model includes of an engineered dermis comprised of normal human epidermal keratinocytes cocultured with dermal fibroblasts seeded in a collagen substratum to represent the thickness and structure of the dermis. Furthermore, the use of viable tissue models allows the evaluation of any cytotoxicity observed after a 24-hour application of the novel immunization patch, through the use of metabolic assays.

## **MATERIALS AND METHODS**

### *HRP DELIVERY STUDY*

#### *Solutions*

Polyvinylpyrrolidone (PVP) of M.W. 1,300,000 from Sigma-Aldrich was dissolved at 0.075mM concentration in absolute ethanol.

Immuno Pure Horseradish Peroxidase (HRP) obtained as a salt-free lyophilized powder from Pierce [Rockford, IL] was reconstituted in phosphate buffered saline (PBS) at a concentration of 0.598 units/ $\mu$ l.

The electrospinning solution consisted of 80% of polymer solution by volume and 20% of the enzyme solution, to obtain the final concentration of 0.1196 units/ $\mu$ l.

The HRP solution used as a positive control in the delivery study was obtained by further diluting the stock with PBS to a final concentration of 0.10 units/ $\mu$ l.

#### *HRP/PVP Matrix*

The electrospinning solution consisting of 20 % HRP by volume was magnetically stirred for five minutes before being placed into a glass syringe, and placed into the programmable syringe pump. The HRP/PVP coating was generated by ejecting 600  $\mu$ l of the electrospinning solution at a flow rate of 10  $\mu$ l/min into an electric field of 1.7 kV/cm with a 10 cm distance between the needle and the target.

The matrix was collected onto an 8x10 cm block covered with aluminum foil to which 24 4x4 mm silicon wafers [Silex Microsystems, Boston, MA] were attached. The wafers were positioned as 12 pairs of closely located wafers to allow for an estimation of HRP deposition for each wafer used in the tissue study. A “control” experiment was carried out, where one of the paired wafers was dissolved in 500 µl of tissue culture media in the absence of a skin model. The control wafer media was harvested and analyzed for HRP content at two time points of 4 and 24 hours.

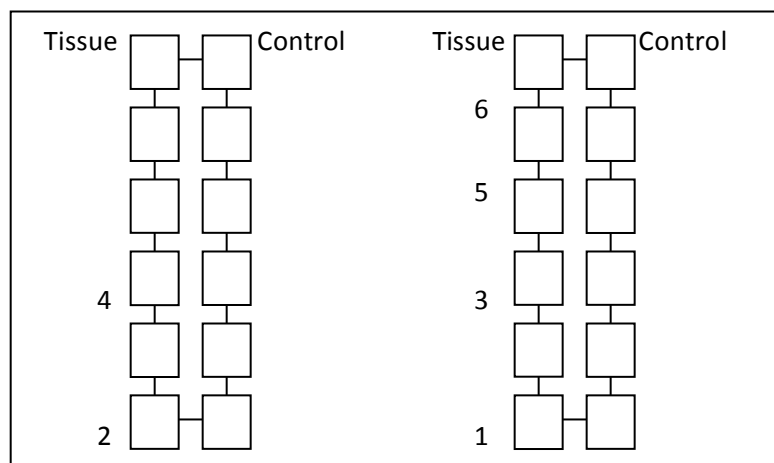


**Figure 4.1.** The electrospinning collector with 4x4 mm silicon wafer pairs used for the HRP delivery experiment in dry and tissue studies. Drawing not to scale.

To aid with efficient loading of HRP/PVP matrix wafers onto the tissue models, we employed ultra-clear microcentrifuge tubes with a diameter of 8mm that were cut to a height of approximately 1 cm. The tubes were sterilized overnight with a 70% ethanol soak and subsequently dried in the sterile environment of the tissue culture hood for approximately a half hour, by being placed onto stainless steel screws, as depicted in Figure 4.2.

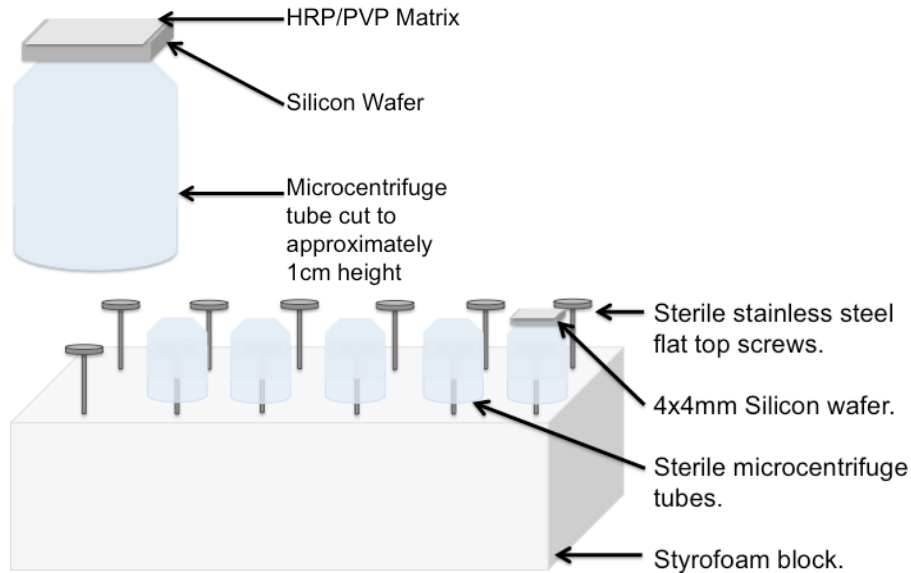


**Figure 4.2.** The HRP/PVP Matrix sample attached to the sterile microcentrifuge tube bottoms.

### *Full Thickness Human Skin Constructs*

To study the HRP delivery profiles we employed the EpiDerm Full Thickness (EFT-300) tissue models from MatTek Corporation. The tissue units were handled under sterile conditions and according to the supplier's directions [135]. The adjustments of the maintenance media volume from 1mL to 0.5mL and switching from a 6-well to a 12-well plate for the duration of the delivery experiment were the only alterations from the supplied protocol. The 24 tissue samples were divided into four groups of n=6. The test groups consisted of Untreated Controls (UTC), HRP Solution, HRP/PVP Solution and HRP/PVP Matrix. To eliminate variability between study groups, all of the liquid antigen formulations were constrained to a volume of 10  $\mu$ l to limit any hydrostatic contribution to payload entry. The HRP/PVP Matrix samples were attached

to plastic vials with crazy glue, and placed on top of the tissue holders, thus beginning the 24 hour study.

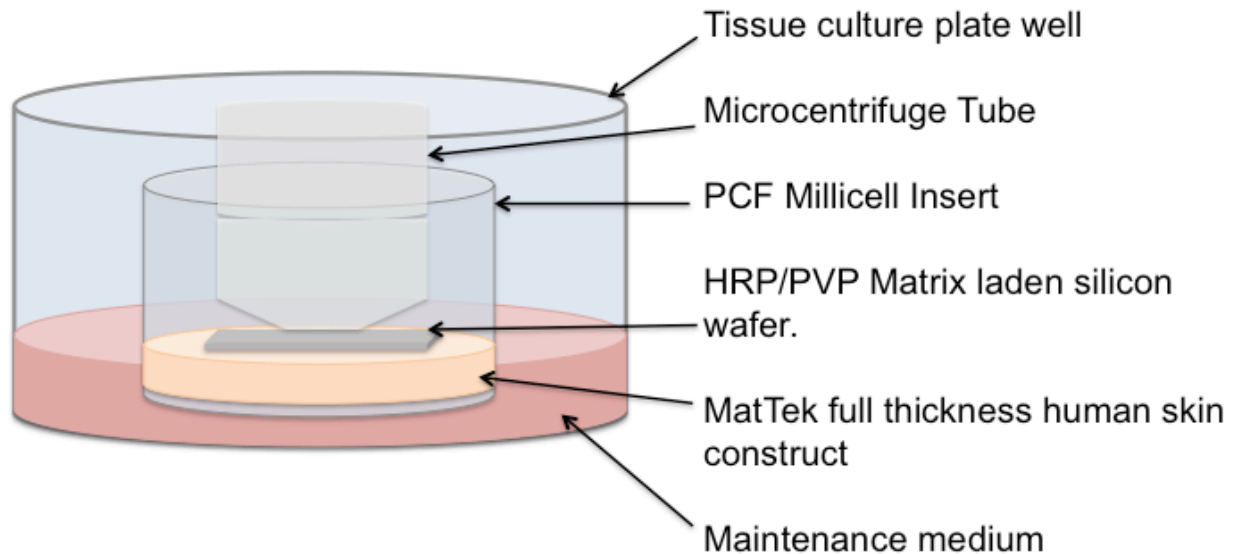


**Figure 4.3.** The MatTek HRP/PVP Matrix sample attached to the sterile microcentrifuge tube bottoms.

The tissue experiment had three time points of 1 hour, 4 hours, and 24 hours, where the tissue insert was moved to a fresh 0.5mL of maintenance media, while the previous time point medium was collected and analyzed using the colorimetric HRP assay.

To compare the integrity of the tissue samples between the test groups and the untreated control group at the conclusion of the 24 hours delivery study, we employed the alamar blue assay. Since the viability assay's interaction interfered with the colorimetric HRP assay, we used only the first two tissue samples from each group. The alamarBlue reagent [LifeTechnologies Corp, Grand Island, NY] was diluted down to

10% concentration with the maintenance media utilized in the delivery study, and incubated the tissues in the reagent/media mix at 37°C for four hours. At the conclusion of the four hour incubation, the liquid was harvested and analyzed in duplicates. The results were measured using the CYTOFLUOR 2300 [Millipore, Billerica, MA] fluorescence reader with an excitation wavelength of 530/25 nm and an emission filter of 590/35 nm. The obtained values were corrected for blank alamarBlue/media mix background signal.

To extract the HRP delivered into the tissue models we homogenized the tissue after the 24 hours media harvest. Samples 3-6 for each test group were cut out of the holders using scalpels and placed into 1.5 mL centrifuge tubes together with 500 µl of fresh tissue culture media. With the use of a tooth polisher and a pellet pestle [Sigma-Aldrich, Milwaukee, WI] the tissue was pulverized. The mixture was centrifuged until all of the debris settled and the liquid portion was collected and analyzed using the previously described HRP assay.

## *PT DELIVERY STUDY*

### *Solutions*

50 µg of lyophilized, salt-free, 117 kDa Pertussis Toxin (PT) [List Biological Labs, Campbell, CA] was reconstituted in 0.80ml of sterile Hank's buffered saline (HBSS) resulting in a concentration of 62.5 ng/µl PT in HBSS.



The PT standards employed as positive controls for the cell culture assay were made with HBSS dilutions of stock PT to obtain a range of concentrations from 5 to 50 ng/ml PT in HBSS.

Polyvinylpyrrolidone (PVP) of M.W. 1,300,000 from Sigma-Aldrich was dissolved at 0.10 mM concentration in absolute ethanol.

The electrospinning solution consisted of 70% of the polymer solution by volume and 30% of the PT stock solution, to result in a final concentration of 18.75 ng/ $\mu$ l.

The PT Liquid formulation was diluted with HBSS to a final concentration of 1.875 ng/ $\mu$ l, delivering 20  $\mu$ l per tissue.

#### *PT/PVP Matrix*

The electrospinning solution consisting of 30% PT by volume was magnetically stirred for five minutes before being placed into a glass syringe, and placed into the programmable syringe pump. The PT/PVP coating was generated by ejecting 1250  $\mu$ l of the electrospinning solution at a flow rate of 10  $\mu$ l/min into an electric field of 1.5 kV/cm with a 10 cm distance between the needle and the target.

The matrix was collected onto a target covered with aluminum foil that 52 4x4 mm silicon wafers [Silex Microsystems, Boston, MA] were adhered to. From previous studies, it has been established that approximately 80% or 1000  $\mu$ l of the ejected electrospinning solution would deposit onto the 8x10 cm collector, and therefore each of the wafers would collect 37.5 ng PT as each occupies 0.2% of the total collector

surface area. To confirm the presence of biologically functional PT within the PT/PVP matrix a “control” study was conducted. 1, 2, 4 and 6 wafers were dissolved in 1.5ml of EPI-100 media. The wafers employed in the tissue study were loaded onto sterilized microcentrifuge tubes as described above and depicted in Fig 4.2.

### *Human EpiDerm Constructs*

To study the novel PT/PVP matrix’s ability to deliver the toxin into and through the outer most layers of human skin we employed the EpiDerm™ (EPI-200) tissue model obtained from MatTek Corporation. As previously noted the EPI-200 model consists of multilayered/highly differentiated normal, human-derived epidermal keratinocytes as well as a stratified SC. The tissue samples were handled under sterile conditions and according to the supplier’s directions [135]. The two changes to the supplied protocol were, adjustment of the maintenance media volume from 1ml to 0.75ml and switching from a 6-well to a 12-well plate for the duration of the delivery experiment. The 14 tissue samples were divided into three groups. The test groups consisted of Untreated Controls (UTC) n=4, PT Solution n=4, and PT/PVP Matrix n=6. The PT/PVP Matrix wafers were attached to plastic vials with crazy glue, and placed on top of the tissue holders, beginning the 24-hour study. The basal maintenance media was collected 24 hours after the delivery sample application.

We employed the MTS cell viability assay to compare the integrity of the tissue units between the PT loaded groups to that of the untreated control group. The MTS reagent CellTiter 96® AQueous One Solution [Promega, Madison, WI] was diluted down

to 15% concentration with HBSS. 300  $\mu$ l aliquots of the diluted solution were placed in each well of a 24-well plate. After triple rinses with PBS and blot drying on a paper towel the tissue units were placed into the MTS, and incubated at 37°C for three hours. At the conclusion of the incubation all the tissue units were collected for the homogenization process, described below. The optical density of the resultant MTS reagent was measured at a wavelength of 490nm using the Versa Max Microplate Reader [Molecular Devices, Sunnyvale, CA]. The samples were analyzed in duplicates and the obtained values were corrected for blank MTS/HBSS mix background signal.

To extract the PT delivered into the tissue models, we pulverized the tissue after the 24 hours media harvest. All the samples were cut out of the holders using scalpels and placed into 1.5 mL glass vials together with 750  $\mu$ l of fresh EPI-100 media. The tissue was homogenized with the use of a tooth polisher and a pellet pestle [Sigma-Aldrich, Milwaukee, WI]. The ground tissue was allowed to settle, the liquid portion was collected and analyzed using the CHO cell assay.

#### *Chinese Hamster Ovary (CHO) Cells*

Confluent CHO-K1 ATCC CCL-61 cells were trypsinized and plated into four sterile 96-well flat bottomed cell culture plates at a concentration of  $2.7 \times 10^4$  cells/cm<sup>2</sup>, equivalent to 0.20 ml of  $3.78 \times 10^4$  cells/ml, except for the peripheral rows and columns with HBSS to avoid the edge effect previously observed for CHO cells cultured in 96-well plates. The cells were allowed to adhere over a 24-hour incubation period, at the

end of which the original medium was replaced with duplicate 200 µl aliquots of the samples listed below:

- PT standards: 0.0, 6.25, 12.5, 25.0, 37.5, 50.0 ng/ml in EPI-100.
- Dissolved control wafers, where triplicates of 1, 2, 3 or 4 wafers were dissolved in 1.5ml of EPI-100.
- Untreated tissue control medium 1 through 4, at time points 24, and homogenized.
- PT liquid formulation tissue sample medium 1 through 4, at time points 24, and homogenized.
- PT/PVP Matrix tissue sample medium 1 through 4, at time points 24, and homogenized.

The plates were examined for the characteristic CHO cell clumping in the presence of functional PT at 12-hour intervals for a 48-hour time period. The microscopic observations were recorded at 48 hours post dosing, using a qualitative grading range from 0 to 2, where a grade of zero indicated no observable clumping.

### *Statistical Analysis*

All of the data used for statistical evaluations were checked for normality and equality of variance, using the Shapiro-Wilk and Levene's tests, followed by appropriate tests for the given experiment. All statistical tests were performed using SPSS software [IBM, Somers, NY] assuming a significance level of  $p < 0.05$ .

## RESULTS

The HRP assay was employed to obtain an HRP standard curve, which would allow the conversion of sample absorbance into HRP units in the given sample. With the correlation coefficient of  $R^2=0.97802$ , the standard curve trend line equation was utilized to establish the HRP concentration of the experimental samples.

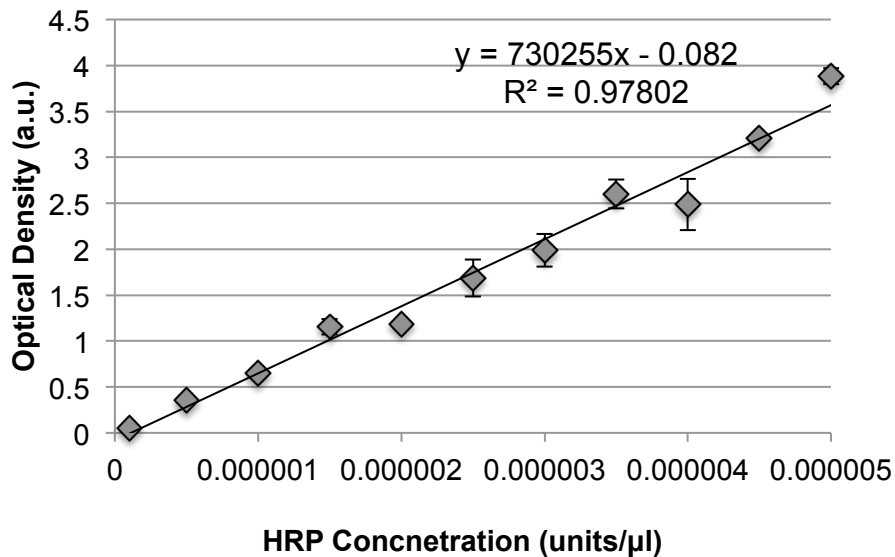


**Figure 4.4.** The standard curve for HRP.

The delivery profiles were represented in both concentrations of HRP as well as percentage of the expected enzyme concentration. The variation between the concentrations of HRP delivered was caused by the varying amount of enzyme delivered through the different preparations tested, as depicted in table 4.1.

| Sample                     | HRP Solution          | HRP/PVP Solution          | HRP/PVP Matrix                   |
|----------------------------|-----------------------|---------------------------|----------------------------------|
| <b>Description</b>         | HRP in PBS            | 20% HRP –80% PVP solution | 20% HRP –80% PVP electrospun mat |
| <b>Concentration</b>       | 0.10 units/ $\mu$ l   | 0.1196 units/ $\mu$ l     | N/A                              |
| <b>HRP Units Predicted</b> | 1.0 unit (10 $\mu$ l) | 1.196 units (10 $\mu$ l)  | 4x4mm wafer<br>0.1148 units      |

**Table 4.1.** The amount of HRP delivered for each sample.

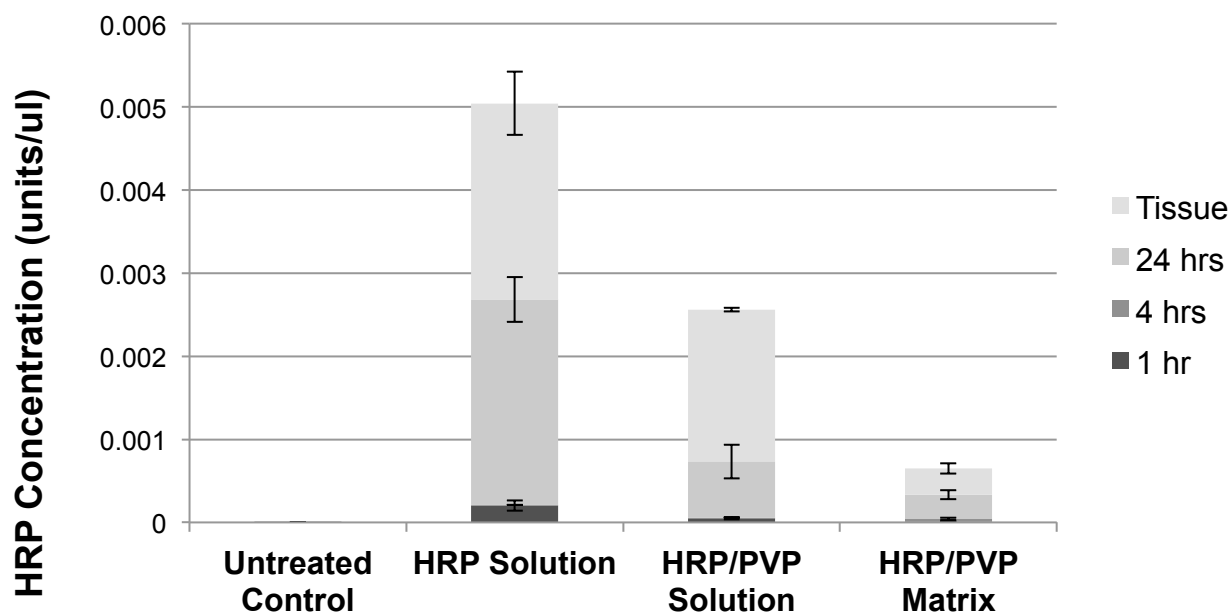


**Figure 4.5.** The average HRP delivery profile for the various platforms tested on the MatTek EFT-300 tissue engineered human skin constructs. The error bars represent the standard error of the mean between the samples within each group for a specific time point (n=6).

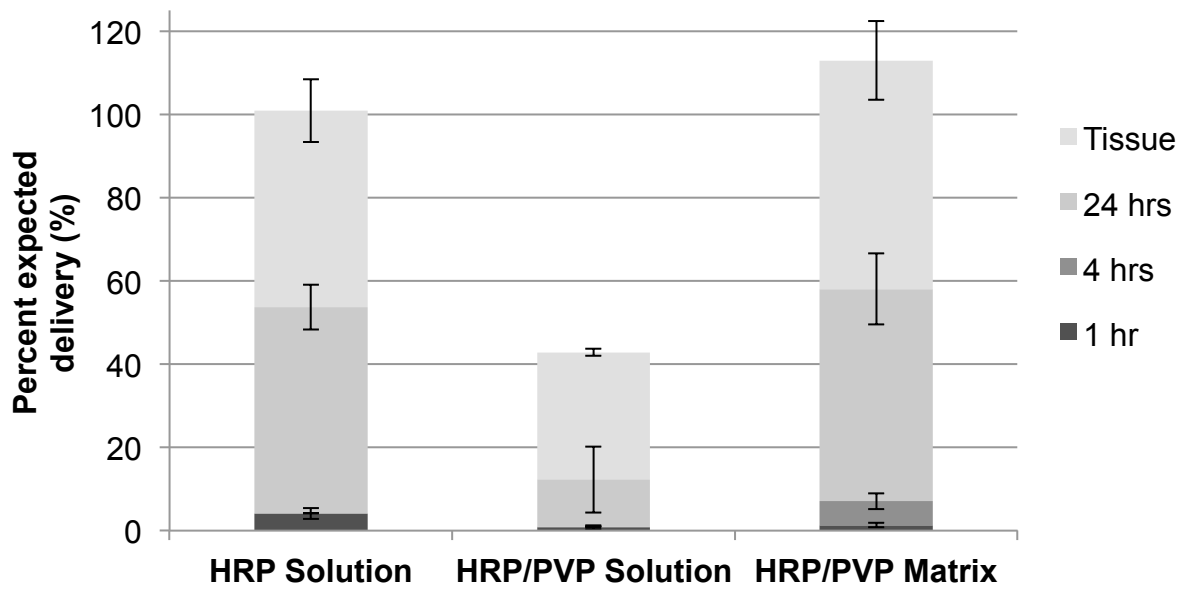


**Figure 4.6.** The average percentage of HRP delivered by the various platforms tested on the MatTek EFT-300 tissue engineered human skin constructs. The error bars represent the standard error of the mean between the samples within each group for a specific time point (n=6).

An overall comparison of the delivered HRP concentrations (%) revealed a statistically significant difference between the groups for the following time points: 1 hour, 4 hours, and 24 hours using the nonparametric Kruskal-Wallis test ( $p=0.02$ ,  $p=0.001$ ,  $p=0.006$  respectively). The pulverized tissue samples were not different from each other ( $p=0.37$ ). To understand which of the groups differed from each other at a given time point we performed the Mann-Whitney U test. The results revealed that the HRP Solution group had higher scores than the HRP/PVP Solution group at 1, 4, and 24 hours after delivery (all  $p$ -values = 0.004). When we compared the HRP Solution group to the HRP/PVP Matrix we observed higher scores for the solution for the first two time points ( $p = 0.055$  and  $p = 0.004$ , respectively). At the 24-hour time point, the percent delivery of enzyme solution to that of the polymer matrix showed no significant

difference. Finally, the Mann-Whitney U test comparing the HRP/PVP Matrix to the HRP/PVP Solution yielded higher scores for the Matrix at 4 ( $p = 0.004$ ) and 24-hours ( $p = 0.01$ ) after delivery

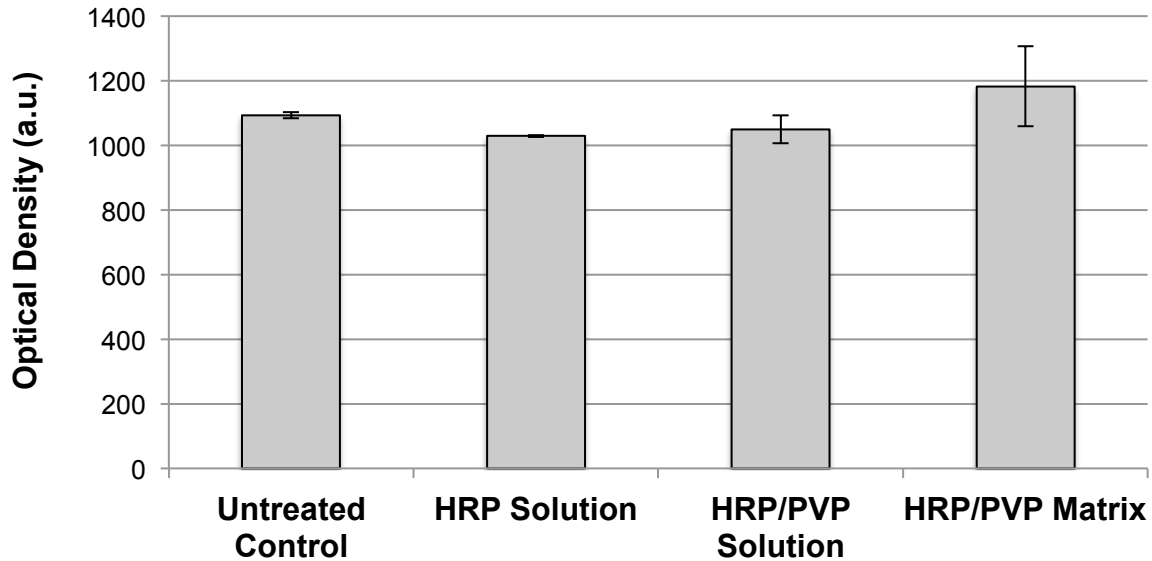


**Figure 4.7.** The alamaBlue cell viability assay absorption at 590 nm observed after the 24-hr delivery study for two tissue samples from each test group. The error bars represent the standard of deviation between the two tissue samples tested for each group ( $n=2$ ).

To confirm that the tissue viability was not compromised during the delivery we compared the absorbance values across the groups using the nonparametric Kruskal-Wallis test. The values were not significantly different from each other ( $p=0.14$ ), suggesting that the tissue was not compromised during the delivery.



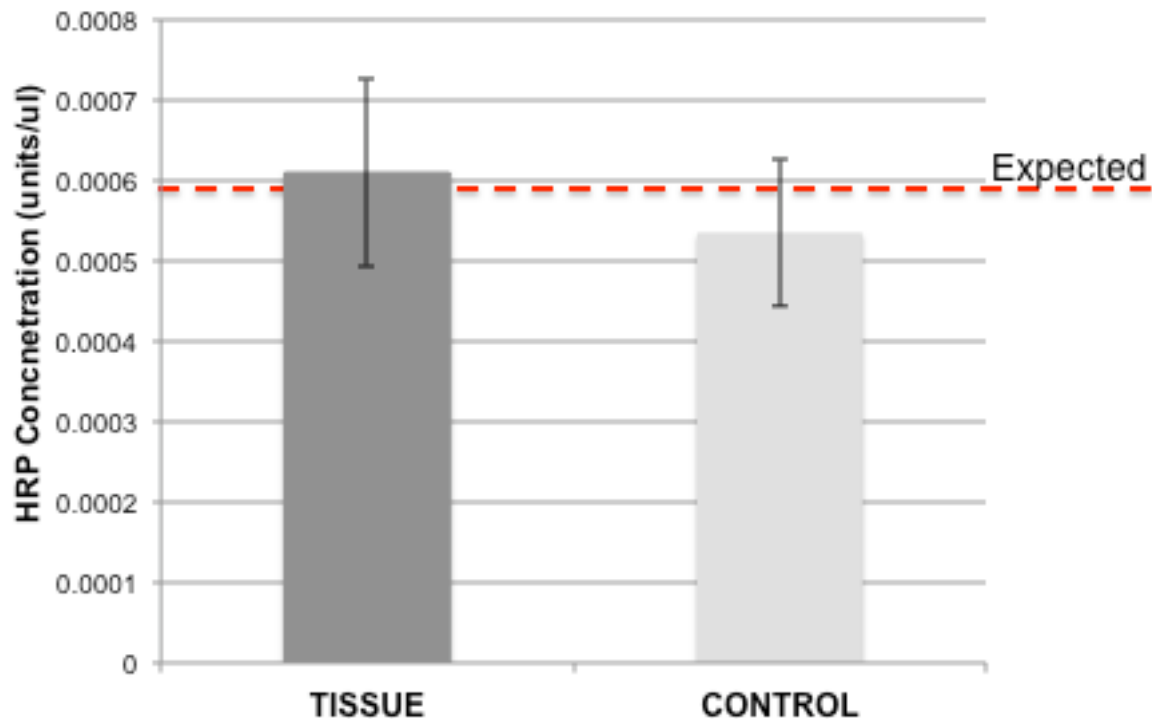


**Figure 4.8.** Comparison of HRP concentrations obtained from the electrospun HRP/PVP Matrix wafers in tissue experiment versus the control dissolution study. The error bars represent the standard error of the mean between the samples within each group for a specific time point (n=4; samples 1 and 2 of homogenized tissue were compromised with the alamar blue assay).

*PT Results*

| PT Concentration<br>(ng/ml) | PT Standard Solution |                       | PT/PVP Standard Solution |                       |
|-----------------------------|----------------------|-----------------------|--------------------------|-----------------------|
|                             | Average              | Standard of Deviation | Average                  | Standard of Deviation |
| 0                           | 0                    | 0                     | 0                        | 0                     |
| 6.25                        | 1                    | 0                     | 1                        | 0                     |
| 12.5                        | 1                    | 0                     | 1                        | 0                     |
| 25                          | 2                    | 0                     | 2                        | 0                     |
| 37.5                        | 2                    | 0                     | 1.5                      | 0.7                   |
| 50                          | 2                    | 0                     | 2                        | 0                     |

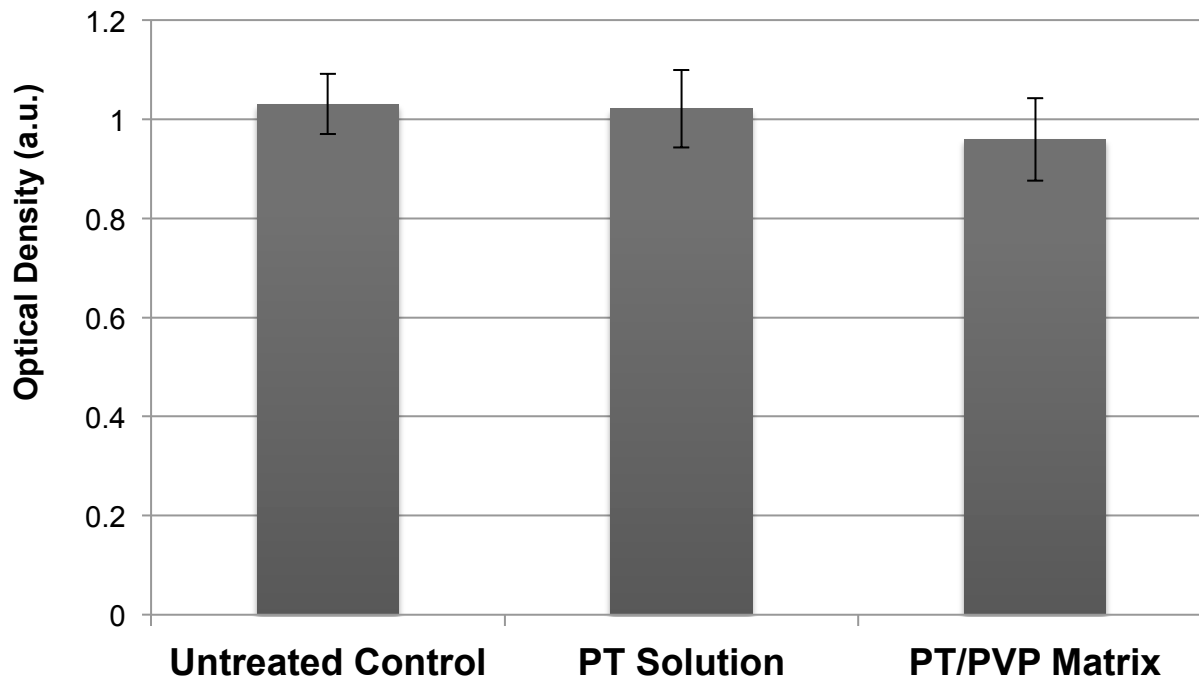
**Table 4.2.** The level of CHO cell clumping observed 48 hours after dosing with duplicates of the control solutions of PT standard as well as the electrospinning solution (n=2).

| Tissue Sample          | 24 Hours |                       | Homogenized |                       | # Tissue Units |
|------------------------|----------|-----------------------|-------------|-----------------------|----------------|
|                        | Average  | Standard of Deviation | Average     | Standard of Deviation |                |
| Untreated Control      | 0        | 0                     | 0           | 0                     | 4              |
| PT Liquid Formulations | 1        | 0                     | 1           | 0                     | 4              |
| PT/PVP Matrix          | 1        | 0                     | 1           | 0                     | 6              |

**Table 4.3.** The level of CHO cell clumping observed 48 hours after dosing with the media collected from the PT delivery EPI-200 tissue experiment.

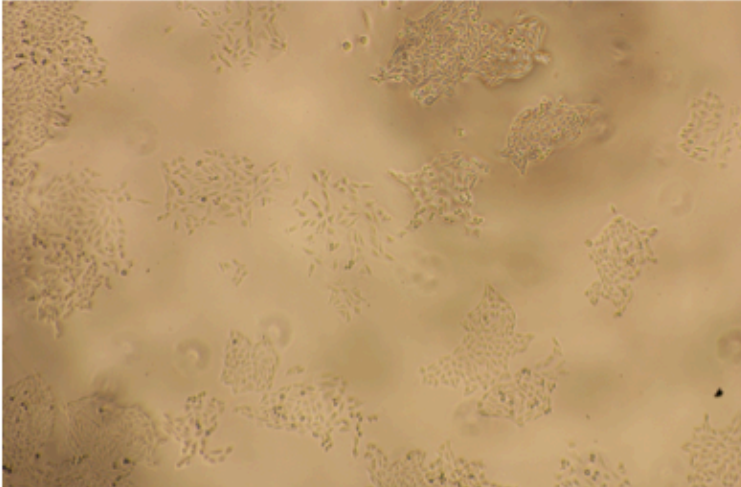
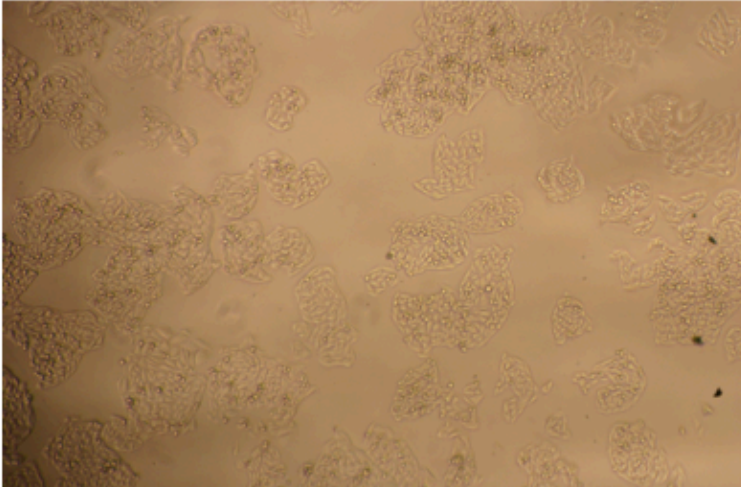
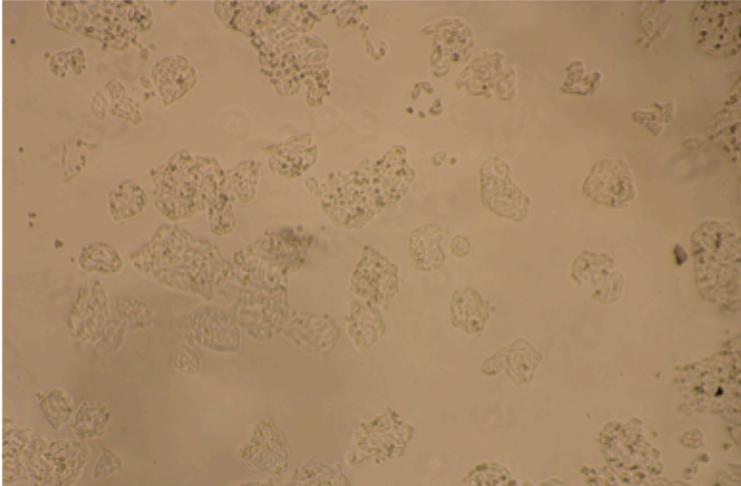
To confirm that the results obtained for the PT/PVP Matrix were not due to chance we employed the nonparametric binomial test. Results showed that the score of 1 observed for the PT/PVP Matrix rejects the null hypothesis that the scores of 0 or 1

were equally likely to happen ( $p=0.03$ ). Although the PT Liquid Formulation data are in the same direction, the  $n=4$  wasn't enough to reach significance using the binomial test.



**Figure 4.9** Average MTS viability assay absorbance reading after the 24-hour PT delivery study ( $n=4$  for UTC and PTSolution;  $n=6$  PT/PVP Matrix).

To confirm that the tissue viability was not compromised during the delivery we compared the absorbance values across the groups using the nonparametric Kruskal-Wallis Test. The values were not significantly different from each other ( $p=0.28$ ), suggesting that the tissue was not compromised during the delivery.

| Clumping score | Representative Image   | Sample                  |
|----------------|--|-------------------------|
| 0              |    | EPI-100 Media           |
| 1              |   | Dissolved PT/PVP Matrix |
| 2              |  | PT Solution Standard    |

**Figure 4.10** Representative images of the CHO cell clumping observed in the presence of the PT samples.

## DISCUSSION

The chief objective of this study was to evaluate the efficacy of the novel nanofibrous matrix to transport biologically functional antigen-like macromolecules into and across the commercially available tissue engineered human skin models. After a 24-hour administration of the nanocomposite HRP/PVP matrix we were able to detect 51% of the enzyme load in the media underlying the full thickness skin model. The process of tissue pulverization accounted for the remaining HRP load embedded within the tissue. The alamar blue cell viability assay detected no significant reduction in viability of HRP/PVP matrix laden tissues to that of untreated control units. The successful transport of the 44kDa enzyme across the full thickness tissue engineered human skin model led to experimentation with a potential antigen. The 117 kDa, pertussis toxin (PT) was encapsulated within a nanocomposite PT/PVP matrix, and applied to the EPI-200 tissue engineered model of human epidermis for a 24-hour time period. The underlying media as well as the liquid separated from pulverized tissue units resulted in the characteristic clumping of CHO cells observed in the presence of functional PT. The viability of the tissue units was not compromised by the PT/PVP matrix application as confirmed by the MTS assay.

Skin, as the largest organ of the human body, protects internal organs and tissues by posing an impermeable membrane to toxins, disease-carrying bacteria and viruses with its structure and composition [13]. Its outermost layer, the stratum corneum, is composed of tightly packed cornified keratinocyte lamellae cemented with lipid mortar. The 10-20  $\mu\text{m}$  thick SC successfully limits penetration of fluids, large molecules, particles and microbes to the underlying epidermis. The prominent

presence of the primary antigen-presenting cells (APC), the Langerhans cells (LC), in the epidermal layer renders it a principal target for vaccine delivery. The transport of antigens into the immunocompetent regions of the skin has been limited to technologies that either strip or puncture the SC structure [14-28].

Our novel immunization patch omits the need for physical force to penetrate the permeation barrier posed by the skin, and instead exploits the transepidermal water loss mechanics of the temporary accordion-like stretching of the SC in the presence of topical, which has been shown to allow the penetration of otherwise inadmissible molecules [132,133]. The commercially available tissue engineered human skin model units utilized in the *in vitro* delivery studies reported here, are housed individually in plastic chambers that allow for topical liquid deposition to stay in place. The observed permeation of both the HRP and PT liquid formulations implies that the skin models emulated the reversible swelling phenomenon documented *in vivo* in the presence of topical hydration. The hypothesized mechanism of antigen delivery from the solid state patches depends on three distinct events. Initially, the occlusive patch must attach to skin, while maximizing the surface area or reactivity between the two. Secondly, the hygroscopic matrix will draw up transepidermal moisture to the outermost layers of the stratum corneum, where it dissolves the nanofibrous patch. Finally, the embedded payload will be released from the hydrated/dissolved matrix, resulting in a large localized concentration gradient expected to aid the thermodynamically favored diffusion of the payload into the skin. Thus the morphology and composition of the novel immunization patch, both played a crucial role in the solid-state matrix's ability to deliver viable macromolecules into the immunocompetent regions of the skin.

The sensitive and cost effective quantitative assay of HRP functionality was the chief proponent for its utility as a primary model for the *in vitro* study of intracutaneous delivery of macromolecules to human skin. Delivery of the enzyme was analyzed in terms of the amount delivered as well as percentage of the expected deposition. The stacked graphs of Fig 4.6 and 4.7 depict group averages for each time point. Although both liquid formulations were expected to deliver equal amounts of the HRP units recovered from the tissue media as well as the pulverized tissue for the electrospinning solution group was half of the pure enzyme formulation. One of the potential explanations of this finding is the viscous nature of the polymer solution, which may have resulted in a repeated pipetting error for the small volume of 10  $\mu$ l. Another possibility is that the organic solvent employed in the polymer formulation may have hindered the functionality of the active enzyme present in solution over the 24 hour incubation period. Many of the commercially available skin patches are composed of dried polymer-based gels [13-24], but as seen in this study as a viscous solution the gelous load was not successful at delivering a large percentage of the load. Due to the size limitation posed by the tissue chambers the HRP/PVP Matrix samples were constrained to applying only one wafer per tissue, thus constituting only 10% of the enzyme load found in either liquid formulation. However the analysis in terms of percent delivery for every time point provided a more insightful picture of the patch's efficacy in delivering viable enzyme into and through the full thickness human skin model. Both liquid formulations as well as the solid-state patch showed very limited (<6%) delivery of the enzyme within the first four hours of the study. Thus implying the tissue model's ability to pose a substantial permeation barrier such as expected of

health human skin. The combined percentages of enzyme delivered at the conclusion of the 24-hour incubation were 54%, 12% and 58% for the HRP Solution, HRP/PVP Solution and HRP/PVP Matrix respectively. With the bulk of the remaining enzyme recovered from the pulverized tissue, except for that of the HRP/PVP Solution units. The 24-hour incubation of the pure HRP solution showed minimal drop in its enzymatic activity/concentration. The secondary goal of this experiment was to evaluate the validity of pairing the matrix wafers by position on the collector. The pairing system proved a reliable indicator for the amount of enzyme collected on each wafer, it further confirmed the estimated 0.2% of total deposition collecting on each wafer, as seen in Fig 4.7. The control HRP/PVP Matrix study confirmed that the dissociation of the nanocomposite material and release of the enzyme in the absence of tissue occurs almost completely within the first four hours upon contact with the media.

The immediate clinical need for an improved pertussis vaccine, and the vast amount of available information, described in the first chapter, rendered the whooping cough immunization an attractive candidate for the *in vitro* proof of principal experiment of cutaneous antigen delivery from the novel immunization patch. Based on the information deduced from the enzyme delivery study we had forgone the earlier collection times and modified the harvest protocol to 24 hours after application and pulverized tissue. The other modification to the delivery study was to change from the full thickness to the EpiDerm™ human skin constructs, since epidermis is the primary target for antigen delivery. To assess the presence of viable toxin we employed the highly sensitive, qualitative *in vitro* assay, explained in length in Specific Aim 2. In short, under normal culture conditions the adherent CHO cells proliferate in sprawling



monolayers, as seen in Figure 4.10 cultured with the EPI-100 media, however in the presence of functional PT the cells lose contact inhibition and within 24-48 hours form compact clusters, as depicted by the lower two images of Figure 4.10. To further enhance the qualitative assay, we adapted an interval scale of grading, from 0 to 2. The lowest score meant no visible cell clusters, the score of 1 was given wells that presented some clusters, and finally the score of 2 was given to wells, where clusters were the predominant cell morphology. To ensure the integrity of the CHO cell assay, each plate contained duplicate stock PT dilutions ranging from 6.25-50.0 ng/ml, where the concentrations of 6.25 and 12.5 ng/ml resulted in a score of 1, while the higher PT concentrations were assigned the score of 2. The grading scale also served as a rough correlate for the amount of PT extracted from the subjacent media as well as the homogenized tissue units. To confirm the presence of viable PT released from the PT/PVP Matrix we dissolved a number of control wafers and dosed the liquid onto the CHO cells along side the other test samples. Based on the 0.2% per wafer deposition model, the expected amount of PT collection was calculated to be 37.5 ng per wafer resulting in a PT concentration of 25 ng/ml in EPI-100 media, CHO clustering of 2. The score of 1, observed for the PT Solution and PT/PVP Matrix formulations used in the tissue delivery study suggests levels of recovered PT lower than the expected 37.5 nanograms. The similar levels of clustering observed for both formulations which were prepared to present equal amounts of PT to the tissue samples, suggests that the reduction in the amount of active PT was an experimental error. One of the potential sources of error may have been the pulverization step. Due to PT's affinity to plastic surfaces, we employed glass vials, which did not allow for centrifugation and instead

required slow sedimentation of the homogenized tissue. The subjective nature of the CHO cell assay assessment presents a potential for misgraded samples due to human error.

To evaluate the cytotoxic effects the novel immunization patch had on human skin constructs we employed two different cell viability assays [135]. The integrity of the EpiDermFT™ models was assessed at the conclusion of the 24-hour HRP delivery study using the alamar blue assay. The assay measured the presence of fluorescent resorufin product that results from the reduction of resazurin, the active ingredient of the alamar blue assay, by the healthy cells [135]. The comparison of fluorescence levels detected for the untreated control units to that of enzyme laden tissue samples, both liquid formulations as well as the novel HRP/PVP matrix was presented in Fig4.7 showed no significant decline in the absorbance across the test groups. Viability of EpiDerm™ units employed in the PT delivery study was assessed using the non-lytic MTS assay. Metabolic activity of the cells was measured through the reduction of tetrazolium salt to the colorimetric product, formazan. As demonstrated in Figure 4.9 the absorption levels across all of the test groups were unvarying, between the untreated units to those of laden tissue samples, both in the liquid formulation as well as the novel PT/PVP matrix. The results of the non-lytic viability assays employed in both of the delivery studies suggest that the surface contact with the novel immunization patch presents no cytotoxic effect on the human skin cells present in the MatTek tissue samples.

The novel nanofibrous matrix developed as an innovative intradermal immunization patch was shown to successfully transport two biologically functional

macromolecules into and across the commercially available tissue engineered human skin models. 24-hour administration of the HRP containing patch resulted in over half of the enzyme load penetrating the full thickness skin model, without a detectable drop in tissue viability as measured by the alamar blue assay. 24-hour administration of the PT laden patch resulted in detectable amounts of the antigen present in the media subjacent to the epidermis human skin model, as well as in the homogenized tissue. Both *in vitro* delivery studies render the patch an attractive painless method of macromolecule delivery that circumvents the need for physical disruption of the skin's barrier. Utilization of engineered human skin equivalents offered a high throughput *in vitro* permeability comparison without the complications arising from natural variability of cadaveric human skin samples reported in experiments using Franz cells as experimental assay tools. The quality control of the skin models and limited variability between tissue units offers a more practical strategy for patch optimization than would be possible with individual Boyden chamber-like units utilized with cadaveric skin. The *in vitro* approach also reduces reliance on animal testing and furthermore lowers the costs of acquiring and maintaining the test subjects.

## Chapter 5

### *Specific Aim 4*

## **Specific Aim IV**

*To evaluate the efficacy of the proposed whooping cough vaccine in vivo in the Sprague-Dawley rat model.*

## **INTRODUCTION**

The largest organ of the human body, the skin, has evolved into an immunocompetent structure that is capable of launching a systemic response to pathogens delivered in situ. The large population of resident antigen presenting cells (APCs) captures and processes the delivered antigens as part of the innate immune response [136]. Upon presentation of the immunogens to naïve T and B cells in draining lymph nodes a specific adaptive response to the delivered antigens follows [137]. This adaptive response may be detected as the appearance of specific circulating antibodies at a rate that can equal or exceed that triggered by delivery of antigen via intramuscular injection. Lower doses of immunogens delivered into the APC-rich layers of the skin have been shown to elicit an immune response comparable to that achieved with intramuscular injection [138, 139].

To date the challenge of needle-less dermal delivery has been addressed by a variety of techniques that temporarily overcome the skin's permeability barrier, the impermeable "brick and mortar" outer layer of the stratum corneum (SC) [131, 132]. Currently explored innovations that either strip or puncture the SC present a more practical option than the Mantoux injection method; however, their use during a spreading pandemic is limited by the logistical challenges they present. The costly

production, multistep administration, as well as issues similar to those faced with administering intramuscular injections, such as, mobilization of trained personnel to carry out or supervise the procedures, biohazardous waste disposal to prevent blood borne pathogen transmission as well as no reported improvement of formulation stabilization than that of liquid injections [13-24]. The intradermal antigen delivery platform offered here is based on electrospun nanofibrous antigen-laden matrices. It represents a single step, painless and convenient strategy for patient administered immunizations. Additional logistical advantages of the proposed system result from its formulation as a solid-state material that require less stringent storage conditions, and simplified transport and disposal. The patient administered patch eliminates the necessity for highly trained medical personnel and therefore offers an expeditious immunization of large populations.

Several of the immunization platforms described by others and summarized in Chapter 1, have been employed for delivery of antigens *in vivo*, utilizing animal models. The above highlighted technologies were all intended to deliver various antigens into the skin of different animal models. Some of the animals employed include, but are not limited to, mice, rats, hairless guinea pigs, and rabbits. The lack of consensus on the appropriate animal model to be used for intradermal antigen delivery makes cross comparison between the studies very problematic. Based on the similarities in thickness of the SC and the epidermis between rat skin and human skin, it is believed that tissues from the two sources share similar permeation rates. This project will employ a depilated immunologically intact rat model in evaluating the efficacy of the proposed whooping cough intradermal vaccine.

Pertussis toxin (PT), secreted by *Bordetella pertussis*, is considered to be the major causative agent in the pathogenesis of whooping cough [58-92]. Long-term immunity against the disease is said to be dependent on circulating PT-neutralizing antibodies. The current resurgence of whooping cough in the general population is said to be a result of multiple causes: the suboptimal quality of the traditional vaccine, cyclic variations in the pattern of exposure to *B. pertussis*, and emergence of new strains of the bacterium that are no longer effectively cleared by the immune mechanisms mobilized by classic vaccination protocols. We have demonstrated successful encapsulation of active pertussis toxin within an electrospun polyvinylpyrrolidone nanofibrous matrix as described in Specific Aim 1. Furthermore, we confirmed retention of biological functionality throughout the electrospinning process, as described in Specific Aim 2, and successfully delivered the toxin into organotypic human skin, as described in Specific Aim 3. The obtained results substantiated our selection of pertussis toxin (PT) as an optimal model antigen for the “proof of principle” *in vivo* immunization study. To evaluate the efficacy of the novel immunization platform to generate the levels of anti-PT antibodies comparable to that of the intramuscular injection without adverse local reactions at the patch site in depilated Sprague-Dawley rats.

## **MATERIALS AND METHODS**

### *Solutions*

The polymer carrier solution consisted of polyvinyl pyrrolidone (PVP) M.W.~1,300,000 g/mol [Sigma-Aldrich, Milwaukee, WI] prepared as a 0.075 mM solution in absolute ethanol (EtOH).

Lyophilized pertussis toxin, obtained from List Biological Labs [Campbell, CA], was reconstituted to a stock concentration of 143 ng/ $\mu$ l in sterile Hank's Buffered Saline Solution (HBSS) [Gibco, Grand Island, NY].

The electrospinning solution with a final PT concentration of 50 ng/ $\mu$ l, was prepared as follows:

- 35% by volume PT (143 ng/ $\mu$ l) - 490  $\mu$ l
- 65% by volume PVP (0.075mM in EtOH) – 910  $\mu$ l.

### *The animal model*

The animal model chosen for this study was the Sprague-Dawley rat. 10-week old Sprague Dawley male rats from Charles River Laboratories (Wilmington, MA), weighing approximately 300 grams, were randomly selected and divided into two groups of five: animals in the first group received PT via intramuscular injection while animals in the second group received PT administered via our "PT-Patch." To aid in identification, the animals were marked at the base of their tails and housed individually throughout the course of the study. Proper handling, housing, care, and standard rodent food was given to the animals according to the guidelines posted by Stony



Brook's Institutional Animal Care and Use Committee (IACUC) and Stony Brook's Division of Laboratory Resources (DLAR).

### *Intramuscular injection*

The intramuscular injection solution was prepared via a dilution of stock PT to a final concentration of 9.6 ng/ $\mu$ l of PT in sterile HBSS; each dose of 100  $\mu$ l, containing 960 ng of PT, was injected directly into the quadriceps muscle of the hind leg using a 25-gauge needle.

### *Patch Design*

Based on a conservative estimate for deposition (Specific Aim 1), we have concluded that approximately 80% of electrospun payload solution accumulates on the aluminum foil-wrapped 8x10 cm target plate. Since each of the 4x4 mm silicon wafers [Silex Microsystems, Boston, MA] utilized for the patch occupies 0.2% of the target's total surface area, it can be deduced that approximately 0.2% of the total electrospun solution would be deposited on each of the eighty wafers attached to the foil.

The electrospinning solution was magnetically stirred for five minutes before being placed into a glass syringe, and placed into the programmable syringe pump. The PT/PVP coating was generated by ejecting 1000  $\mu$ l of the electrospinning solution at a flow rate of 20  $\mu$ l/min into an electric field of 1.7 kV/cm with a 10 cm distance between the needle and the target. The process was paused for 1 minute at 10 minute intervals to enhance deposition.



**Figure 5.1.** Silicon wafers attached to aluminum foil to be wrapped over the target plate of the electrospinning apparatus.

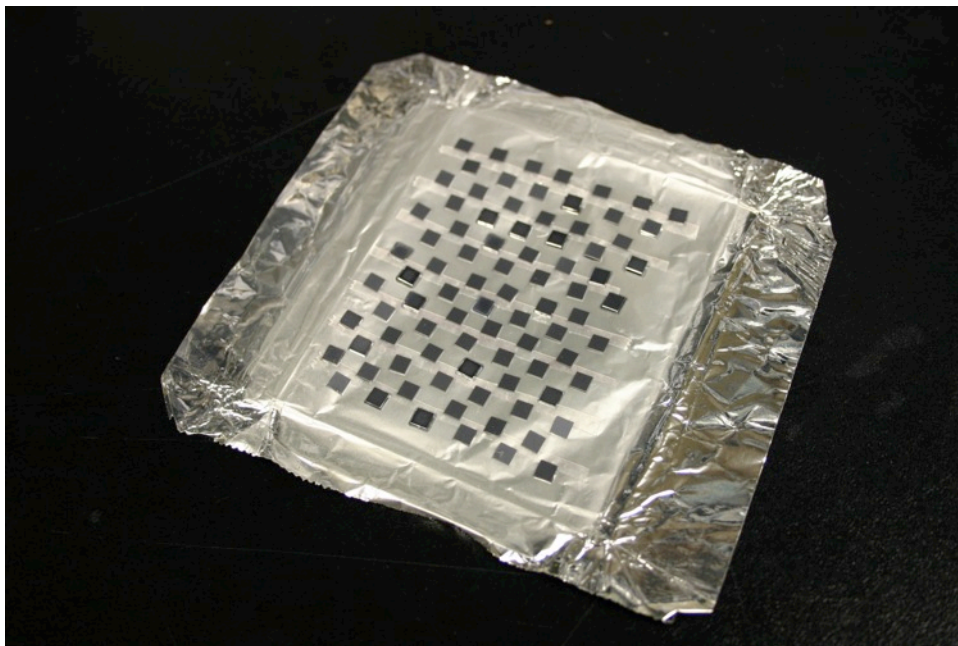


**Figure 5.2.** Electrospun PT/PVP matrix collected on the wafers.

The amount of PT collected on each wafer has been correlated to its surface area. The 4x4mm wafer occupies 0.2% of the collector's area. The parameters utilized for electrospinning of the composite have been observed to result in an 80% deposition

rate of material on the collection plate. A total of 40,000ng of PT accumulated on the entire foil, indicating that each silicon wafer coating contained approximately 80ng of PT.

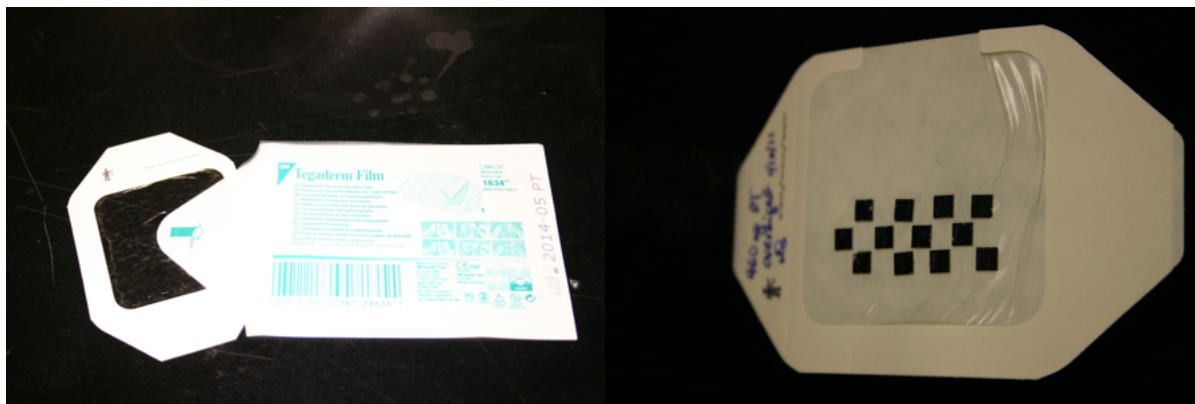


**Figure 5.3.** The PT-patch; 12 silicon wafers attached to Tegaderm.

The PT-Patch was constructed by adhering 12 PT-PVP wafers to a Tegaderm transparent film dressing [3M, Saint Paul, Minnesota]. The waterproof dressing is said to allow for water vapor and oxygen exchange while providing a barrier to bacterial and viral contamination. The wafers were attached in a staggered formation of three rows with four wafers each, to maximize adhesion between the skin and patch. The patch was then returned to its packaging and stored in an airtight plastic container with desiccant until it was attached to the animal's back, approximately one hour later.

### *Blood collection and immunization*

The animals were sedated using isoflurane inhalation anesthesia for each blood collection and vaccine administration. All of the animals were immunized on days 0 and 21. Blood samples were obtained using the retro-orbital method prior to the initial

immunization, and again on days 14, 28 and 42. All whole blood samples were collected into 1cc blood collection vials, and centrifuged at 3000 rpm for 10 minutes. Approximately 200µl of plasma was obtained from each sample and was divided into 20 µl aliquots and stored at -20°C to allow for simultaneous determination of antibody titers.



**Figure 5.4.** The PT-patch after application to the depilated dorsal surface of a rat; the sturdy backing material on the Tegaderm film was removed once the film was applied to each animal's back.

The PT-patches were applied immediately after blood collection on days 0 and 21. The dorsal surface of each animal receiving a PT-patch was shaved with an electric razor to remove bulk of the hair, and further depilated with an application of Nair hair-removing cream “for sensitive skin.” The skin was then cleaned with wet gauze to remove any excess cream. Prior to application of the PT-Patch, the skin surface was cleaned with 70% isopropyl alcohol wipes and allowed to dry. After application to the dorsal surface, the patch was bandaged over with Vetwrap to protect it from the

grooming efforts of the animals. To further discourage the grooming efforts we taped over the animals' feet to prevent them from removing the patch. The patch, bandage and tape were left in place for 24 hours after application.



**Figure 5.5.** The PT-patch bandaged over with a Vetwrap.

After removal of the patch, the site was wiped clean with sterile saline to remove any residual material. A secondary goal of this study was to evaluate any local responses of the skin at the application site upon removal of the patch and bandage. The immunization site was photographed and qualitatively examined for signs of edema and erythema at the site within fifteen minutes after patch removal, as well as 1, 3, and 7 days after each administration.

### *Serology*

The body's ability to produce neutralizing antibodies to a delivered immunogen has been established as a highly relevant measurement of effective delivery of the antigen to the immunocompetent layers of the skin. The sera obtained at the previously

mentioned time points were analyzed for a humoral response in rats by a custom designed enzyme linked immunosorbent assay (ELISA).

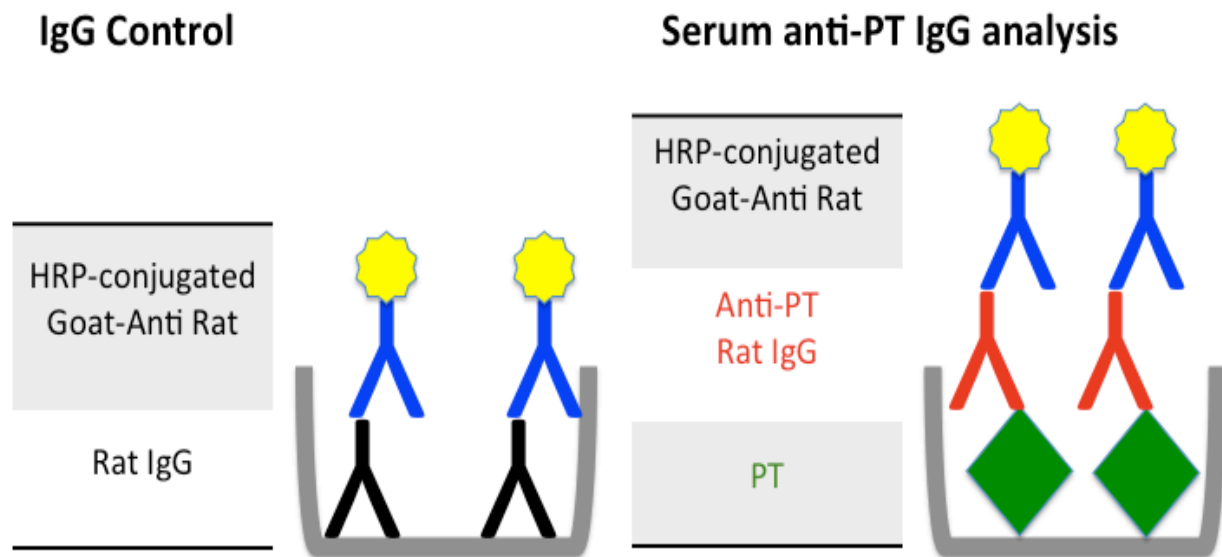


**Figure 5.6.** Schematic representation of the PT ELISA design.

The ELISAs were carried out in 96-well plates [BD Biosciences, Franklin Lakes, NJ]. The wells were coated with 200  $\mu$ l aliquots of either PT antigen used for immunization (150 ng/well) or a serial dilution of control Rat IgG antibody in PBS at the concentrations of 0, 0.005, 0.075, 0.150, 0.225, 0.300, 0.375, 0.450 and 0.600 ng/ $\mu$ l, and incubated overnight on a plate shaker at room temperature. Next day the antigen was dumped, and after three washes with PBS the plate wells were blocked with 200  $\mu$ l of 20% BSA-PBS for three hours on a plate shaker. Once the blocking step was completed, the plate was washed three times with 0.01% Tween-PBS and once with PBS. The next step was to allow capture of any anti-PT antibodies in the serum

samples, which was achieved by a two hour incubation of 100  $\mu$ l of a 1:100 serum dilution in 4% BSA-PBS added to each washed PT well. The contents of the plate were once again dumped and the plate was washed three times with 0.01% Tween-PBS and once with PBS. Quantitation of the captured anti-PT antibodies was achieved by incubating each well with 100  $\mu$ l of peroxidase-conjugated AffiniPure Goat Anti-Rat IgG (H+L) [Jackson ImmunoResearch Laboratories, West Grove, Pennsylvania] at a dilution of 1:5000 in 4% BSA-PBS for one hour. The plate was once again washed and then incubated for 30 minutes with 100  $\mu$ l of stabilized tetramethylbenzidine (TMB) substrate [Pierce; Rockford, IL], followed by an addition of 100  $\mu$ l of 2M sulfuric acid to stop the reaction and convert the product to its final yellow color. Measurements of optical density were taken at a wavelength of 650 nm for the kinetic reaction of the conjugated peroxidase with TMB over a time course of 30 minutes, followed by a second read at 450 nm for the end point.

### *Statistical Analysis*

All of the data used for statistical evaluations were checked for normality and equality of variance, using the Shapiro-Wilk and Levene's tests, followed by appropriate tests for the given experiment. All statistical tests were performed using SPSS software [IBM, Somers, NY] assuming a significance level of  $p < 0.05$ .

Each test group consisted of five animals. To assess the changes of IgG titer levels across time points within each group we employed the nonparametric Friedman's test. To compare two time points, the Wilcoxon Signed Rank Test was used.

## RESULTS

The reference Rat IgG ELISA standards produced a linear regression line with the formula of  $y=7.119x-0.263$  and a coefficient of determination of 0.97107.

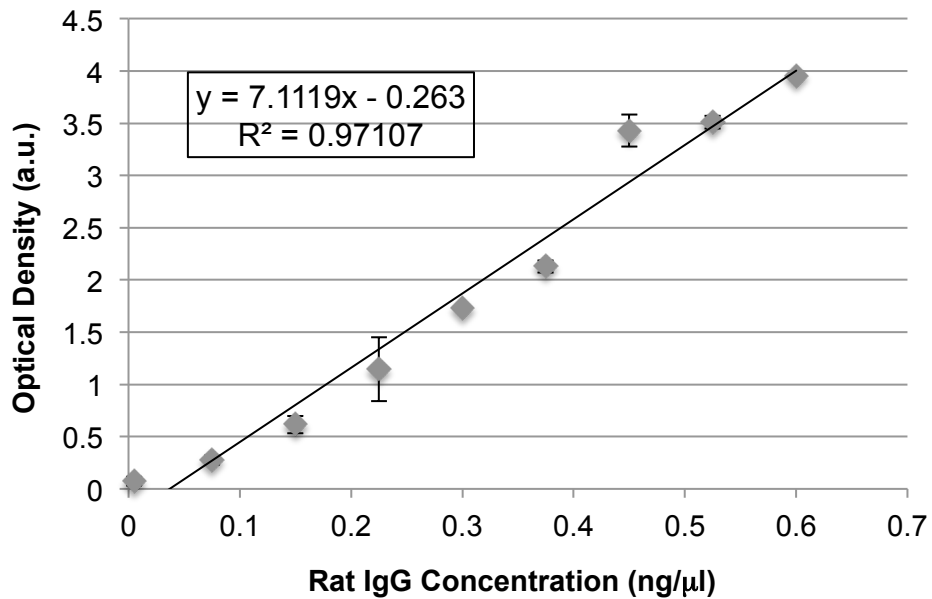


**Figure 5.7.** Rat IgG standard curve.

The obtained formula was then utilized to convert the optical density values observed for the study sera to calculate Anti-PT IgG concentrations. The data were corrected for the baseline values for any anti-PT IgG detected prior to the initial immunization. The error bars depicted show the variation between the duplicate wells of the ELISA.



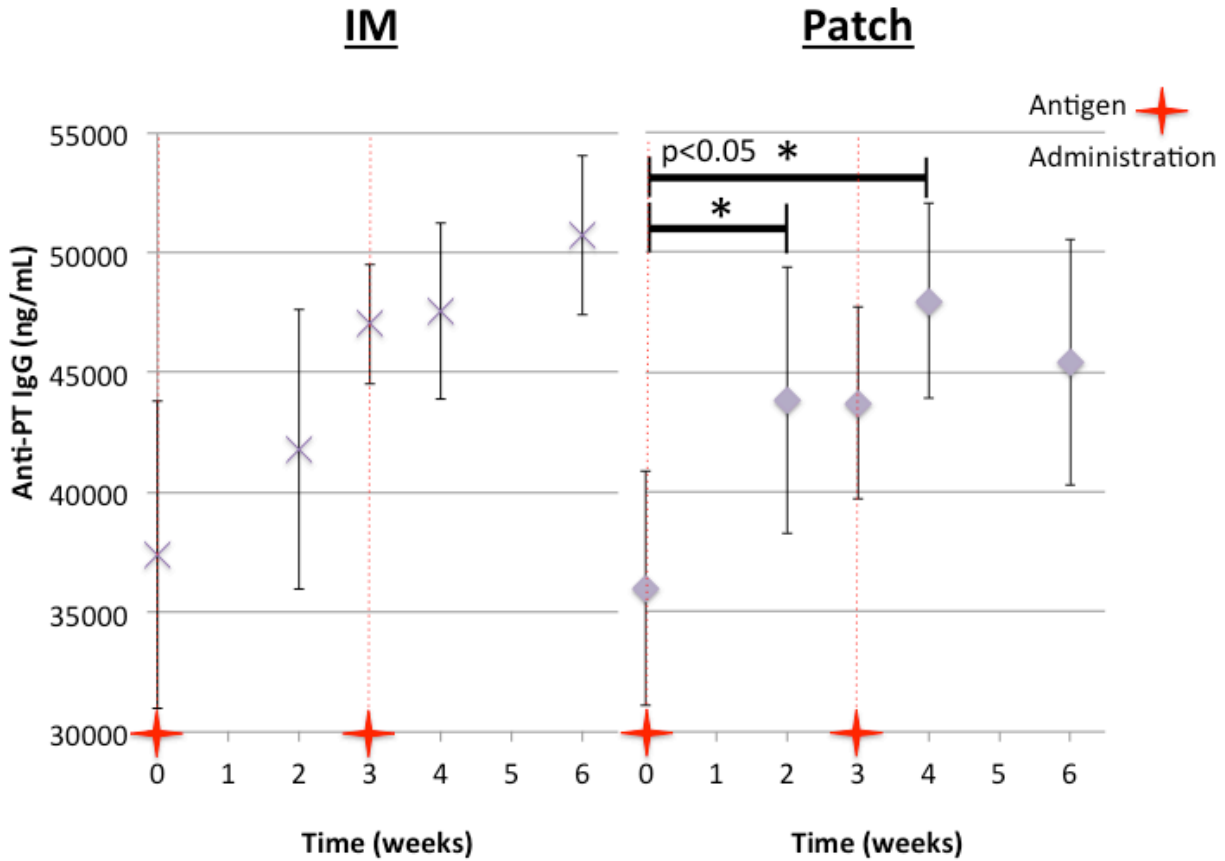


**Figure 5.8.** Mean ( $\pm$ SEM) anti-PT IgG levels in rats receiving PT either via intramuscular injection (IM) or the PT-Patch (n=5 for both groups). The blood collection occurred prior to the antigen administration at weeks 0 and 3.

An overall comparison of the time points within each group indicated that the values obtained for the PT-Patch (Friedman's test,  $p=0.05$ ) but not the IM injection ( $p=0.28$ ) changed significantly over time. To understand which time points differed from each other we performed the Wilcoxon Signed Rank Test. The PT-Patch values increased significantly from week 0 to week 2 and from week 0 to week 4 ( $p<0.05$ ). The PT-Patch values also tended to increase from week 0 to 3, 2 to 4, and 3 to 4 ( $p=0.08$ ). A trend was also observed for the intramuscular injection group; IgG levels tended to be higher after 6 weeks compared to 3 weeks ( $p=0.08$ ).

The secondary goal of this study was to evaluate the local skin tolerance to the occlusive patch. Images were taken immediately after patch removal.

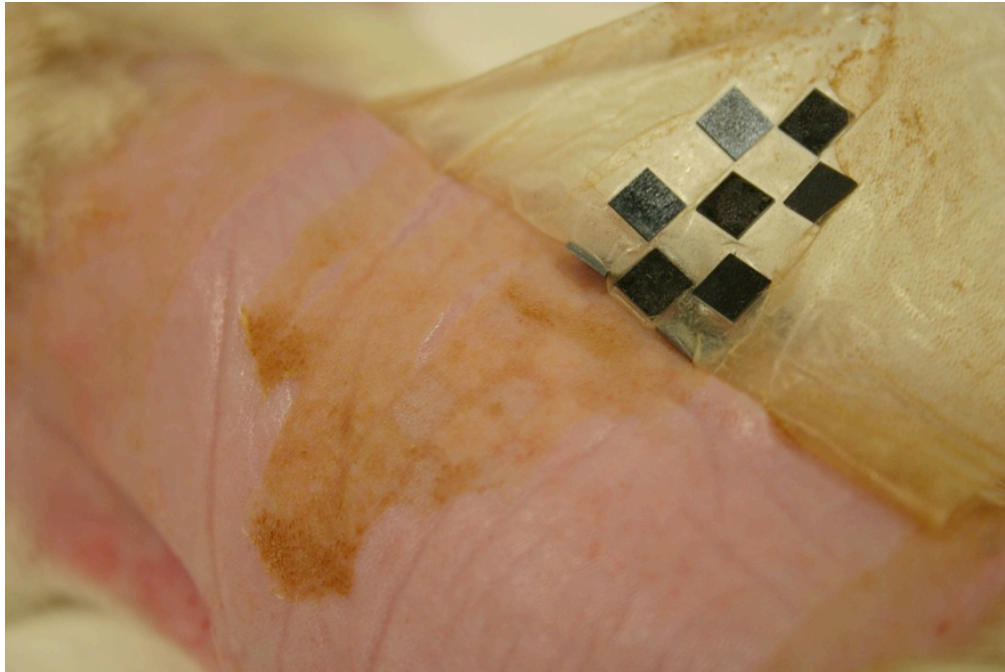


**Figure 5.9.** The PT-Patch being removed from the animal's back after a 24 hour occlusion.



**Figure 5.10.** The PT-Patch freshly removed from the animal post experiment.

## DISCUSSION

The chief objective of this study was to evaluate the efficacy of the novel immunization platform to deliver pertussis toxin to the immunocompetent regions of the skin and to generate production of antigen specific antibodies without adverse local reactions at the patch site. The nanocomposite PT-Patch administered for 24 hours on days 0 and 21 evoked a significant humoral response in the Sprague-Dawley rat model with mean anti-PT IgG concentrations comparable to those triggered by intramuscular injection of the antigen. The change in anti-PT antibody concentrations increased significantly in response to each PT-Patch administration, and were more robust than those observed for IM animals. Clinically employed wound dressing, Tegaderm adhesive film, used as the occlusive backing on the PT-Patch, appeared to leave the animal skin with limited temporary irritation, but the silicon wafers onto which the PT-PVP nanocomposite was deposited provoked no visible reaction.

Human skin defends against foreign pathogens both physically, with the barrier posed by its architecture, as well as immunologically, with the large population of resident antigen presenting cells (APCs) [5-10]. It has been reported that lower doses of immunogens delivered into the APC-rich layers of the skin can elicit an immune response comparable to that achieved with intramuscular injection [149, 150]. Because of this robust immune response, intradermal delivery of antigens has been seen as an attractive alternative method of rapid distribution of easily administered vaccines to large populations under the time constraints of a spreading pandemic [10-13]. A major challenge for intradermal delivery of antigens to the intrinsically immunocompetent epidermis has been the effective barrier the structure of the skin poses to antigen entry.

The four competing technologies reported in the literature all attempted to overcome the permeability barrier presented by the SC via mechanical disruption, as summarized by Table 5.1

| <u>IS™ Patch</u>  | <u>MACROFLUX®</u>                      | <u>SSBMS</u>  | <u>PVP<br/>MICRONEEDLES</u>  |
|---|--|---|--|
| Abrasion with a pumice pad or emery paper and tape stripping. | 200-650 μm titanium microneedle array. | A spring-loaded high velocity impactor with 200μm dissolvable microneedles. | 650μm antigen containing polyvinyl pyrrolidone (PVP) microneedles. |

**Table 5.1.** Methods of physical disruption of the SC used by competing technologies.

All of the newly developed methods have generated immune responses to their delivered antigens. However the technologies have not reduced the need for costly design, production, and disposal of the materials used in vaccination protocols. The vaccine patch developed in this study offers an attractive solution to the logistical problems associated with the competing technologies.

Gillenius et al. reported generation of PT neutralizing antibodies in mice, guinea pigs and rabbits after intraperitoneal immunization with pertussis toxin. To date there are no *in vivo* studies that employ intradermal delivery of pertussis toxin. The variety of animal models utilized for the *in vivo* evaluation of the competing technologies discussed above, has rendered cross comparisons among the studies very problematic; however all of the reported work compares titer levels obtained via the proposed platform to that obtained with intramuscular injection of an equivalent amount of antigen.

The so-called “universal immunostimulating” IS™ patch [Iomai, MD, USA] has been employed with adjuvants such as cholera toxin (CT) or heat-labile enterotoxin (LT) and has been shown to induce systemic immune responses in animal and human subjects [13-15]. Aided by the physical disruption of the skin, delivery of vaccine by patch achieved an enhanced immune response using transcutaneous delivery that resulted in antibody levels comparable to those observed after delivery of the vaccine by injection. The Macroflux patch of titanium microneedles coated with ovalbumin was used to deliver an antigen to hairless guinea pigs, resulting in a specific immune response comparable to that achieved after intramuscular injection [25]. The spring-loaded high velocity impactor device that was employed to drive a solid-state biodegradable microstructure (SSBMS) array loaded with levels of antigen equal to those used for intramuscular injection resulted in generation of IgG levels in the host animal superior to those achieved by IM injection [27]. Finally, the dissolvable, 650µm antigen-containing polyvinyl pyrrolidone (PVP) microneedle patch employed to deliver influenza antigen intradermally into mice successfully induced a humoral response in the test animals [28]. Antibody levels were initially slightly lower than those induced by intramuscular injection of an equivalent quantity of antigen, but by day 28 the titers were comparable to those induced by injection.

The mean anti-PT IgG values were measured in serum samples collected prior to the initial and booster immunization at weeks 0 and 3 as well as at weeks 2, 4 and 6. The anti-PT IgG levels observed for the novel PT-PVP Patch were compared to those measured in animals receiving two doses of antigen via intramuscular injection. The time points were selected to capture both the primary and secondary immune

responses as well as to relate the findings to those found in literature. The time course for the immune response, presented in Figure 5.8, showed that the antibody levels achieved by application of the PT-Patch were comparable to those induced by intramuscular vaccination. Each application of the PT-Patch resulted in a robust response, faster than that triggered by the standard route of inoculation. Furthermore the increase in the antibody levels observed for the Patch group achieved statistical significance 2 weeks after the initial administration, and 1 week after the booster administration at 3 weeks. The rapid response observed in the rats receiving the PT-Patch may reflect the involvement of the large numbers of APC residing in the epidermis of the animals that are preferentially mobilized by the intradermal delivery protocol to capture antigens [147]. It has been established that activated or migrating dendritic cells undergo a sequence of steps in the course of phenotypic and functional maturation that can be detected as unregulated levels of cell surface markers, including major histocompatibility complex I and II (MHC I and II), and co-stimulatory molecules such as inflammatory cytokines [16]. These APC amplify the immune response via priming and differentiation of CD8<sup>+</sup> T cells into effector cells and also activate the adaptive immune response mediated by CD4<sup>+</sup> T cells, which in turn promote production and release of antigen-specific antibodies by B cells. The chain of activation events eventually results in establishment of a population of antigen-specific memory B cells.

The novel immunization platform evaluated in this study circumvents the need for mechanical disruption of the skin's outermost layer by exploiting its ability to swell and contract during the naturally observed transport of liquids within the epidermis. The unmatched surface area to volume ratio offered by the electrospun nanofibrous matrix

enhances skin contact with the patch, while its hygroscopic composition tends to draw up epidermal fluid, which then releases the reversibly encapsulated payload. The previously dehydrated outermost lamellae of the stratum corneum are then put into direct contact with the layer of liquid in which the antigen is dissolved. The favorable concentration gradient of solubilized payload can then effectively facilitate transport of the previously encapsulated proteins through the “brick and mortar anatomy” of the SC [131-134]. In summary, water is transudated through the epidermis, and the resulting local concentration gradient of the released payload drives it across the hydrated (and thus permeable) stratum corneum. The accordion-like mechanism of delivery has been depicted in Figure 5.14.

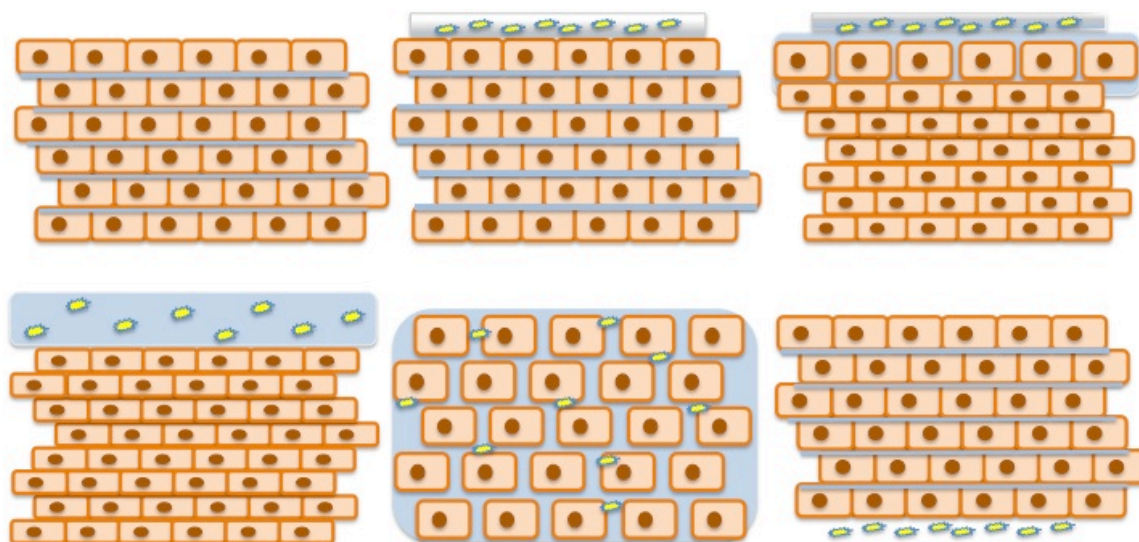


**Figure 5.8.** The proposed mechanism of antigen delivery *in vivo*.

Based on visual observations, we can conclude that that the PT-patch administration site exhibited no local irritation after 24 hours of contact with payload-coated silicon wafers held in place by a conventional occlusive film.

Although specific antibody titer levels provide the most relevant measurement of successful delivery of the immunogen to antigen presenting cells in this animal model, such specific antibody levels might not be equated to levels of protection from disease. Moreover, it would be highly premature to conclude that positive results found in rats would also hold true for human subject studies. Nevertheless, this study provides meaningful insight into the efficacy of the novel immunization platform.

In conclusion, this study has established the efficacy of the novel immunization platform to successfully deliver pertussis toxin to the immunocompetent regions of the skin, and result in a more robust production of antigen specific antibodies than that achieved via an intramuscular injection. The nanocomposite PT-Patch applied to the skin for 24 hours on day 0 and again on day 21 evoked a significant humoral response in the Sprague Dawley rat model with mean anti-PT IgG concentration levels comparable to those elicited by intramuscular injection of the antigen. The novel PT-Patch was applied to the animal skin for 24 hours without adverse local reactions to the occlusive patch.



## Chapter 6

### *Conclusions and Limitations*

The integumentary system's immunocompetence has been said to allow for significantly lowered antigen doses to achieve an immune response comparable to that achieved by intramuscular injection, thus allowing protection of larger population sectors with lower amounts of precious vaccines. Recently, innovative immunization methods have concentrated on various forms of mechanical disruption of the stratum corneum to effectively deliver the antigen to the immunocompetent regions of the skin. Ranging from physical abrasion to puncture penetration, each of the described solutions complicates the design, and cost for production and distribution of the vaccination product, and still requires training of patients and health care providers. In addition, the proper disposal of biohazardous materials to avoid blood borne pathogen spread may become more crucial during a pandemic threat. The waste generated by the use of metal microneedle arrays in some of the currently proposed devices would simply substitute, replace, or add to the amount of waste produced by the current disposal of conventional hypodermic needles. Other explored methods of administration, such as high velocity spring loaded impactors or a multistep skin treatment prior to administration, add more complexity to the system and therefore present the potential for lower patient compliance and suboptimal utilization by health care providers. The long-term goal of this study is to generate a novel antigen delivery platform that will aim to eradicate some of the stringent requirements posed by the use of traditional liquid formulations for immunizations.

The objective of Specific Aim 1 was to optimize the electrospinning process parameters for synthesis of nanofibrous matrices of a model macromolecule, horseradish peroxidase. The chief limitation of this study was the assumption that the

variations in payload and polymer solutions employed would have a miniscule effect on the solubility profile for the nanocomposite matrix obtained. The aim evaluated solubilization and release of only one payload, however the sensitive, direct and cost effective quantification assay for HRP allowed for simple and reproducible protocols of evaluating dissolution for each of the macromolecules. The second limitation was the initial attempt at evaluating the novel matrices' solubility in bulk scale. It was anticipated that the small quantities of deposited payload on the silicon wafers in comparison to the solvent used for washing may not adequately showcase the impressive solubility of electrospun nanofibrous matrices applied directly to the skin, as is expected to occur upon close contact with the SC, however the bulk dissolution of HRP from the PVP matrix confirmed the preservation of enzymatic activity throughout the process of electrospinning. We established that the most favorable mixture for HRP deposition was 20% HRP – 80% 0.075 mM, it resulted in a collection of 92% of the electrospun enzyme on the collector. The bolus release of HRP in the presence of a large volume led to the development of a novel protocol for release, which utilized a 0.4  $\mu\text{m}$  PCF Millicell® tissue sample holder to create a barrier between the electrospun coating and available moisture. The developed setup resulted in a slow release of the enzyme from the electrospun wafers during a 2 hour time period. SEM analysis of the electrospun enzyme matrices presented an average diameter of 40nm, presenting with continuous 3D porosity and an advantageous surface area to volume ratio. Lastly we were able to validate the effect of brief pausing on the matrix morphology, i.e. bead formation.

The purpose of Specific Aim 2 was to establish retention of functionality and immunoreactivity for antigens immobilized within a nanofibrous matrix, as well as to

evaluate the long-term storage stability of the antigen-containing matrix. Functionality of Pertussis toxin (PT) evaluated through the highly sensitive CHO cell *in vitro* assay showed preservation of antigen activity in the presence of the polymer vehicle as well as after being solubilized from the electrospun nonwoven nanofibrous matrix. The same assay was employed to evaluate the long-term stability of PT formulated in solution, as a dried PT/PVP coating and finally the novel PT/PVP Matrix. The 20-week observation period successfully showcased the denaturation of the dry coated and solution samples, and established the superior storage capacity of the novel matrix. Scanning electron microscopy evaluation of the matrix morphology confirmed the presence of a highly porous nonwoven mat of fibers with an average diameter of 72 nm. The preservation of the antigen's immunorecognition was established using the 15 amino acid hemagglutinin peptide, widely utilized as an antigen in the already developed avian influenza vaccines. The utilization of the Slot-Blot apparatus allowed for quantification of HA exuded from the dissolved matrix to be within the acceptable range of the expected concentration. The greatest limitation of the study was that functionality and immunoreactivity was not assessed for the same antigen. The antigen functionality assays employed require the use of cellular responses and only allowed for semi-quantitative analysis of the payload, and required the use of an untreated standard to serve as a control to be compared with the experimental samples. The immunoreactivity analysis allowed for a quantitative analysis of immunogen concentration over a limited range, but also demanded that a standard be employed in each trial for comparison to the experimental samples. The long term stability study was only evaluated for two out of the four antigens, PT and PA. The time course and the

selected intervals described above may not be sufficient to precisely monitor payload activity loss.

The chief objective of Specific Aim 3 was to evaluate the efficacy of the novel nanofibrous matrix to transport biologically functional antigen-like macromolecules into and across the commercially available tissue engineered human skin models. Both studies evaluated a 24-hour administration of the nanocomposite matrix. The HRP/PVP patch delivered 51% of the enzyme load into the media underlying the full thickness skin model, and the remainder of the encapsulated HRP was recovered from within the pulverized tissue. The alamar blue cell viability assay detected no significant reduction in viability of HRP/PVP matrix laden tissues to that of untreated control units. The successful transport of the 44kDa enzyme across the full thickness tissue engineered human skin model led to experimentation with the whooping cough antigen. The 117 kDa pertussis toxin (PT) was encapsulated within a nanocomposite PT/PVP matrix, and applied to the EPI-200 tissue engineered model of human epidermis for a 24-hour time period. The underlying media, as well as the liquid separated from pulverized tissue units resulted in the characteristic clumping of CHO cells observed in the presence of functional PT. The viability of the tissue units was not compromised by the PT/PVP matrix application as confirmed by the MTS assay. Utilization of engineered human skin equivalents offers a high throughput *in vitro* alternative for evaluating the release of an antigen payload. Although the employed method offers the advantages of increased reliability, and its application to the evaluative studies proposed here may provide a more efficient means to narrow the range of conditions in future tests, it presents intrinsic limitations. Even though the results offer insight into the antigen delivery

profiles from electrospun nanofiber mats containing horseradish peroxidase or pertussis toxin, the data obtained cannot be directly extended to *in vivo* studies, especially with other payloads.

The main purpose of Specific Aim 4 was to evaluate the efficacy of the novel immunization platform to deliver pertussis toxin to the immunocompetent regions of the skin and to generate production of antigen specific antibodies without adverse local reactions at the patch site. The nanocomposite PT-Patch administered for 24 hours on days 0 and 21 evoked a significant humoral response in the Sprague-Dawley rat model with mean anti-PT IgG concentrations comparable to those triggered by intramuscular injection of the antigen. The changes in anti-PT antibody concentrations increased significantly in response to each PT-Patch administration, and were more robust than those observed for IM animals. The clinically employed wound dressing Tegaderm adhesive film, used as the occlusive backing on the PT-Patch, appeared to leave the animal skin with limited temporary irritation, but the silicon wafers onto which the PT-PVP nanocomposite was deposited provoked no visible reaction. Although specific antibody titer levels would provide the most relevant measurement of successful delivery of the immunogen to antigen presenting cells in this animal model, such specific antibody levels might not be equated to levels of protection from disease. In conclusion, the proposed study will provide meaningful insight into the efficacy of the novel immunization platform; however, it would be premature to conclude that positive results found in rats would also hold true for human subject studies.

The interdependence of the specific aims carried out in this study posed a potential limitation to the overall success of the proposed study. However, sufficient

alternative approaches developed along the way allowed the study to continue. The successful completion of the outlined study has established the novel immunization platform as a viable solution of a logistically favorable intradermal vaccine. Furthermore, data collected throughout the study have enhanced the fields of electrospinning, encapsulation, immobilized protein stability, applications of organotypic models for *in vitro* delivery and *in vivo* immunization delivery.

## References

1. Balicer, R.D., Huerta, M., Davidvitch, N., Grotto, I., “*Cost benefit of stockpiling drugs for influenza pandemic*”, *Emerging Infectious Diseases*, 11(\*), 2005, p.1280-1282.
2. Renewal of Public Health in Canada, “*Learning from SARS: Renewal of Public Health in Canada*”, Chapter 12, 2003, p.211-214.
3. Rowthorn, R. E., Laxminarayan, R., & Gilligan, C. a. (2009). Optimal control of epidemics in metapopulations. *Journal of the Royal Society, Interface / the Royal Society*, 6(41), 1135–44. doi:10.1098/rsif.2008.0402.
4. Riedel, S., “*Edward Jenner and the history of smallpox and vaccination*”, *Baylor University Medical Center Proceedings*, 18(1), 2005, p.21-25.
5. Merad, M., Ginhoux, F., Collin, M. (2008). “*Origin, homeostasis and function of Langerhans cells and other langerin-expressing dendritic cells*”, *Nature Reviews: Immunology*, 8, 935-945.
6. Bousso, P. (2008). “*T-cell activation by dendritic cells in the lymph node: lessons from the movies*”, *Nature Reviews: Immunology*, 8, 675-684.
7. Batista, F.D., Harwood, N.E. (2009). “*The who, how and where of antigen presentation to B cells*”, *Nature Reviews: Immunology*, 9, 15-27.
8. Roediger, B., Ng, L.G., Smith, A.L., de St Groth, B.F., Weninger, W. (2008). “*Visualizing dendritic cell migration within the skin*”, *Histochem Cell Bio*, 130, 1131-1146.
9. Kaplan, D.H., Kissenpfennig, A., Clausen, B.E. (2008). “*Insights into Langerhans cell function from Langerhans cell ablation models*”, *Eur. J. Immunol.*, 38, 2369- 2376.
10. Baxter, D. (2007). Active and passive immunity, vaccine types, excipients and licensing. *Occupational medicine (Oxford, England)*, 57(8), 552–6. doi:10.1093/occmed/kqm110
11. Website <http://www.textbookofbacteriology.net/immune.html>, November 21, 2010.
12. Stansfield, W.D., “*Serology and Immunology A clinical approach*”, 1981
13. Glenn, G.M., Kenney, R.T., Ellingsworth, L.R., Frech, S.A., Hammond, S.A., Zoetweij, J.P., “*Transcutaneous immunization and immunostimulat strategies:capitalizing on the immunocompetence of the skin*”, *Expert Review of Vaccines*, 2 (2), 2003
14. Glenn, G.M., Kenney, R.T., Hammond, S.A., Ellingsowrth, L.R., “*Transcutaneous immunization and immunostimulant strategies*”, *Immunology and Allergy Clinics of*



- North America, 23, 2003, p.787-813.
15. Glenn, Gregory M, Kenney, R. T., Hammond, S. a, & Ellingsworth, L. R. (2003). Transcutaneous immunization and immunostimulant strategies. *Immunology and Allergy Clinics of North America*, 23(4), 787–813. doi:10.1016/S0889-8561(03)00094-8
  16. Angel, C.E., George, E., Ostrovsky, L.L., Dunbar, P.R., “*Comprehensive analysis of MHC-II expression in healthy human skin*”, *Immunological Cell Biology*, 85(5), 2007, 363-369.
  17. Auewarakul, P., Kositanont, U., Sornsathapornkul, P., Tthong, P., Kanyok, R.,Thongcharoen, P., “*Antibody responses after dose-sparing intradermal influenza vaccination*”, *Vaccine*, 25, 2007, p. 659-663.
  18. Kenney et al. “*Dose sparing with Intradermal Injection of Influenza Vaccine*”,*The New England Journal of Medicine*, 2004. 351: 2295-2301.
  19. Glenn, G.M, Taylor, D.N., Li, X., Frankel,S., Montemarano, A., Alving, C.R., “*Transcutaneous immunization: A human vaccine delivery strategy using a patch*”, *Nature Medicine*, 6(12), 2000, p.1403-1406.
  20. Matyas, G.R., Friedlander, A.M., Glenn, G.M., Little, S., Yu, J., Alving, C.R., “*Needle Free Skin Patch Vaccination Method for Anthrax*”, *Infection and Immunity*, 2004, p.1181-1183.
  21. Look, J.L., Butler, B., Al-Khalili, M., Lai, Y-H., Frolov, V., Zhang, C., Yang, J., Smyla,D., Mayo, A., Yu, J., Guebre-Xabier, M., Frech, S, Ellingsowrt, L., Seid, R., Glenn, G., *The Adjuvant Patch: “A univeral dose sparing approach for Pandemic and Conventional Vaccines*”, Supplement to Bio Pharm International, 2007.
  22. Mkrtychyan, M., Ghochikyan, A., Movsesyan, N., Karapetyan, A., Begoyan, G., Yu, J., Glenn, G.M., Ross, T.M., Agadjanyan, M.G., Cribbs, D.H., “*Immunostimulant adjuvant patch enhances humoral and cellular immune response to DNA immunization*”, *DNA and Cell Biology*, 27(1), 2009, p.19-24.
  23. Frolov, V.G., Seid, R.C., Odutayo, O., Al-Khalili, M., Yu, J., Frolova, O.Y., Vu, H., Butler, B.A., Look, J.L., Ellingsworth, L.R., Glenn, G.M. (2008). “*Transcutaneous delivery and thermostability of a dry trivalent inactivated influenza vaccine patch*”, *Influenza and Other Respiratory Viruses*, 2, 53-60.
  24. Frerichs, D.M., Ellingsworth, L.R., Frech, S.A., Flyer, D.C., Villar, C.P., Yu, J., Glenn,

- G.M. (2008). "Controlled, single-step, stratum corneum disruption as a pretreatment for immunization via a patch", *Vaccine*, 26, 2782-2787.
25. Matriano, J.A., Cormier, M., Johnson, J., Young, W.A., Buttery, M., Nyam, K., Daddona, P.E., "Macroflux Microporjection Array Patch Technology: A New and Efficient Approach for Intracutaneous Immunization", *Pharmaceutical Research*, 19(1), 2002, p. 63-70.
  26. Widera, G., Johnson, J., Kim, L., Libiran, L., Nyam, K., Dadona, P.E., Cormier, M., "Effect of delivery parameters on immunization to ovalbumin following intracutaneous administration by a coated microneedle array patch system", *Vaccine*, 2006, 24, p.1653-1664.
  27. Wendorf, J.R. Gharthey-Tagoe, E.B., Williams, S.C., Enioutina, E., Singh, P., Cleary, B.W., "Transdermal Delivery of Macromolecules Using Solid-State Biodegradable Microstructures", *Pharmaceutical Research*, 2010, Published Online.
  28. Sullivan, S.P., Koutsonanos, D.G., Martin, M.d.P, Lee, J.W., Zarnitsyn, V., Choi, S.O., Murthy, N., Compans, R.W., Skountzou, I., Prausnitz, M.R., "Dissolving polymer microneedle patches for influenza vaccination", *Nature Medicine*, 16, 2010, p. 915-920.
  29. Sawicka, K.M, Roemer, E.J., Simon, S.R., *Enzyme composite nanofibers as novel transdermal delivery coating*, 2007, NEBEC Proceedings, Stony Brook, NY.
  30. Knockenhauer, K.E., Sawicka, K.M., Simon, S.R., *Encapsulation within Nanofibers Confers Stability to the Protective Antigen Protein*, 2010, NEBEC Proceedings, New York, NY.
  31. Hadgraft, J., Lane, M.E., "Skin permeation: The years of enlightenment", *International Journal of Pharmaceutics*, 305, 2005, p. 2-12
  32. Godin, B., Touitou, E., "Transdermal skin delivery: Predictions for humans from in vivo, ex vivo and animal models", *Advanced Drug Delivery Reviews*, 59, 2007, p. 1152-1161
  33. Korinth, G., Schaller, K.H., Drexler, H., *Is the permeability coefficient  $K_p$  a reliable tool in percutaneous absorption studies?*, *Archives of Toxicology*, 2005, 79, p.155-159.
  34. Barry, B.W., "Novel mechanisms and devices to enable successful transdermal drug delivery", *European Journal of Pharmaceutical Sciences*, 14, 2001, p.101- 114.
  35. Rosen, H., Abribat, T., "The rise and rise of drug delivery", *Nature Review Drug Delivery*, 4(5), 2005, p. 381.

36. Lotte, C., Rougier, A., Wilson, D.R., Maibach, H.I., *"In vivo relationship between transepidermal water loss and percutaneous penetration of some organic compounds in men: effect of anatomic site"*, Archives of Dermatological Research, 1987, 279, p.351-356.
37. Werner, R.R., Stone, K.J., Boissy, Y.L., *"Hydration Disrupts Human Stratum Corneum Ultrastructure"*, Journal of Investigative Dermatology, 120, 2003, p. 275- 284.
38. Wokovich, A.M., Prodduturi, S., Doub, W.H., Hussain, A.S., Buhse, L.F., *"Transdermal Drug Delivery System (TDDS) adhesion as a critical safety, efficacy and quality attribute"*, European Journal of Pharmaceutics and Biopharmaceutics, 64 (1), 2006, p.1-8.
39. Basavaraj, K.H., Johnsy, G., Navya, M.A., Rashmi, R., *"Biopolymers as Transdermal Drug Delivery Systems in Dermatology Therapy"*, Critical Reviews in Therapeutic Drug Carrier Systems, 27(2), 2010, p. 155-185.
40. Kupec, J.M. Houser, J.S., *"Removal of polyvinylpyrrolidone from wastewater using different methods."* Water Environ Res, 2012, 84(12), p.2123-23.
41. Buckton, G., Adeniyi, A., Saunders, M., *"HyperDSC studies of amorphous polyvinylpyrrolidone in a model wet granulation system"*, International Journal of Pharmaceutics, 2006, 312 (1-2). pp. 61-65.
42. Feldstein, M., Tohmakhchi, V., Malkhazov, L., *"International Journal of Pharmaceutics"*, 131, 1996, p.229.
43. Kaneda, Y., Tsutsumi, Y., *Biomaterials*, 25, 2004, p. 3259. 49.Aqil, M., Asgar, A.. *"European Journal of Pharmaceutics and Biopharmaceutics"*, 54, 2002, p.16.
44. Kaneda, Y., Tsutsumi, Y., Yoshioka, Y., Kamada, H., et al, *"The use of PVP as a polymeric carrier to improve the plasma half-life of drugs"*, Biomaterials, 2004, 25, p. 3259-3266
45. Maeda, H., Sasaki, S., Mashita, T., *"Dissipative structure in aqueous polymer solutions"*, Journal of Molecular Liquids, 65/66, 1995, p.341
46. Arcos, D., Cabanas, M.V., Ragel, C.V., *"Ibuprofen release from hydrophilic ceramic-polymer composites"*, Biomaterials, 18, 1997, p.1235-1242.
47. Raghavan, S.L., Kiepfner, B., Davis, A.F., Kazarian, S.G., Hadgraft, J., *"Membrane transport of hydrocortisone acetate from supersaturated solutions; the role of polymers"*,

- International Journal of Pharmaceutics, 221, 2001, p.95-105.
48. Wu, Z., Gong, S., Li, C., “*Novel water-soluble fluorescent polymer containing recognition units: Synthesis and interactions with PC12 cell*”, European Polymer Journal, 41 (9), 2005, p.1985-1992.
  49. Ravin, H. A., Seligman, A. M. & Fine, J. “*Polyvinylpyrrolidone as a plasma expander, studies on its excretion distribution and metabolism*”, New Engl. J. Med., 247, 921-929, 1952.
  50. Fong, H. Chun, I., Reneker, D.H., “*Beaded nanofibers formed during electrospinning*”, Polymer, 40, 1999, p.4585-4592.
  51. Dzenis, Y. (2004). Material science. “*Spinning continuous fibers for nanotechnology*”, Science, 304(5679), 1917-1919.
  52. Sawicka, K.M., Gouma, P. (2006). „*Electrospun composite nanofibers for functional applications*”. Journal of Nanoparticle Research, 8, 769-781.
  53. Formhals, A., U.S. Patent No. 1975504, 1934.
  54. Schiffman, J. D., & Schauer, C. L. (2008). A Review: Electrospinning of Biopolymer Nanofibers and their Applications. *Polymer Reviews*, 48(2), 317–352.  
doi:10.1080/15583720802022182
  55. Sill, T. J., & von Recum, H. a. (2008). Electrospinning: applications in drug delivery and tissue engineering. *Biomaterials*, 29(13), 1989–2006.
  56. Hohman, M. M., Shin, M., Rutledge, G., & Brenner, M. P. (2001), Electrospinning and electrically forced jets. I. Stability theory. *Physics of Fluids*, 13(8), 2201.
  57. K. M. Sawicka, P. Gouma, S. Simon, “*Electrospun biocomposite nanofibers for urea biosensing*”, Sens. Actuators, B, Chem., 2005, 108, p. 585.
  58. Bordet J, Gengou O. Le microbe de la coqueluche. Annales de l'Institut Pasteur 1906;20:731-41.
  59. Guiso, N. (2009). Bordetella pertussis and pertussis vaccines. *Clinical infectious diseases : an official publication of the Infectious Diseases Society of America*, 49(10), 1565–9.
  60. Cherry, J. D. (2010). The present and future control of pertussis. *Clinical infectious diseases : an official publication of the Infectious Diseases Society of America*, 51(6), 663–7.

61. Fuzine, C., & Kende, E. (1961). [Whooping cough in an adult]. *Orvosi hetilap*, 102, 1887–9. Retrieved from <http://www.ncbi.nlm.nih.gov/pubmed/22716993>
62. Van Boven, M., Ferguson, N. M., & van Rie, A. (2004). Unveiling the burden of pertussis. *Trends in microbiology*, 12(3), 116–9.
63. Carbonetti, N. (2010). Pertussis toxin and adenylate cyclase toxin: key virulence factors of *Bordetella pertussis* and cell biology tools. *Future microbiology*, 5, 455–469.
64. Cheung, G. Y. C., Xing, D., Prior, S., Corbel, M. J., Parton, R., & Coote, J. G. (2006). Effect of different forms of adenylate cyclase toxin of *Bordetella pertussis* on protection afforded by an acellular pertussis vaccine in a murine model. *Infection and immunity*, 74(12), 6797–805.
65. Loch, C., Coutte, L., & Mielcarek, N. (2011). The ins and outs of pertussis toxin. *The FEBS journal*, 278(23), 4668–82.
66. Xu, Y., & Barbieri, J. T. (1995). Pertussis toxin-mediated ADP-ribosylation of target proteins in Chinese hamster ovary cells involves a vesicle trafficking mechanism. *Infection and immunity*, 63(3), 825–32.
67. Mangmool, S., & Kurose, H. (2011). G(i/o) Protein-Dependent and -Independent Actions of Pertussis Toxin (PTX). *Toxins*, 3(7), 884–99.
68. Schneider, O. D., Weiss, A. a, & Miller, W. E. (2007). Pertussis toxin utilizes proximal components of the T-cell receptor complex to initiate signal transduction events in T cells. *Infection and immunity*, 75(8), 4040–9.
69. Millen, S. H., Bernstein, D. I., Connelly, B., Ward, J. I., Chang, S., & Weiss, A. A. (2004). Antibody-Mediated Neutralization of Pertussis Toxin-Induced Mitogenicity of Human Peripheral Blood Mononuclear Cells, 72(1), 615–620.
70. *WHO vaccine-preventable diseases: monitoring system 2009 global summary*. (2009) (pp. 1–42).
71. Mansour, M., Brown, R. G., Morris, A., Smith, B., & Halperin, S. a. (2007). Improved efficacy of a licensed acellular pertussis vaccine, reformulated in an adjuvant emulsion of liposomes in oil, in a murine model. *Clinical and vaccine immunology : CVI*, 14(10), 1381–3.

72. Mooi, F. R., van Loo, I. H. M., van Gent, M., He, Q., Bart, M. J., Heuvelman, K. J., Mertsola, J. (2009). Bordetella pertussis strains with increased toxin production associated with pertussis resurgence. *Emerging infectious diseases*, 15(8), 1206–13.
73. Wong, K. H., & Skelton, S. K. (1988). New, practical approach to detecting antibody to pertussis toxin for public health and clinical laboratories. *Journal of clinical microbiology*, 26(7), 1316–20.
74. Marconi, G. P., Ross, L. a, & Nager, A. L. (2012). An upsurge in pertussis: epidemiology and trends. *Pediatric emergency care*, 28(3), 215–9.
75. Meyer, C. U., Zepp, F., Decker, M., Lee, M., Chang, S.-J., Ward, J., Edwards, K. M. (2007). Cellular immunity in adolescents and adults following acellular pertussis vaccine administration. *Clinical and vaccine immunology*, 14(3), 288-292.
76. Higgs, R., Higgins, S. C., Ross, P. J., & Mills, K. H. G. (2012). Immunity to the respiratory pathogen Bordetella pertussis. *Mucosal immunology*, 5(5), 485–500.
77. Halperin, Scott A, & Serres, G. De. (2006). Has the change to acellular pertussis vaccine improved, 175(10), 1227–1228.
78. Litt, D. J., Neal, S. E., & Fry, N. K. (2009). Changes in genetic diversity of the Bordetella pertussis population in the United Kingdom between 1920 and 2006 reflect vaccination coverage and emergence of a single dominant clonal type. *Journal of clinical microbiology*, 47(3), 680–8.
79. Heininger, U., Cherry, J. D., & Stehr, K. (2004). Serologic response and antibody-titer decay in adults with pertussis. *Clinical infectious diseases : an official publication of the Infectious Diseases Society of America*, 38(4), 591–4.
80. Ho, S. Y., Chua, S. Q., Foo, D. G. W., Loch, C., Chow, V. T., Poh, C. L., & Alonso, S. (2008). Highly attenuated Bordetella pertussis strain BPZE1 as a potential live vehicle for delivery of heterologous vaccine candidates. *Infection and immunity*, 76(1), 111–9.
81. Mandal, S., Tatti, K. M., Woods-Stout, D., Cassidy, P. K., Faulkner, A. E., Griffith, M. M., Martin, S. W. (2012). Pertussis Pseudo-outbreak linked to specimens contaminated by Bordetella pertussis DNA From clinic surfaces. *Pediatrics*, 129(2), e424–30.
82. Pichichero, M., Deloria, M., Rennels, M., Deforest, A., & Meade, B. (1997). A safety and immunogenicity comparison of 12 acellular pertussis vaccines and one whole-cell

- pertussis vaccine given as a fourth dose in 15-to 20-month-old children. *Pediatrics*, 100(5), 772–788.
83. Pizza, M., Covacci, a, Bartoloni, a, Perugini, M., Nencioni, L., De Magistris, M. T., Bugnoli, M. (1989). Mutants of pertussis toxin suitable for vaccine development. *Science (New York, N.Y.)*, 246(4929), 497–500.
  84. Preston, A. (2005b). Bordetella pertussis: the intersection of genomics and pathobiology. *CMAJ : Canadian Medical Association journal = journal de l'Association medicale canadienne*, 173(1), 55–62.
  85. Van Gent, M., de Greeff, S. C., van der Heide, H. G. J., & Mooi, F. R. (2009). An investigation into the cause of the 1983 whooping cough epidemic in the Netherlands. *Vaccine*, 27(13), 1898–903.
  86. Van Loo, I. H. M., & Mooi, F. R. (2002). Changes in the Dutch Bordetella pertussis population in the first 20 years after the introduction of whole-cell vaccines. *Microbiology (Reading, England)*, 148(Pt 7), 2011–8.
  87. Watanabe, M., Connelly, B., & Weiss, A. A. (2006). Characterization of Serological Responses to Pertussis, 13(3), 341–348.
  88. Vickers, D., Ross, A. G., Mainar-Jaime, R. C., Neudorf, C., & Shah, S. (2006). Whole-cell and acellular pertussis vaccination programs and rates of pertussis among infants and young children. *CMAJ : Canadian Medical Association Journal*, 175(10), 1213–7.
  89. Cherry, J. D. (2012). Why do pertussis vaccines fail? *Pediatrics*, 129(5), 968–70.
  90. Clarke, M. F., Rasiyah, K., Copland, J., Watson, M., Koehler, a P., Dowling, K., & Marshall, H. S. (2012). The pertussis epidemic: informing strategies for prevention of severe disease. *Epidemiology and infection*, 1–9.
  91. Fedele, G., Bianco, M., Debie, A.-S., Loch, C., & Ausiello, C. M. (2011). Attenuated Bordetella pertussis vaccine candidate BPZE1 promotes human dendritic cell CCL21-induced migration and drives a Th1/Th17 response. *Journal of immunology (Baltimore, Md. : 1950)*, 186(9), 5388–96.
  92. Fry, S. R., Chen, A. Y., Daggard, G., & Mukkur, T. K. S. (2008). Parenteral immunization of mice with a genetically inactivated pertussis toxin DNA vaccine induces cell-mediated immunity and protection. *Journal of medical microbiology*, 57(Pt 1), 28–35.

93. Polizzi, K. M., Bommarius, A. S., Broering, J. M., & Chaparro-Riggers, J. F. (2007). Stability of biocatalysts. *Current opinion in chemical biology*, 11(2), 220–5.
94. Bischof, J. C., & He, X. (2005). Thermal stability of proteins. *Annals of the New York Academy of Sciences*, 1066, 12–33.
95. Giteau, A., Venier-Julienne, M.-C., Marchal, S., Courthaudon, J.-L., Sergent, M., Montero-Menei, C. Benoit, J.-P. (2008). Reversible protein precipitation to ensure stability during encapsulation within PLGA microspheres. *European journal of pharmaceutics and biopharmaceutics : official journal of Arbeitsgemeinschaft für Pharmazeutische Verfahrenstechnik e.V*, 70(1), 127–36.
96. Menon, A., Somasekharan, K.N., “*Velocity, acceleration & jerk in electrospinning*”, Internet Journal of Bioengineering, 2010, 4(2).
97. Medeiros, E.S., Glenn, G.M., Klamczynski, A.P., Orts, W.J., Mattoso, L.H.C, (2009). “*Solution blow spinning: a new method to produce micro- and nanofibers from polymer solutions*”, Journal of Applied Polymer Science, 113, 2322-2330.
98. Kong, C.S., YOO, W.S., JO, N.G., KIM, H.S. (2010) “*Electrospinning mechanism for producing nanoscale polymer fibers*”, J. Macromolecular Sci. Part B: Physics, 49, 122-131.
99. Eremin A, Budnikova L, Sviridov V, Metelitsa D. (2001). Stabilization of Diluted Aqueous Solutions of Horseradish Peroxidase. *Applied Biochemistry and Microbiology*. 38:151-158.
100. Chattopadhyay K. and Mazumda S. (2000). Structural and Conformational Stability of Horseradish Peroxidase: Effect of Temperature and pH. Department of Chemical Sciences, Tata Institute of Fundamental Research. 39: 263-27.
101. Van Aalst, J. a, Reed, C. R., Han, L., Andrady, T., Hromadka, M., Bernacki, S., Lobo, E. G. (2008a). Cellular incorporation into electrospun nanofibers: retained viability, proliferation, and function in fibroblasts. *Annals of plastic surgery*, 60(5), 577–83.
102. Venugopal, J., & Ramakrishna, S. (2005). Applications of polymer nanofibers in biomedicine and biotechnology. *Applied biochemistry and biotechnology*, 125(3), 147–58.
103. Kim, G. M., Lach, R., Michler, G. H., Pötschke, P., & Albrecht, K. (2006). Relationships between phase morphology and deformation mechanisms in polymer nanocomposite



- nanofibres prepared by an electrospinning process. *Nanotechnology*, 17(4), 963–72.
104. Kim, G.-M., Wutzler, A., Radusch, H.-J., Michler, G. H., Simon, P., Sperling, R. a., & Parak, W. J. (2005). One-Dimensional Arrangement of Gold Nanoparticles by Electrospinning. *Chemistry of Materials*, 17(20), 4949–4957.
  105. Lee, C.K., Kim, S.I., Kim, S.J., “*The influence of added ionic salt on nanofiber uniformity for electrospinning of electrolyte polymer, synthetic metals*”, 154, 2005, p.209-212.
  106. Munir, M. M., Iskandar, F., & Okuyama, K. (2008). A constant-current electrospinning system for production of high quality nanofibers. *Review of Scientific Instruments*, 79(9), 093904.
  107. Wnek, G. E., Carr, M. E., Simpson, D. G., Bowlin, G. L., (2003). Electrospinning of Nanofiber Fibrinogen Structures, 1–4.
  108. Lee, S.-W., & Belcher, A. M. (2004). Virus-Based Fabrication of Micro- and Nanofibers Using Electrospinning. *Nano Letters*, 4(3), 387–390.
  109. Wendorf, J. R., Gharthey-Tagoe, E. B., Williams, S. C., Enioutina, E., Singh, P., & Cleary, G. W. (2011). Transdermal delivery of macromolecules using solid-state biodegradable microstructures. *Pharmaceutical research*, 28(1), 22–30.
  110. Hewlett, E. L., Sauer, K. T., Myers, G. a, Cowell, J. L., & Guerrant, R. L. (1983). Induction of a novel morphological response in Chinese hamster ovary cells by pertussis toxin. *Infection and immunity*, 40(3), 1198–203.
  111. Gaines Das, R. E. (1999). Assessment of assay precision: a case study of an ELISA for anti-pertussis antibody. *Biologicals : journal of the International Association of Biological Standardization*, 27(2), 125–31.
  112. Halperin, S A, Bortolussi, R., Kasina, A., & Wort, A. J. (1990). cytotoxicity assay for the rapid diagnosis of Use of a Chinese Hamster Ovary Cell Cytotoxicity Assay for the Rapid Diagnosis of Pertussis, 28(1).
  113. Burns, D. L., Kenimer, J. G., & Manclark, C. R. (1987). alteration of Chinese hamster ovary cell Role of the A Subunit of Pertussis Toxin in Alteration of Chinese Hamster Ovary Cell Morphology, 55(1).

114. Lynn, F., Reed, G. F., & Meade, B. D. (1996). Collaborative study for the evaluation of enzyme-linked immunosorbent assays used to measure human antibodies to *Bordetella pertussis* antigens. *Clinical and diagnostic laboratory immunology*, 3(6), 689–700.
115. Cinatl, J., Michaelis, M., Doerr, H. (2007). “*The threat of avian influenza A (H5N1). Part IV: development of vaccines*”. *Med. Microbiol. Immunol.*, 196, 213-225.
116. Thomas, J.K., Noppenberger, J. (2007). “*Avian influenza: A review*”, *Am J Health-Syst Pharm*, 64, 149-165.
117. Hampton, T. (2007). “*Drug, vaccine research target avian flu*”, *JAMA*, 297 (11), 1179-1180.
118. Straus, W.L. (2005). “*The US vaccine supply: challenges in preparing for an avian influenza pandemic*”. *Yale J Biol and Med*, 78, 251.
119. Subbarao, K., Joseph, T. (2007). “*Scientific barriers to developing vaccines against avian influenza viruses*”, *Nature Reviews: Immunology*, 7, 267-278.
120. Suguitan, A., McAuliffe, J. (2006). “*Live, attenuated influenza A H5N1 candidate vaccines provide broad cross-protection in mice and ferrets*”, *PLoS Med*, 3(9), p. 1541-1555.
121. Chang, L. L., & Pikal, M. J. (2009). Mechanisms of Protein Stabilization in the Solid State, 98(9), 2886–2908.
122. Adams, T., Osborn, S., Rijpkema, S., “*An immuno-diffusion assay to assess the protective antigen content of anthrax vaccine*”, *Vaccine*, 2005, 23, p.4517-4520
123. Bienek, D.R., Loomis, L.J., Biagini, R.E., “*The anthrax vaccine - No new tricks for an old dog*”, *Human Vaccines*, 2009, 5, 3, p.184-189.
124. Bonuccelli, G., Sotgia, F., Frank, P. G., Williams, T. M., de Almeida, C. J., Tanowitz, H. B., Lisanti, M. P. (2005). ATR/TEM8 is highly expressed in epithelial cells lining *Bacillus anthracis*' three sites of entry: implications for the pathogenesis of anthrax infection. *American journal of physiology. Cell physiology*, 288(6), C1402–10.
125. Bradley, K. A., Mogridge, J., Mourez, M., Collier, R. J., & Young, J. A. T. (2001). Identification of the cellular receptor for anthrax toxin, (September), 225–229.
126. Brittingham, K. C., Ruthel, G., Panchal, R. G., Fuller, C. L., Ribot, W. J., Hoover, T. A., Bavari, S. (2005). Implications for Anthrax Pathogenesis 1.
127. Collier, R. J. (2009). Membrane translocation by anthrax toxin. *Molecular aspects of*

- medicine*, 30(6), 413–22.
128. Cybulski, R. J., Sanz, P., & O'Brien, A. D. (2009). Anthrax vaccination strategies. *Molecular aspects of medicine*, 30(6), 490–502.
  129. Griffiths, P.D. (2008). “*Whatever happened to bird flu*”, *Rev. Med. Virol.*, 18, 1-3.
  130. Warner, R R, Boissy, Y. L., Lilly, N. a, Spears, M. J., McKillop, K., Marshall, J. L., & Stone, K. J. (1999). Water disrupts stratum corneum lipid lamellae: damage is similar to surfactants. *The Journal of investigative dermatology*, 113(6), 960–6.
  131. Warner, R.R., Stone, K.J., Boissy, Y.L., “*Hydration Disrupts Human Stratum Corneum Ultrastructure*”, *Journal of Investigative Dermatology*, 120, 2003, p. 275- 284.
  132. Benson, H.A.E., Namjoshi, S., “*Proteins and peptides: strategies for delivery to and across the skin*”, *Journal of Pharmaceutical Sciences*, 2007, 1-20.
  133. Bolzinger, M.-A., Briançon, S., Pelletier, J., & Chevalier, Y. (2012). Penetration of drugs through skin, a complex rate-controlling membrane. *Current Opinion in Colloid & Interface Science*, 17(3), 156–165.
  134. Website: <http://www.mattek.com/pages/products/epiderm>, November 29, 2010.
  135. Angel, C.E., George, E., Ostrovsky, L.L., Dunbar, P.R., “*Comprehensive analysis of MHC-II expression in healthy human skin*”, *Immunological Cell Biology*, 85(5), 2007, 363-369.
  136. Babiuk, S., Baca-Estrada, M., Babiuk, L. A., Ewen, C., Foldvari, M. (2000). „*Cutaneous vaccinated action: the skin as an immunologically active tissue and the challenge of antigen delivery*”, *J. Contr. Release*, 66(2-3), 199-214.
  137. Godin, B., Touitou, E., “*Transdermal skin delivery: Predictions for humans from in vivo, ex vivo and animal models*”, *Advanced Drug Delivery Reviews*, 59, 2007, p. 1152-1161.
  138. Chilcott, R. P., Dalton, C. H., Emmanuel, A. J., Allen, C. E., & Bradley, S. T. (2002). Transepidermal water loss does not correlate with skin barrier function *in vitro*. *The Journal of investigative dermatology*, 118(5), 871–5.
  139. Hadgraft, J., Lane, M.E., “*Skin permeation: The years of enlightenment*”, *International Journal of Pharmaceutics*, 305, 2005, p. 2-12
  140. Arcos, D., Cabanas, M.V., Ragel, C.V., “*Ibuprofen release from hydrophilic ceramic-polymer composites*”, *Biomaterials*, 18, 1997, p.1235-1242.
  141. Asahi-Ozaki, Y, Itamura, S, Ichinohe, T, Strong, P, Tamura, S, et al. (2006) “*Intranasal*

- administration of adjuvant-combined recombinant influenza virus HA vaccine protects mice from the lethal H5N1 virus infection*”, *Microbes Infect.*, 8, 2706-2714.
142. Auewarakul, P., Kositanont, U., Sornsathapornkul, P., Tthong, P., Kanyok, R., Thongcharoen, P., “*Antibody responses after dose-sparing intradermal influezavaccination*”, *Vaccine*, 25, 2007, p. 659-663.
  143. Banks, S. L., Pinninti, R. R., Gill, H. S., Paudel, K. S., Crooks, P. A., Brogden, N. K., Stinchcomb, A. L. (2010). Transdermal Delivery of Naltrexol and Skin Permeability Lifetime after Microneedle Treatment in Hairless Guinea Pigs, *99(7)*, 3072–3080.
  144. Barbero, A. M., & Frasch, H. F. (2009). Pig and guinea pig skin as surrogates for human *in vitro* penetration studies: a quantitative review. *Toxicology in vitro : an international journal published in association with BIBRA*, 23(1), 1–13.
  145. Basavaraj, K.H., Johnsy, G., Navya, M.A., Rashmi, R., “*Biopolymers as Transdermal Drug Delivery Systems in Dermatology Therapy*”, *Critical Reviews in Therapeutic Drug Carrier Systems*, 27(2), 2010, p. 155-185.
  146. Levine, T. P., & Chain, B. M. (1992). Endocytosis by antigen presenting cells: dendritic cells are as endocytically active as other antigen presenting cells. *Proceedings of the National Academy of Sciences of the United States of America*, 89(17), 8342–6.
  147. Crowe, J. H., Crowe, L. M., Carpenter, J. F., & Aurell Wistrom, C. (1987). Stabilization of dry phospholipid bilayers and proteins by sugars. *The Biochemical journal*, 242(1), 1–10.
  148. Kenney et al. “*Dose sparing with Intradermal Injection of Influenza Vaccine*”, *The New England Journal of Medicine*, 2004. 351: 2295-2301.
  149. Look, J.L., Butler, B., Al-Khalili, M., Lai, Y-H., Frolov, V., Zhang, C., Yang, J., Smyla, D., Mayo, A., Yu, J., Guebre-Xabier, M., Frech, S, Ellingsowrt, L., Seid, R., Glenn, G., *The Adjuvant Patch: “A univeral dose sparing approach for Pandemic and Conventional Vaccines*”, Supplement to Bio Pharm International, 2007.